225
5-16

130
ORNL-4855

HEAVY-SECTION STEEL TECHNOLOGY PROGRAM

Semiannual Progress Report

Period Ending August 31, 1972

BLANK PAGE

Printed in the United States of America. Available from
National Technical Information Service
U.S. Department of Commerce
5285 Port Royal Road, Springfield, Virginia 22151
Price: Printed Copy $3.00; Microfiche $0.95

ORNL-4855
UC-80 – Reactor Technology

Contract No. W-7405-eng-26

HEAVY-SECTION STEEL TECHNOLOGY PROGRAM
SEMIANNUAL PROGRESS REPORT
For Period Ending August 31, 1972

F. J. Witt, Program Director

APRIL 1973

OAK RIDGE NATIONAL LABORATORY
Oak Ridge, Tennessee 37830
operated by
UNION CARBIDE CORPORATION
for the
U.S. ATOMIC ENERGY COMMISSION

Contents

BLANK PAGE

Foreword

The Heavy-Section Steel Technology (HSST) Program is a USAEC-sponsored effort for investigating the effects of flaws, variations of properties, stress raisers, and residual stress on the structural reliability of present and contemplated water-cooled reactor pressure vessels. The cognizant engineer for the USAEC is J. R. Hunter, and at ORNL the program is under the Pressure Vessel Technology Program, of which G. D. Whitman is Director. The program is being carried out in very close cooperation with the nuclear power industry. Prior reports in this series are ORNL-4176, ORNL-4315, ORNL-4377, ORNL-4463, ORNL-4512, ORNL-4590, ORNL-4653, ORNL-4681, ORNL-4764, and ORNL-4816.

Summary

The Heavy-Section Steel Technology (HSST) program is one of the major USAEC safety engineering research programs devoted to extending and developing the technology for quantitatively assessing the margins of safety against fracture of the primary containment systems of civilian water reactors. Emphasis is on the massive pressure vessels of these sophisticated systems. Practically all areas of materials technology as related to the pertinent steels and weldments have been or are being investigated. The investigations in progress are discussed in this progress report; prior reports in this series are identified in the Foreword.

An investigation of weldments of the European forging steel 22NiMoCr37 by K. Kussmaul of MPA Stuttgart, West Germany, has indicated susceptibility to intergranular cracking. However, a metallographic examination at ORNL of a submerged-arc weldment of ASTM A533, grade B, class 1 steel has shown no evidence of such cracking. The ASTM A508, class 2 forging welds are under investigation.

A combined experimental and analytical program has been initiated at Westinghouse to evaluate the engineering usefulness of the two leading theories of elastic-plastic fracture: the equivalent-energy approach and the J-integral approach. Under the experimental portion of the program, five uniaxial tensile specimens, six compact-tension specimens, and three center-cracked (fracture theories evaluation) specimens were machined from A533, grade B, class 1 steel (HSST plate 04). The five tensile specimens were tested to provide stress-strain data for input to the analytical portion of the program.

A preliminary elastic analysis of the fracture theories evaluation specimen was performed to study nonuniformities of the displacement field in order to determine a gage length for the elastic-plastic analysis. A more detailed finite-element model of the specimen gage length was then set up for use in the elastic-plastic analysis. This second model has an extremely fine grid in the vicinity of the crack tip to provide the necessary high degree of resolution there.

A program was initiated at Westinghouse to examine low-frequency fatigue-crack growth response of nuclear pressure vessel steels in simulated reactor coolant environments. Previous crack growth rate studies had not indicated a frequency dependence in or out of the reactor coolant environments at cycling rates of 60 and 500 cpm.

Three 2T CT specimens have been tested at a load application frequency of 1 cpm with $R = 0.2$. The results indicate higher crack growth rates in both the PWR and BWR environments than were previously reported in the higher frequency ranges.

The fatigue-crack propagation behavior of A533, grade B, class 1 steel was studied at Hanford Engineering Development Laboratory within the framework of linear-elastic fracture mechanics. Tests were conducted at 75°F (24°C) and 550°F (288°C) on unirradiated material and on material irradiated to 2.3 to 2.8 $\times 10^{19}$ and 5.3 to 5.7 $\times 10^{19}$ neutrons/cm^2 ($E > 1$ MeV). In general, at the cyclic frequency used (600 cpm), neither temperature nor neutron irradiation had a significant effect on the fatigue-crack propagation.

Fracture properties were evaluated by plane strain (K_{Ic}) and lower-bound equivalent-energy (K_{Icd}) measurements for irradiated A533 weldment from the HAZ and fusion line and for A533 base plate material. The lower-bound K_{Ic} of 2 $\times 10^{19}$ neutrons/cm^2 ($E > 1$ MeV) fusion line material was 175 ksi$\sqrt{\text{in.}}$ at test temperature above 250°F; base plate material, at similar

BLANK PAGE

irradiation and test conditions, exhibited a K_{Ic1} of approximately 190 ksi$\sqrt{in.}$ Weldment material from the HAZ after irradiation to 0.5×10^{19} neutrons/cm^2 gave a value of 149 ksi$\sqrt{in.}$ at room temperature; however, upper-shelf lower-bound toughness was not yet attained at that temperature.

Six 4T compact-tension specimens are to be irradiated in the Battelle Research Reactor (BRR) by Westinghouse to midthickness fluence levels of 5×10^{19} neutrons/cm^2 ($E > 1$ MeV). An encapsulation arrangement has been designed in order to ensure relative uniformity of the fluence and temperature distributions in the specimens during irradiation. Detailed thermal analysis has been performed to confirm the design and demonstrate that the temperature distribution will be in the desired range during irradiation. Preliminary measurements were made in the BRR to characterize the neutron environment and the gamma radiation fields adjacent to the core. The capability to monitor three-dimensional distribution of temperature and fluence has been incorporated in the capsule design.

The final series of 6-in.-thick tensile specimens, including one unflawed specimen, were tested at Southwest Research Institute. Test temperatures ranged from -40 to 200°F.

Mechanical properties data were obtained from the prolongation of intermediate vessel V-1, including drop-weight, room-temperature tensile, standard Charpy V-notch impact, and slow-bend precracked Charpy V-notch tests.

Forging prolongation material from the first and second HSST intermediate pressure vessels was fabricated by Westinghouse into 4T and 0.85T compact-tension specimens. These specimens were tested over a temperature range of 0 to 200°F in order to establish a lower-bound curve of the fracture toughness of the pressure vessel material.

Six 0.85-in.-thick model vessels fabricated from the prolongation of intermediate vessel V-1 were flawed, instrumented, and burst. These results were used to select the test temperature for the first intermediate test vessel under prescribed conditions of failure.

The hydraulic pulsing crack-sharpening technique previously developed for the 6-in.-thick tensile specimens was further developed to apply to the intermediate test vessels. Further development effort was also required to permit monitoring of the flaw growth by ultrasonic testing.

Vessel V-1 was instrumented with strain gages and thermocouples internally and externally mounted, a crack-opening displacement device, and with acoustic emission transducers. The instrumenting, monitoring, and evaluation of the acoustic emissions were performed by Southwest Research Institute. The vessel was successfully tested, and in general the performance was as expected.

Battelle Columbus laboratory conducted two tests investigating mode III crack extension of full-scale reactor piping with variations in flaw size, pressure, and temperature between the two tests.

1. Program Administration and Procurement

The Heavy-Section Steel Technology (HSST) Program is oriented toward developing a technology that can be used to assess the margins of safety against failure of the primary containment systems of civilian water-reactor power stations. Major emphasis is placed on the conditions necessary to initiate failure in the massive pressure vessels, particularly catastrophic failure. The areas of research interest and support, however, cover the gamut of material technology, with particular emphasis on the effects of fast-neutron irradiation. The HSST program is coordinated with efforts by other government agencies and the manufacturing and utility sectors of the nuclear power industry both in the United States and abroad. These total efforts should result in the quantification of safety assessments which are needed by the USAEC regulatory bodies, the professional code-writing bodies, and the nuclear power industry.

The activities of the HSST program are carried out under 12 separate tasks. About 75% of the task activities are performed under subcontract by research facilities throughout the United States and through informal cooperative efforts abroad. Currently there are eight research and development subcontracts in force. In addition, a panel of 28 scientists and engineers with expertise in materials technology has been organized to serve in an advisory capacity to the program. Four technical reports and one progress report were issued during this reporting period.[1-5]

The major procurement items of the HSST program are the intermediate test vessels. Four vessels have been received, and six more are in various stages of fabrication.

Administratively, the HSST program is carried out as task activities; however, for reporting purposes here, the research areas are discussed under investigations of unirradiated materials, investigations of irradiated materials, and pressure vessel and piping investigations.

---

1. S. C. Grigory, *Six-Inch-Thick Flawed Tensile Tests, First Technical Summary Report, Longitudinal Specimens 1 through 7*, HSSTP-TR-18 (SwRI 03-2520), Southwest Research Institute (June 1972).
2. P. N. Randall, *Effects of Strain Gradients on the Gross Strain Crack Tolerance of A533-B Steel*, HSSTP-TR-19, TRW Systems Group (May 1, 1972).
3. S. C. Grigory, *Tests of Six-Inch-Thick Flawed Tensile Specimens, Second Technical Summary Report, Transverse Specimens Numbers 8 through 10, Welded Specimens Numbers 11 through 13*, HSSTP-TR-20, Southwest Research Institute (June 1972).
4. S. A. Leitge, *Effects of Fracture Mechanics Parameters of Displacement Measurement Geometry for Varying Specimen Sizes*, WCAP-7926, Westinghouse Electric Corporation (June 1972).
5. *HSST Program Semiannu. Progr. Rep. Feb. 29, 1972*, ORNL-4816.

2. Investigations of Unirradiated Materials

The materials investigations under the HSST program are divided, in general, into studies of unirradiated materials and studies of irradiation effects. The studies of unirradiated materials, which include inspection, characterization, metallurgy, variability determinations, transition temperature investigations, fracture mechanics studies, and fatigue-crack propagation tests, are discussed here. No work specifically under the transition temperature task is in progress. Additional results for unirradiated materials are presented in Chap. 3.

INVESTIGATION OF WELD METAL HEAT-AFFECTED ZONE

D. A. Canonico

Intergranular cracking in the heat-affected zone (HAZ) of thick-section weldments representative of those employed in the fabrication of nuclear pressure vessels was reported by K. Kussmaul of MPA Stuttgart, West Germany, at the 1972 Annual Information Meeting of the HSST Program.[1] This report prompted the initiation of studies of the HAZ of a number of the weldments used in the HSST studies. Until recently, these welds were prepared for weld characterization studies and, for the most part, have been used in the assessment of their fracture toughness. These welds are between 6- and 12-in. plates of ASTM A533, grade B, class 1 steel. The fabrication of the intermediate test vessels has provided weldments between 6-in.-thick shells of ASTM A508, class 2 forging steel. This forging grade of steel is nearer in chemical composition to the European 22Ni-Mo-Cr37 steel used in the Kussmaul study. The HAZ of the ASTM A508, class 2 steel is under study.

Reported herein are the preliminary results of an investigation of the HAZ from a portion of submerged-arc weldment,[2] HSST plate 57C. The steel plates joined were 6-in.-thick ASTM A533, grade B, class 1 steel. After welding, the weldment was stress relieved at 1150°F for 6 hr. Our study concentrated on a location near one end of the weldment plate; Fig. 2.1 shows the location from which the HAZ study specimen was taken. The specimen, which was 3 in. long, was sectioned as shown in Fig. 2.2. The specimens (four), approximately 3 in. long and 1½ in. wide, were prepared so that the polished surface was perpendicular to the welding direction, and the metallographic investigation progressed from the base metal (BM) through the HAZ to the weld metal (WM). Figure 2.3 contains photomacrographs taken at various distances below the initially polished surface. Point zero in Fig. 2.3 is mostly unaffected BM. (A light coloration near the center and at the bottom indicates a location nearer the weld than the remainder of the specimen.) As the metal is removed, indications of different microstructures are evident by the variance in coloration. Note, particularly in the photomacrographs taken after the removal of

1. K. Kussmaul and D. Sturm, "Research Activities at the MPA Stuttgart in the Field of Nuclear Pressure Vessel Technology: Materials – Welding – Safety," presented at the Sixth Annual Information Meeting of the Heavy-Section Steel Technology Program, ORNL, Apr. 25–26, 1972.

2. C. E. Childress, *Fabrication Procedures and Acceptance Data for ASTM A-533 Welds and a 10-in.-thick ASTM A-543 Plate of the HSST Program*, ORNL-4313-3 (January 1971).

BLANK PAGE

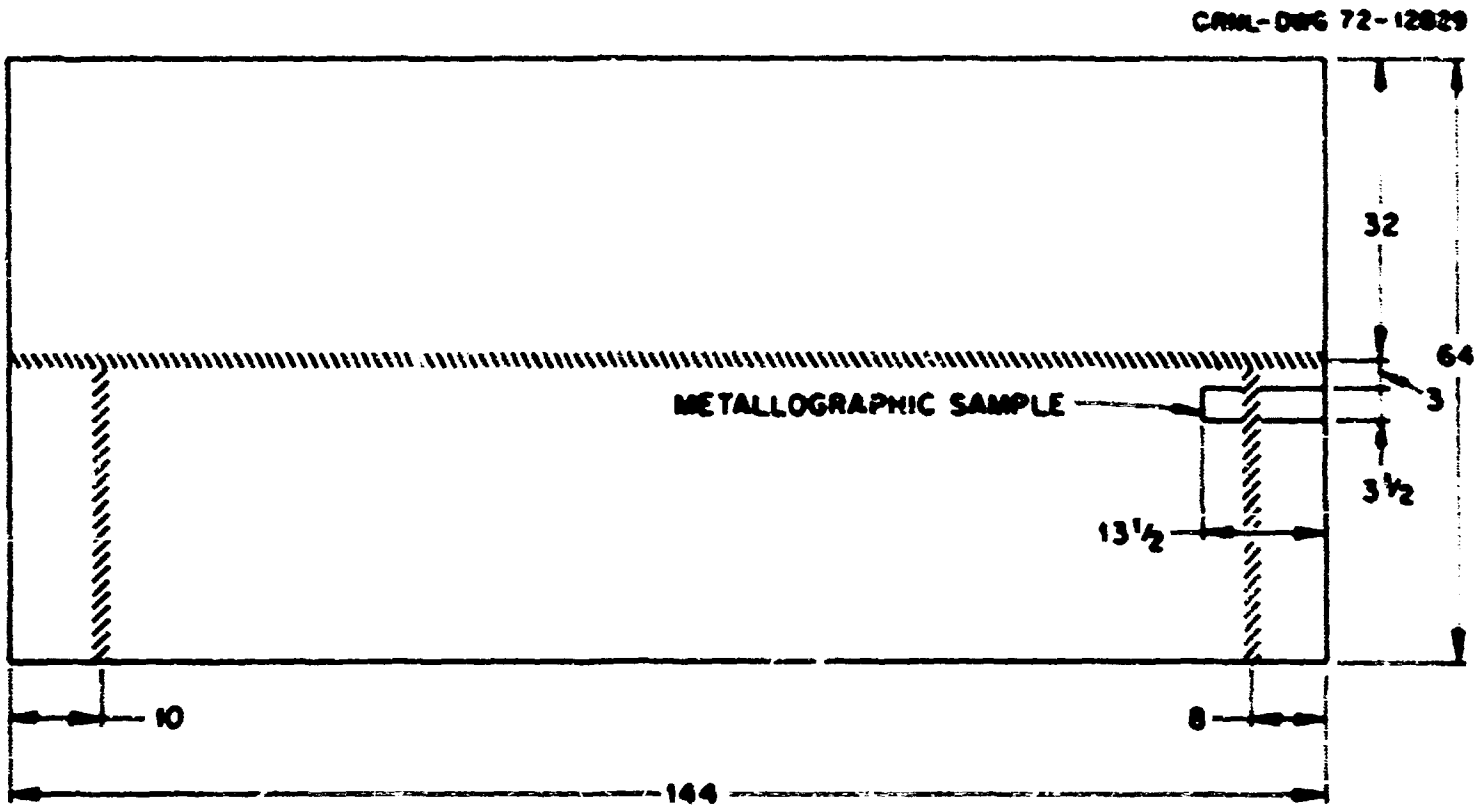

DIMENSION IN INCHES

////// - WELD

Fig. 2.1. HSST plate 57C, showing size of plate and location of the submerged-arc welds. The location of the sample used in this investigation is identified. The plate used to make the weldment is 6-in.-thick A[illegible]TM A533, grade B, class 1.

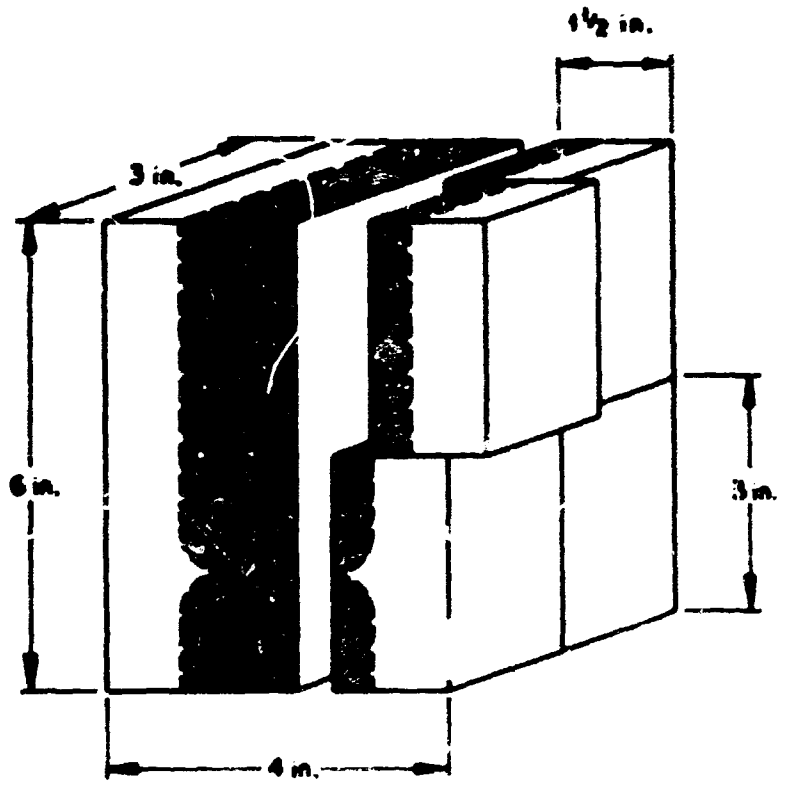

Fig. 2.2. Sketch showing method of specimen removal for metallographic study.

0.1676 to 0.1879 in. of metal, that the individual weld passes are clearly delineated.

Extensive metallographic investigations were conducted at the various depths of metal removal, and no indication of cracking of any type was observed. This is true regardless of the microstructure observed in the HAZ. Figure 2.4 is included because it is representative of the microstructure present at the fusion line. The bottom of Fig. 2.4 (a four-photomicrograph montage) is weld metal, and the top is the coarse-grained austenitic region in the HAZ immediately adjacent to the fusion line. The microstructure is tempered martensite.

Our studies to date have revealed no signs of intergranular cracking in the HAZ. We are continuing the metallographic study and are investigating samples from weldments from 6- and 12-in.-thick ASTM A533, grade B, class 1 steel and part of the prolongation from vessel V-4.

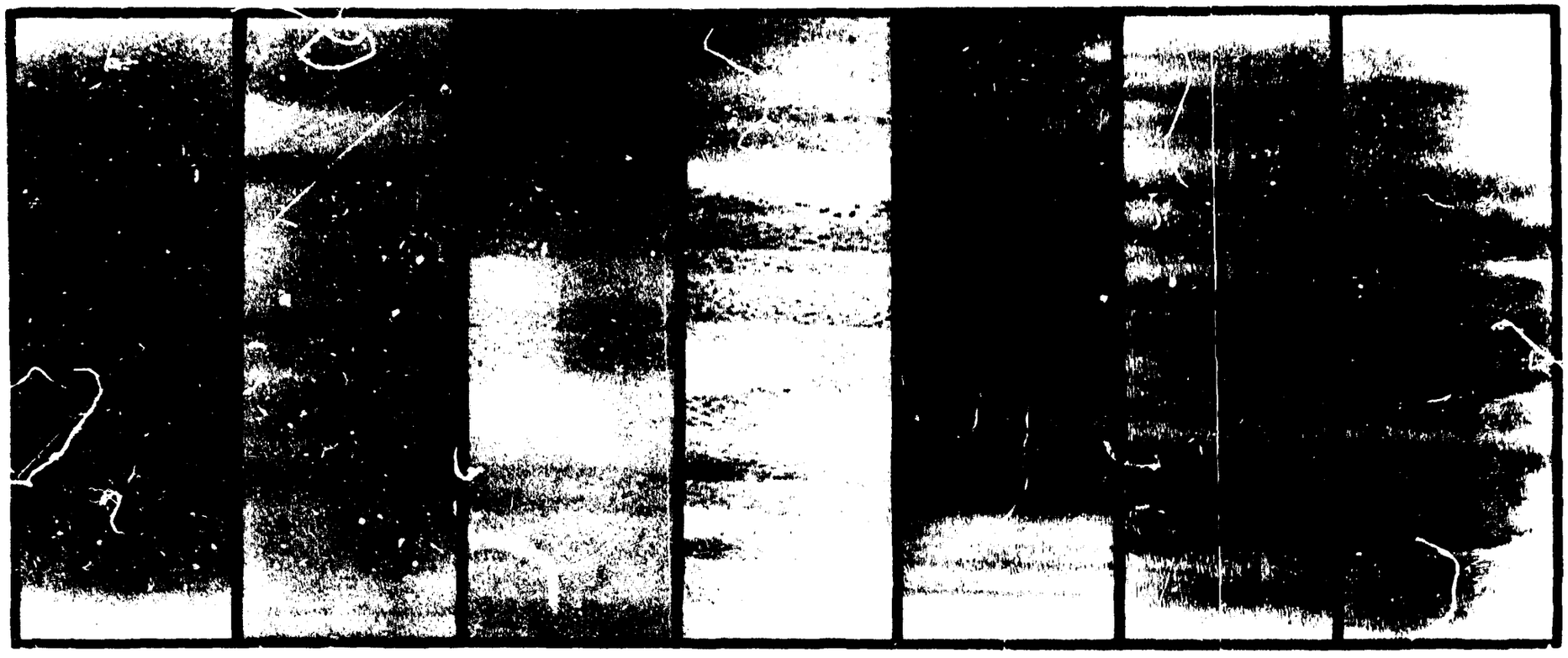

Fig. 2.3. Photomacrographs of ORNL Metals and Ceramics Division metallographic specimen 73662. This specimen, along with three others, has been extensively studied. The numbers on top of the photomacrographs indicate amount of metal removed. The individual weld passes are clearly delineated by their effect on the microstructure in the heat-affected zone.

PHOTO Y-116153

Fig. 2.4. Montage of photomicrographs representative of the microstructure seen at the fusion line in HSST weldment 57C. The fusion line is shown. The bottom of the montage is weld metal, and the top is the coarse-grained austenite region of the HAZ. (The microstructure is tempered martensite.) Note the weldment soundness and cleanliness. No cracks were observed in any of the regions studied.

FRACTURE MECHANICS INVESTIGATIONS

J. G. Merkle

The objectives of the fracture mechanics investigations are (1) to establish the applicability of fracture mechanics methods as currently understood to the low-alloy steels being used in reactor pressure vessels, (2) to extend the applicability of this knowledge to cover the tougher behavior at higher temperatures, and (3) to develop new methods specifically applicable for predicting the fracture behavior of steels that undergo gross plastic strains before fracture. These objectives are being pursued through a series of investigations with related tasks (described elsewhere) contributing significantly to the developments. Several of these activities have been completed, and only one activity assigned specifically to this task is in progress.

Experimental and Analytical Elastic-Plastic Fracture Theories Evaluation Program[3]

P. C. Riccardella
Westinghouse Electric Corporation

J. L. Swedlow
Carnegie-Mellon University

Introduction

Neither of the two leading theories of elastic-plastic fracture (J-integral and equivalent energy) has yet been subjected to a critical evaluation to demonstrate its applicability to complex loading and geometric configurations such as those which exist in nuclear reactor pressure vessels. Both theories rely heavily upon the experimental load-deflection curve of a test specimen to predict failure. However, in a reactor vessel, no single parameter represents applied load, and no single displacement value is pertinent to the overall problem. The degree of loading can only be estimated using sophisticated, two-dimensional analysis techniques, such as the finite-element technique, which are capable of considering geometric discontinuities, pressure stresses, and complex thermal gradients.

The objective of this effort is to apply both fracture theories to a relatively simple test specimen using a two-dimensional finite-element computer program which has enough generality that it can later be applied to more complex reactor vessel problems. The test specimen chosen is a center-cracked plate geometry (hereafter referred to as the fracture theories evaluation specimen), which is illustrated in detail in Fig. 2.5. Critical failure parameters (load and deflection) will be predicted by both fracture theories from the analysis, and the accuracy of the predictions will be evaluated by comparison with actual experimental results.

In order to ensure a meaningful evaluation of the two theories, the tests are to be performed in the transition range between linear elastic (frangible) behavior and fully ductile behavior. To satisfy this constraint, a test temperature of +50°F has been chosen.

Experimental program

A total of 14 specimens have been machined from HSST plate section 04-A for the fracture theories evaluation program. A sawing sketch showing the location from which each specimen was taken is given in Fig. 2.6. Note that the flame-cut edges of the plate and 2 in. each of top and bottom surface material have been removed prior to machining of the specimens.

Five standard 0.505 uniaxial tensile specimens[4] have been machined as shown in Fig. 2.6. Three specimens were taken in the longitudinal (RW) direction (at the ¼ plate thickness, center plate thickness, and ¾ plate thickness depths), and two were taken in the transverse (WR) direction (at the ¼ plate thickness and ¾ plate thickness depths). All five specimens were tested at the test temperature of +50°F, and the resulting true stress-strain data are summarized in Fig. 2.7. The strain rate for all five tests was 0.0008 sec^{-1}. The data in Fig. 2.7 indicate that the stress-strain properties of the material are essentially homogeneous and isotropic. The material exhibits a yield point instability at approximately 70,000 psi, and nonstrain hardening behavior at 66,000 psi between yield strain and about 1.0%. At 1.0% the material begins to strain harden up to about 95,000 psi and 9% strain.

Four 2T and two 4T compact-tension (CT) fracture mechanics specimens[5] have been machined from the plate as shown in Fig. 2.6. The 2T CT specimens were taken at the one-quarter thickness, center thickness, and three-fourths thickness depths, and the 4T CT specimens spanned the thickness. All the compact-tension specimens were taken in the longitudinal (RW)

---

3. Work sponsored by HSST Program under UCCND Subcontract No. 3196 between Union Carbide and Westinghouse Electric Corporation.

4. Standard Methods of Tension Testing of Metallic Materials, ASTM-E8-69, 1969.

5. Tentative Method of Test for Plane Strain Fracture Toughness of Metallic Materials, ASTM-E399-70T, 1970.

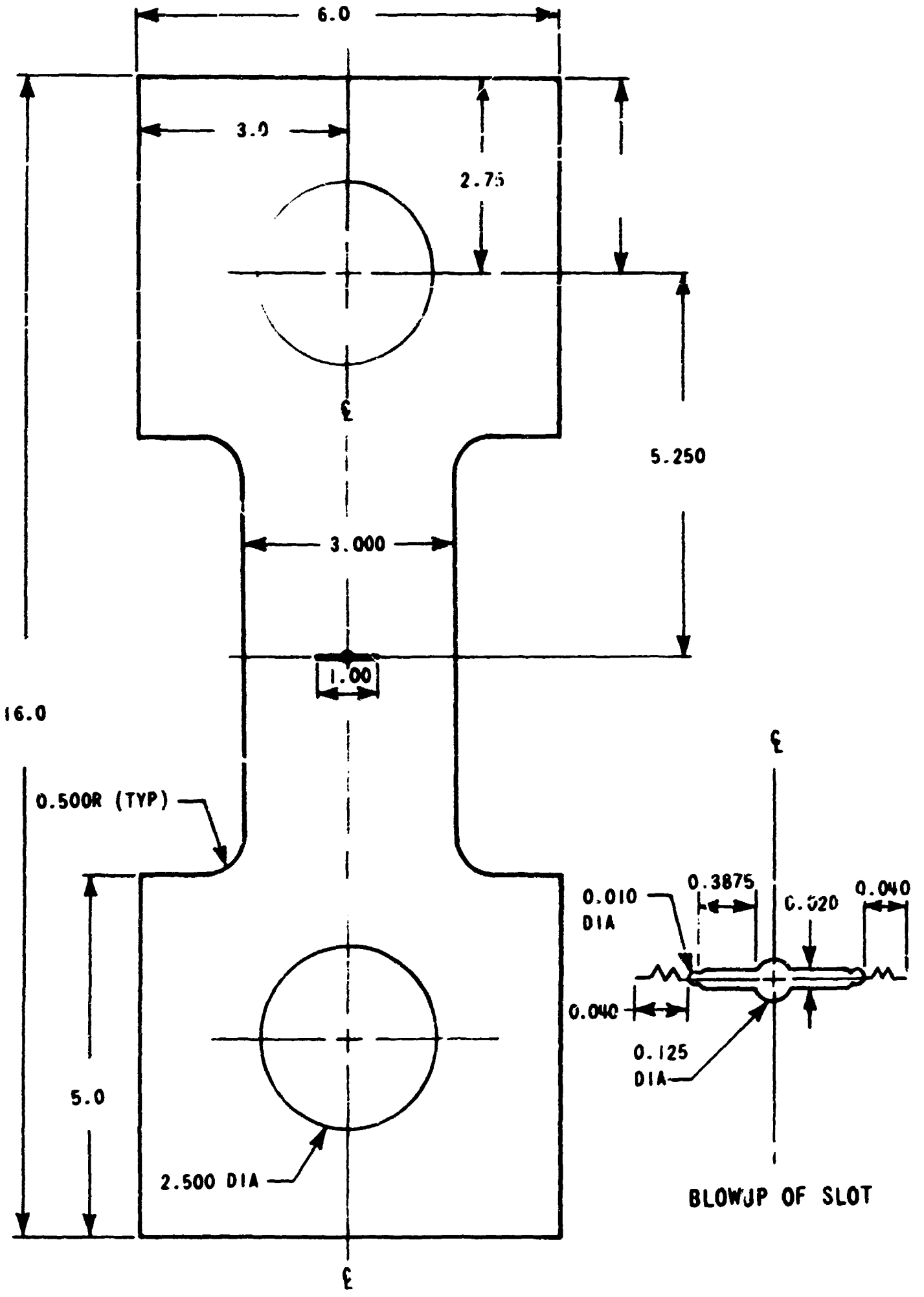

Fig. 2.5. Fracture theories evaluation specimen.

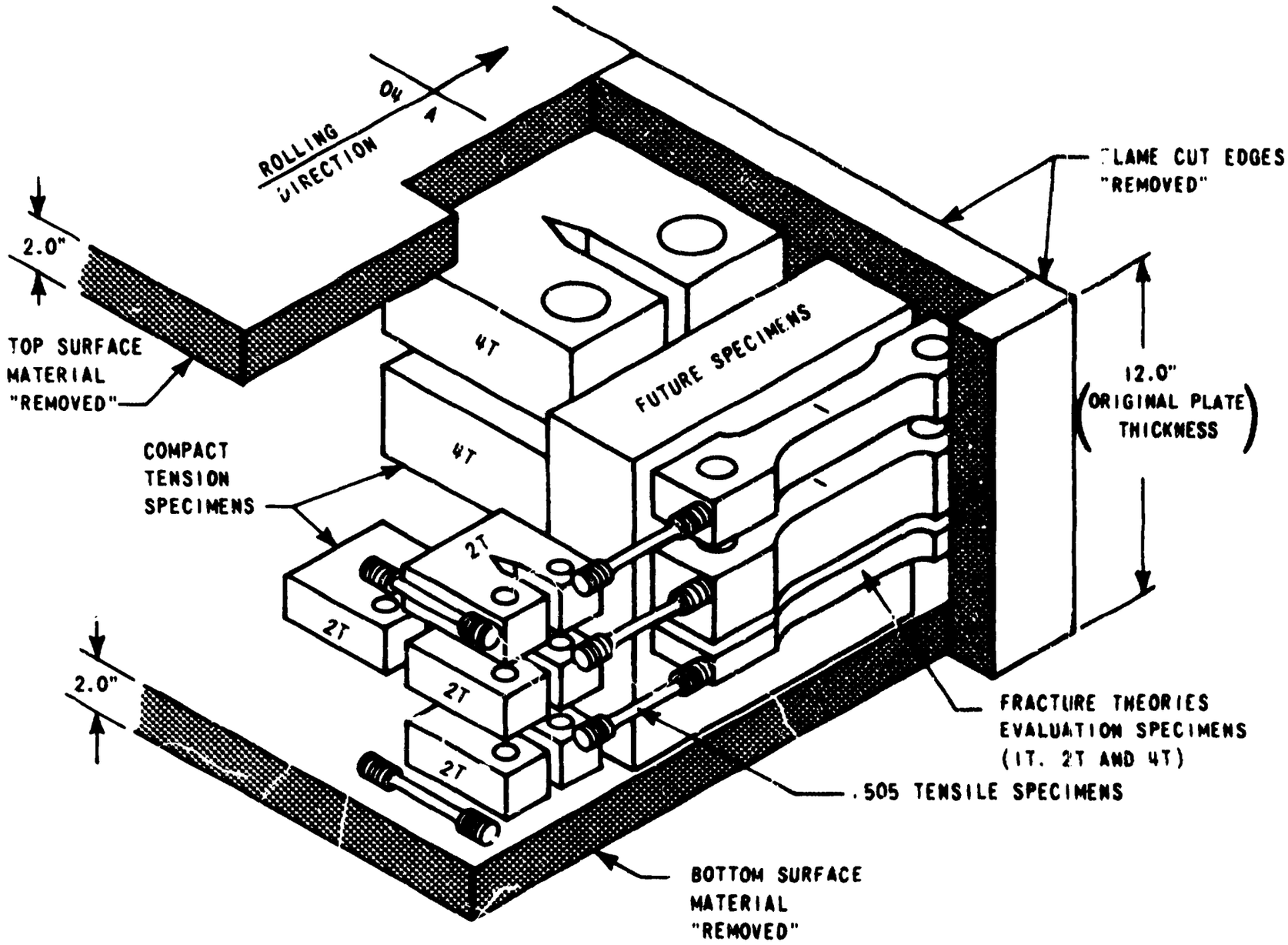

Fig. 2.6. Specimen sawing sketch for fracture theories evaluation program.

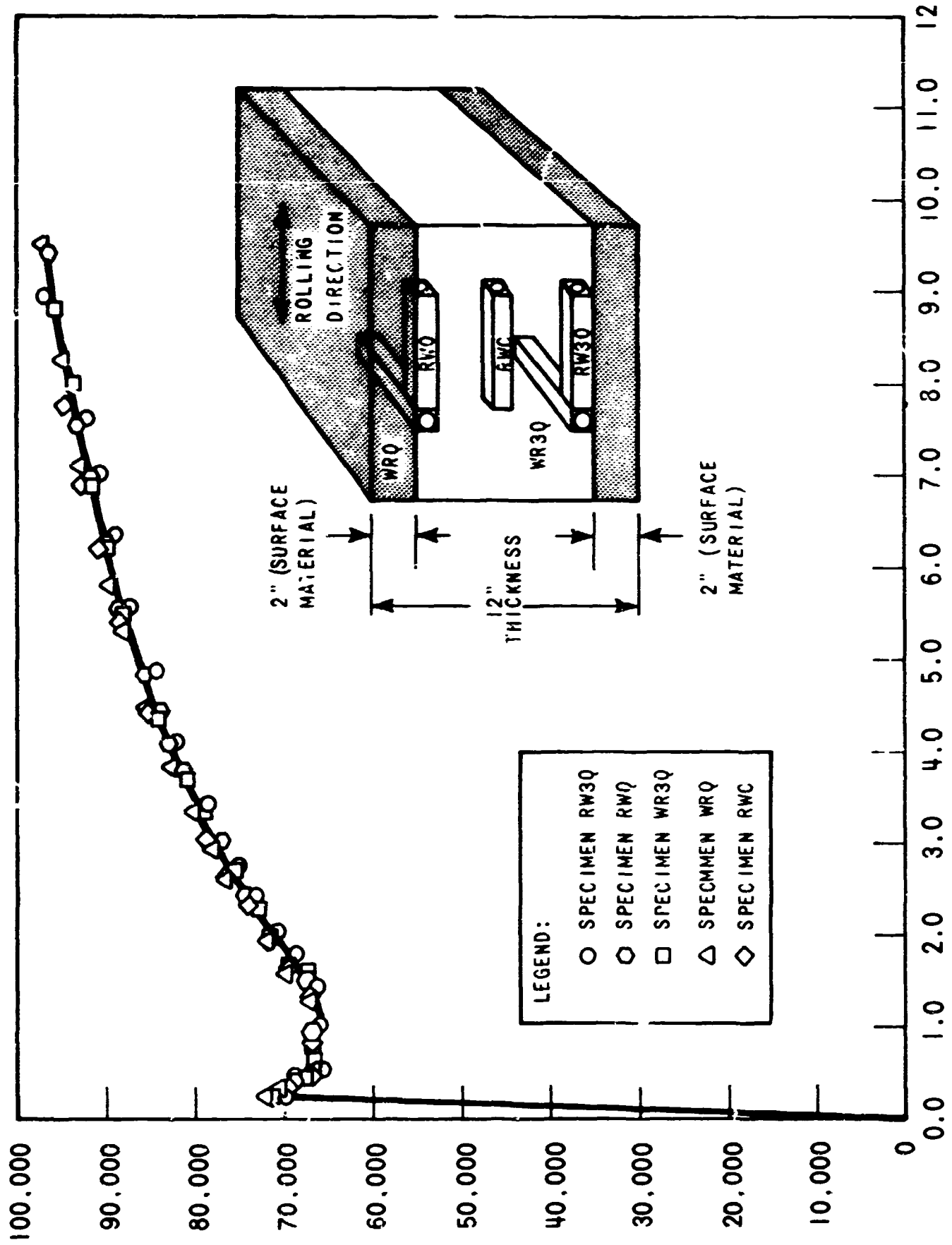

Fig. 2.7. Stress vs strain data from uniaxial tensile tests.

direction. These specimens will be tested at the test temperature (50°F) to study the variability of the material fracture toughness (as determined by both J_{Ic} and K_{Icd} interpretations) at this temperature.

Finally, three fracture theories evaluation specimens were machined from the plate as shown in Fig. 2.6. The in-plane dimensions of these specimens are given in Fig. 2.5, and specimens with thickness of 1, 2, and 4 in. were fabricated in order to study the approach to plane strain behavior. The center slot was machined using electrical discharge machining (EDM), as shown in Fig. 2.5, and will be fatigue sharpened to a final length of 1.0 in. prior to testing.

Analytical program

A relatively simple elastic model of the fracture theories evaluation specimen was set up in order to perform preliminary studies on the specimen (see Fig. 2.8). Two symmetry lines were used to reduce the size of the model. Axial loading was applied along the upper half of the loading hole, and the axial deflection results in the gage region of the specimen are shown in Fig. 2.9. Near the crack plane, the deflection of the center line of the specimen is much greater than that of the edges, while near the specimen grips, the deflection at the edges is much greater. In the region approximately 1.5 to 1.75 in. from the crack plane, the displacement is essentially uniform. The ideal choice for gage length for the specimen is within this uniform displacement region. Thus the effective half gage length has been chosen to be 1.75 in. (total gage length = 3.5 in.).

Since the displacement pattern at the ends of the gage length region was uniform in the elastic case, it can be assumed that this displacement pattern will also be essentially uniform for the elastic-plastic case. Therefore, when setting up the more detailed model for elastic-plastic analysis of the specimen, only the gage length region was modeled. The elastic-plastic model is shown in detail in Figs. 2.10 and 2.11. Note that an extremely fine grid was used in the vicinity of the crack tip to provide the necessary high degree of resolution there.

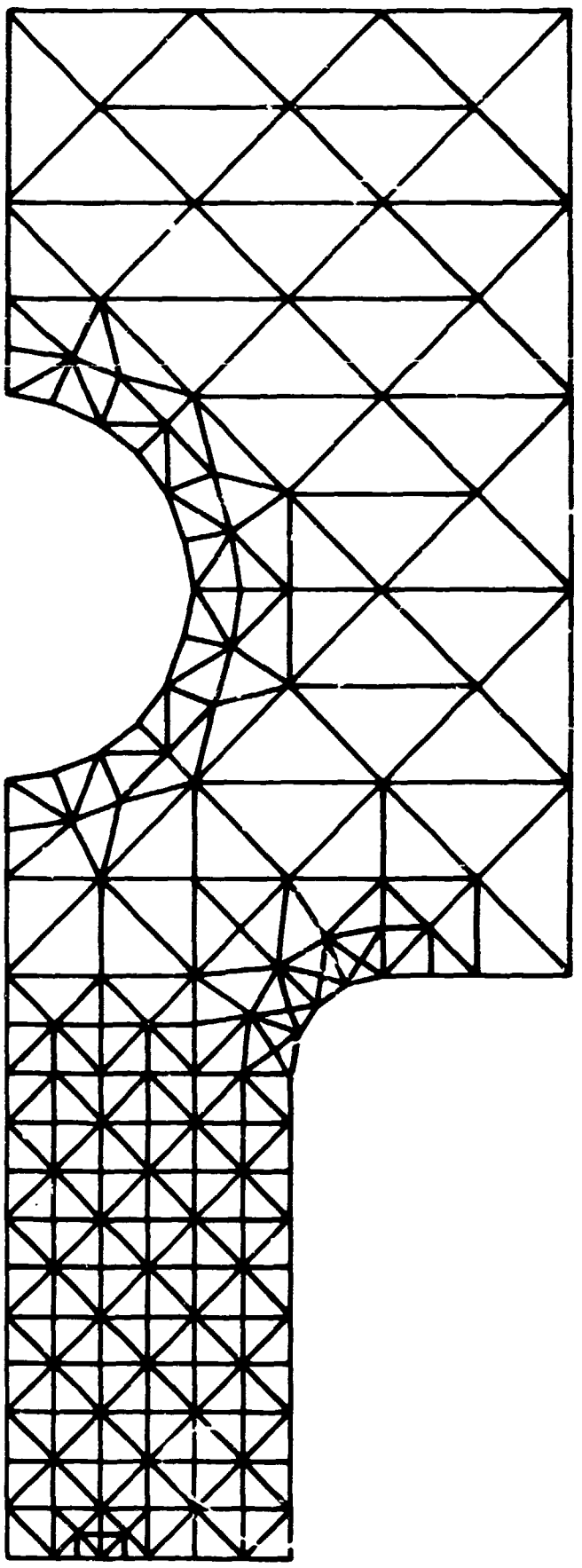

Fig. 2.8. Elastic model of fracture theories evaluation specimen used to determine gage length.

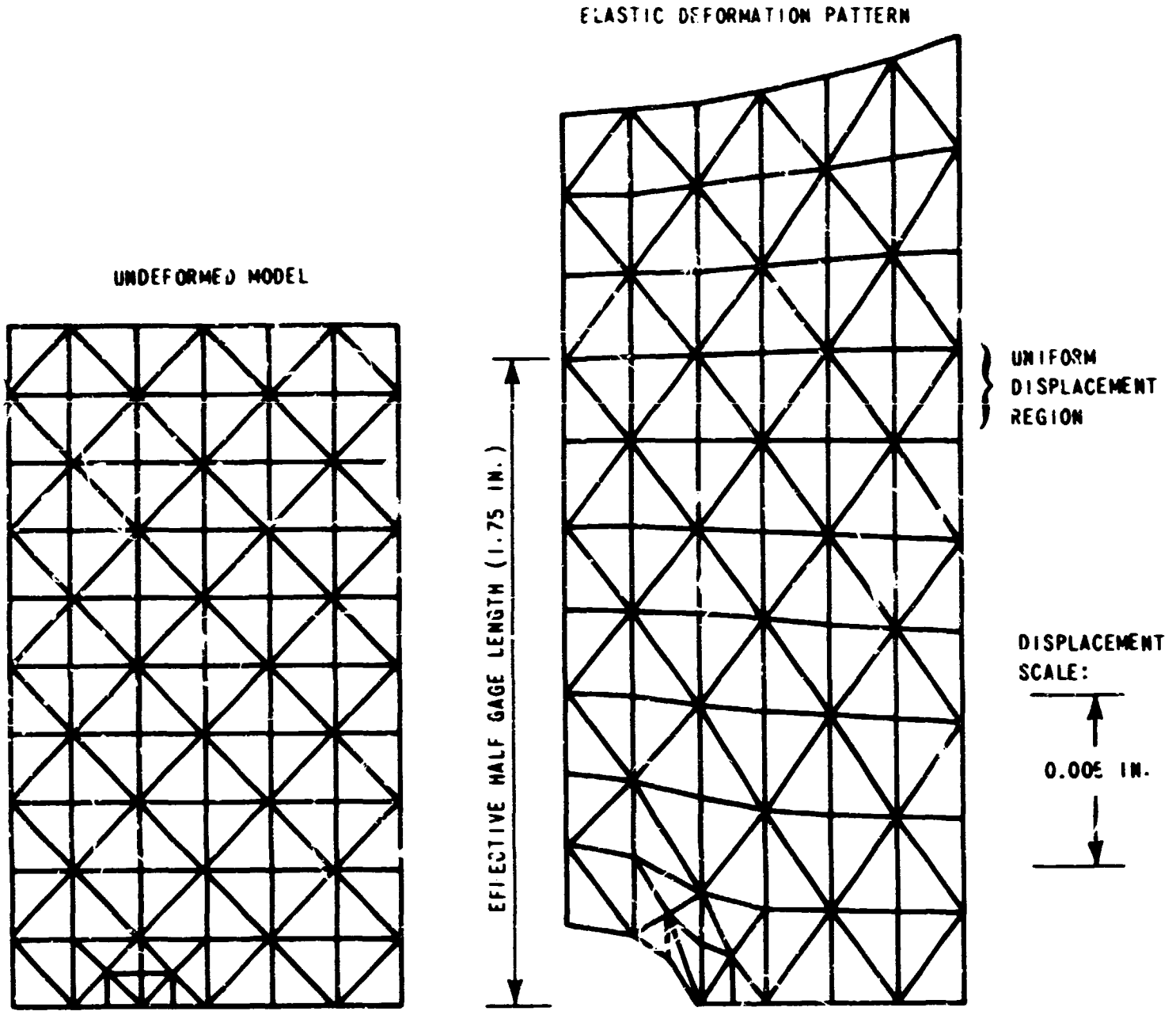

Fig. 2.9. Deflection results of elastic analysis of fracture theories evaluation specimen.

EFFECTS OF HIGH-TEMPERATURE PRIMARY REACTOR WATER ON THE SUBCRITICAL CRACK GROWTH OF REACTOR VESSEL STEEL[6]

S. A. Legge T. R. Mager
Westinghouse Electric Corporation

Introduction

A program was initiated this report period to examine low-frequency fatigue crack growth response in nuclear pressure vessel steels in simulated reactor coolant environments. Previous crack-growth-rate studies had not indicated a frequency dependence in or out of the reactor coolant environments at cycling rates of 60 and 600 cpm.[7]

Three 2T CT specimens have been tested at a load application frequency of 1 cpm with R = 0.2. The results indicate higher crack-growth rates in both the PWR and BWR environments than were previously reported in the higher frequency ranges.

Experimental Procedure

Six precracked 2T CT specimens (KW orientation) were fabricated from HSST plate 02 for the study. The

---

6. Work sponsored by HSST Program under UCCND Subcontract No. 3290 between Union Carbide and Westinghouse Electric Corporation.

7. T. R. Mager and V. J. McLoughlin, *The Effect of an Environment of High Temperature Primary Grade Nuclear Reactor Water on the Fatigue Crack Growth Characteristics of A533 Grade B Class 1 Plate and Weldment Material*, Heavy-Section Steel Technology Program Technical Report No. 16 (October 1971).

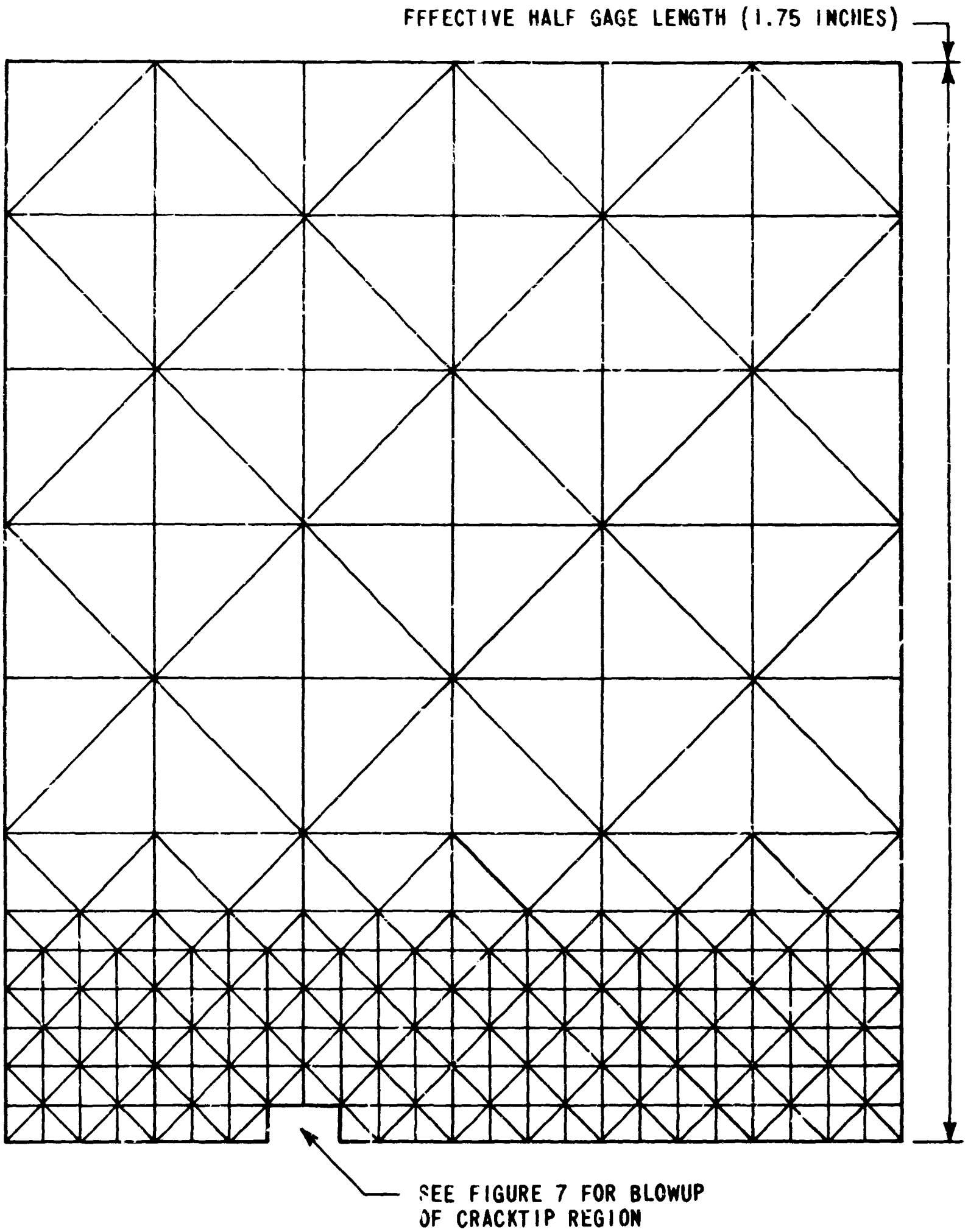

Fig. 2.10. Elastic-plastic model of fracture theories eva.. ation specimen.

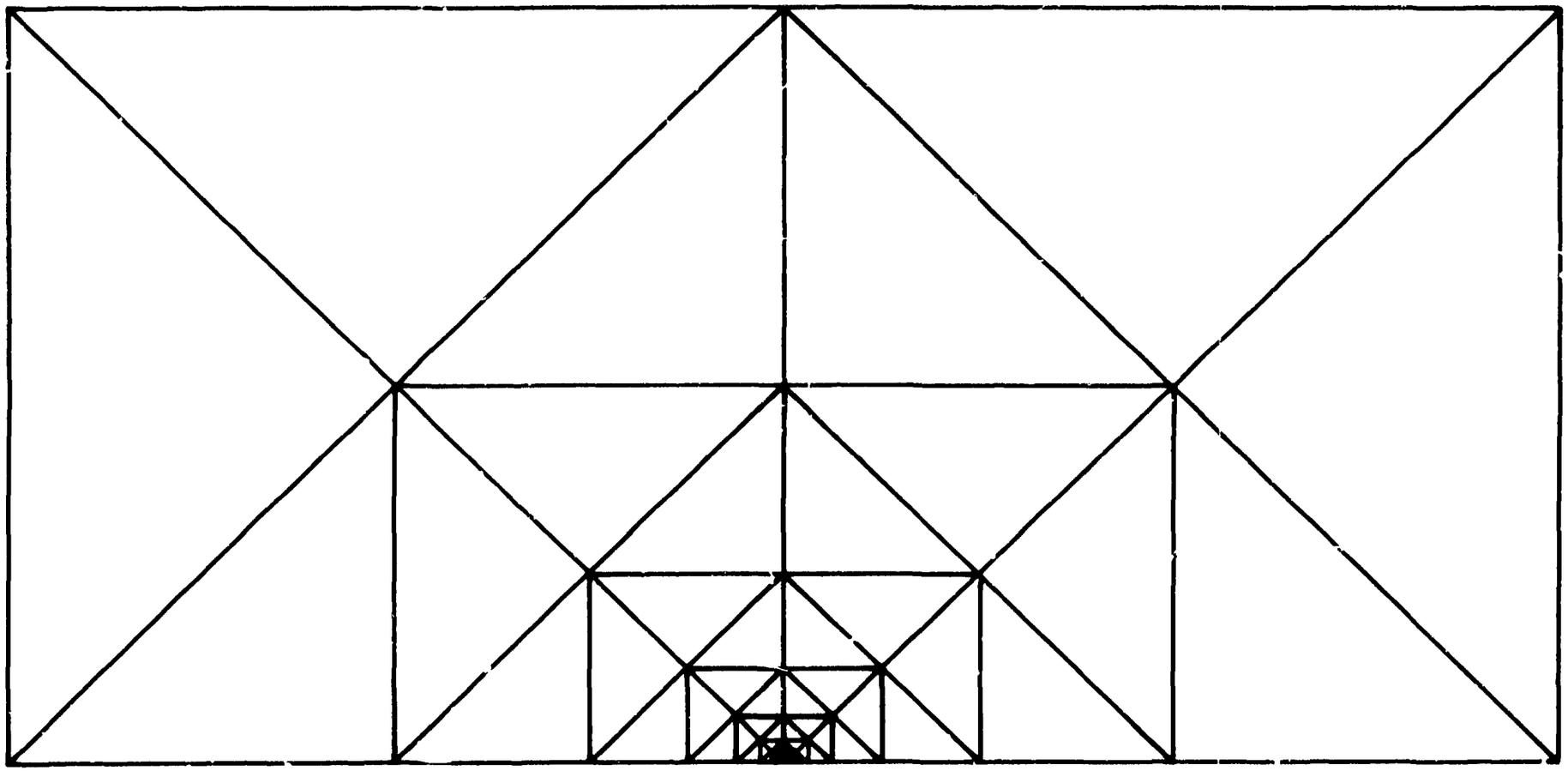

Fig. 2.11. Elastic-plastic model of fracture theories evaluation specimen (blowup of crack tip region).

load cycle was held constant at a frequency of 1 cpm with maximum load at 20,000 lb. Two specimens were tested in a PWR environment (2000 psi, 550°F) and one specimen in a BWR environment (1200 psi, 550°F), and the water chemistries were controlled to the specifications give in Table 2.1. A fourth test is under way in air (2000 psi, 550°F).

Experimental Results

The resultant crack length vs number of cycles data were reduced to fracture mechanics parameters. In Fig. 2.12, the crack growth rate (*da/dn*) is plotted as a function of the independent variable, stress intensity factor (ΔK), for the three tests completed. For convenience, a reference line has been included on the plot

Table 2.1. Environmental water chemistry

	Pressurized-water reactor	Boiling-water reactor
Oxygen, ppm	<0.1	<0.3
Chloride, ppm	<0.15	<0.1
Fluoride, ppm	<0.15	<0.1
Total suspended solids, ppm	<1.0	<0.2
Boron, ppm	0 - 4000 (2500 av)	
Solution pH	4.2 – 10.5 (5.1 av)	Neutral
Electrical conductivity, μmhos/cm	<1 - 40	0.1
Hydrogen, cc (STP)/kg	25 - 35	0.037
LiOH, *m*	0.3×10^{-4} 3.2×10^{-4}	

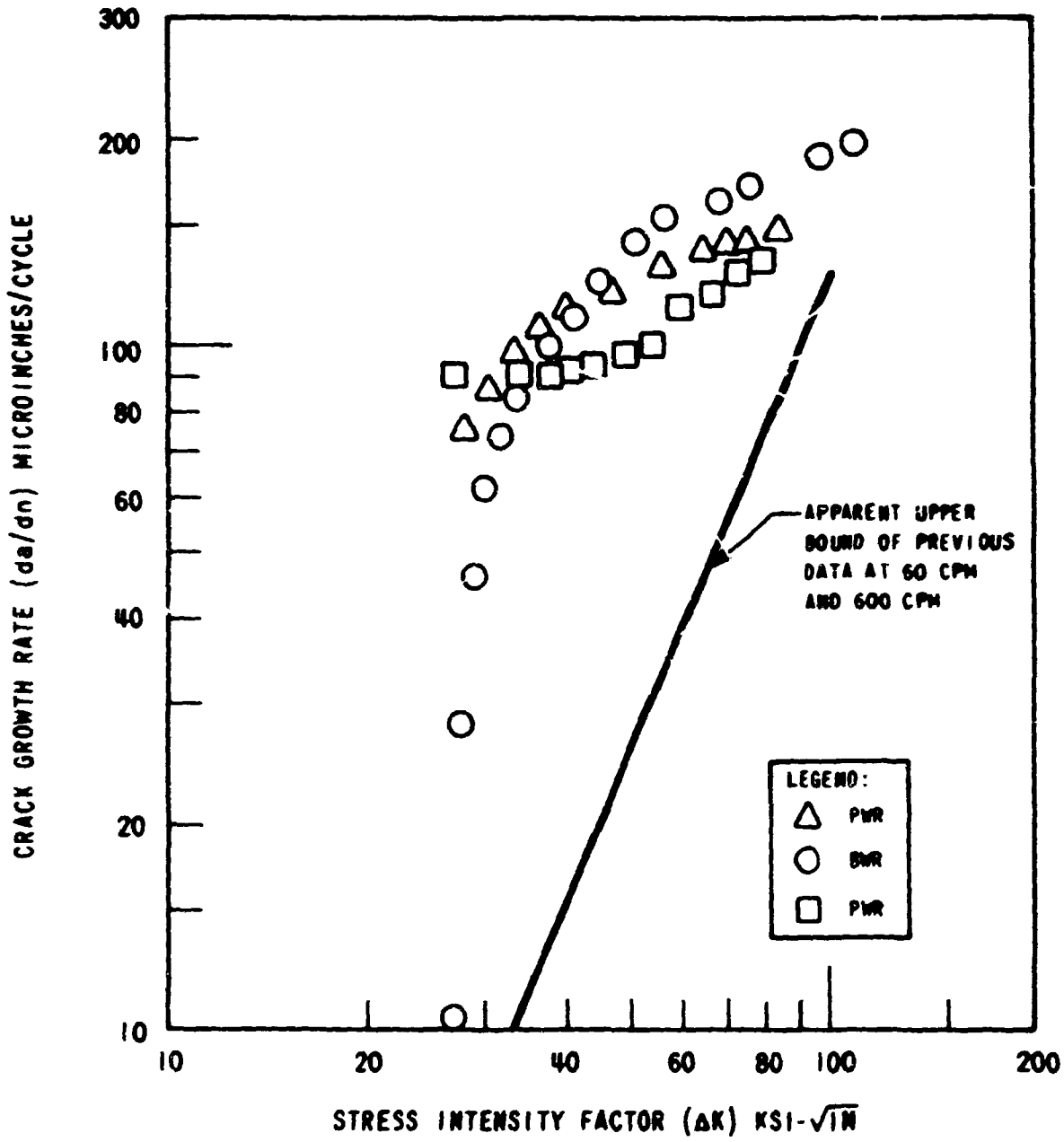

Fig. 2.12. Crack growth rates for HSST 02 material at 1 cpm frequency in PWR and BWR environments.

representing an upper bound for all previous crack-growth-rate data generated on HSST plate 02 at frequencies of 60 and 600 cpm.[7] It is apparent that at the lower frequencies crack growth rates are accelerated. These results are in general agreement with other studies,[8] which have been conducted on austenitic stainless steel, in which frequency-dependent behavior is demonstrated to obey a power law of the type

$$da/dn = A(f)(\Delta K)^n ,$$

where $A(f)$ is an empirically determined frequency function that increases with decreasing frequency.

---

8. L. A. James. *The Effect of Frequency upon the Fatigue Crack Growth of Type 304 Stainless Steel at 1000°F*. HEDL-SA-243, WADCO Corporation.

3. Investigations of Irradiated Materials

One of the environmental factors that must be considered in safety evaluations of reactor pressure vessels is irradiation, because the mechanical properties of metals may be modified thereby to a degree that is of considerable engineering significance. Irradiation effects were investigated by Hanford Engineering Development Laboratory (HEDL) and by Westinghouse Electric Corporation. The areas of primary interest to the HSST program are the temperature range 450 to 600°F and the fast-neutron ($E > 1$ MeV) fluence range 1 to 8×10^{19} neutrons/cm^2.

This chapter summarizes the research performed by HEDL and Westinghouse.

IRRADIATION EFFECTS ON THE FRACTURE OF HEAVY-SECTION PRESSURE VESSEL STEELS[1]

J. A. Williams L. A. James
Hanford Engineering Development Laboratory

Two areas of irradiation investigations are in progress at Hanford Engineering Development Laboratory. One is a study of the effect of irradiation on the cyclic fatigue crack growth behavior of the ASTM A533, grade B, class 1 steel. The other is the determination of both the static fracture toughness K_{Ic} and the lower bound thereof up to 550°F of the pertinent plate and forging steels and weldments. These two efforts are discussed below.

Fatigue-Crack Propagation of Irradiated ASTM A533, Grade B, Class 1 Steel

Cracking behavior of the A533-B HSST plate 02 steel is being determined for use in design or safety analyses of flaw or crack propagation resulting from cyclic service loadings. The present study uses the principles of linear-elastic fracture mechanics to characterize the effects of temperature and neutron irradiation upon the fatigue-crack growth behavior of this steel.

Irradiated A533, grade B, class 1 specimens were obtained from fractured 2-in.-thick compact-tension specimens (2T CT) irradiated in the Babcock and Wilcox Test Reactor. The details of material irradiations and test results are documented by Mager.[2] Irradiations were conducted at 550°F (288°C) to fluences of 2.3 to 2.8 and 5.3 to 5.7 $\times 10^{19}$ neutrons/cm^2 ($E > 1$ MeV); postirradiation yield strength was nominally 90 ksi at room temperature and 78 ksi at 550°F.[2] Specimens from the irradiated material were machined by Oak Ridge National Laboratory, and unirradiated A533, grade B specimens were from section 02GA of HSST plate 02. Nominal yield strength of the unirradiated material is 67 and 55 ksi at room temperature and 550°F respectively.[3] All specimens were of longitudinal (RW) orientation from between one-quarter and one-half the plate thickness position. The irradiated specimens were of the wedge-opening-loading (WOL) type,

1. Research sponsored under Purchase Order No. 11Y-50917V between Union Carbide Corporation and Hanford Engineering Development Laboratory.

2. T. R. Mager, *Postirradiation Testing of 2T Compact Tension Specimens*, WCAP-7561 (August 1970).

3. C. W. Hunter and J. A. Williams, "Fracture and Tensile Behavior of Neutron-Irradiated A 533-B Pressure Vessel Steel," *Nucl. Eng. Des.* 17(1), 131–48 (1971).

and the unirradiated specimens were of the ASTM compact-tension (CT) type.

All specimens were fatigue cycled using load as the control parameter, with a sinusoidal loading waveform at 600 cpm (10 Hz); the cyclic stress ratio, R ($R = \sigma_{min}/\sigma_{max}$), was zero for all tests. Testing was conducted in an air environment at 75°F (24°C) and at 550°F (288°C).

Fatigue-crack growth rates, da/dN, were based on the incremental change in crack length between readings, Δa, divided by the number of loading cycles for that increment, ΔN. Stress intensity factors were computed from Eqs. (1) and (2) for the WOL specimen and the CT specimen respectively:

$$K = \frac{P}{B\sqrt{a}}\left[30.96\left(\frac{a}{W}\right) - 195.8\left(\frac{a}{W}\right)^2 + 730.6\left(\frac{a}{W}\right)^3 - 1186.3\left(\frac{a}{W}\right)^4 + 754.6\left(\frac{a}{W}\right)^5\right], \quad (1)$$

$$K = \frac{P}{B\sqrt{W}}\left[29.6\left(\frac{a}{W}\right)^{0.5} - 185.5\left(\frac{a}{W}\right)^{1.5} + 655.7\left(\frac{a}{W}\right)^{2.5} - 1017.0\left(\frac{a}{W}\right)^{3.5} + 638.9\left(\frac{a}{W}\right)^{4.5}\right], \quad (2)$$

where

K = stress intensity factor, ksi $\sqrt{\text{in.}}$,

P = applied load, lb,

B = specimen thickness, in.,

a = crack length, in.,

W = specimen width, in.,

using the average crack length for each increment. The stress intensity factor range, ΔK, was calculated using

$$\Delta K = K_{max}(1 - R). \quad (3)$$

The data were plotted as log (da/dN) vs log (ΔK) such that the simple power law proposed by Paris and Erdogan[4] results:

$$da/dN = C(\Delta K)^n, \quad (4)$$

where C, n = constants for a given material-environment combination.

The results for the tests conducted at 75°F (24°C) are plotted in Fig. 3.1, and the results for 550°F (288°C) are given in Fig. 3.2. A single power law of the form of Eq. (4) describes the crack growth behavior at both temperatures over a fairly wide range of ΔK values. In both sets of data, there is some suggestion of a slope transition at the lower values of ΔK. The existence of such a slope transition in unirradiated material is confirmed by the study of Paris et al.,[4] which dealt with crack growth rates below 10^{-6} in./cycle (2.54×10^{-5} mm/cycle). In general, the unirradiated material test results of the present study are in good agreement with those of other investigators[5-10] for similar conditions.

Comparison of the results of Figs. 3.1 and 3.2 leads to several observations. First, there is essentially no difference in the cracking behavior of unirradiated material at 75 and at 550°F. This is in agreement with the findings of Clark,[5] who tested at the same frequency (600 cpm) used in the present study. Watson et al.,[6] however, noted an increase in the fatigue-crack growth rate with increasing temperature when the testing was carried out at a frequency of 10 cpm.

Crack growth behaviors of unirradiated and irradiated materials are equivalent at 75°F, as evidenced by Fig. 3.1. This is generally consistent with the data of Watson et al.[6] for the RW orientation. Watson et al., however, have observed differences in behavior of the irradiated

4. P. Paris and F. Erdogan, "A Critical Analysis of Crack Propagation Laws," *J. Basic Eng.* 85(4), 528–34 (1963).

5. W. G. Clark, Jr., "Fatigue Crack Growth Characteristics of Heavy Section ASTM A 533 Grade B, Class 1 Steel Weldments," ASME paper 70-PVP-24, 1970.

6. H. E. Watson, L. E. Steele, and P. Shahinian, *Effects of Irradiation and Temperature on the Fatigue Properties of A 533-B Steel, Irradiation Effects on Reactor Structural Materials*, NRL Memorandum Report 2328, pp. 12–17, U.S. Naval Research Laboratory (August 1971).

7. W. G. Clark, Jr., "Effect of Temperature and Section Size on Fatigue Crack Growth in Pressure Vessel Steel," *J. Mat.* 6(1), 134–49 (1971).

8. P. C. Paris et al., "An Extensive Study on Low Fatigue Crack Growth Rates in A 533 and A 508 Steels," Scientific Paper 71-1E7-FMPWR-P7, Westinghouse Research Laboratories, 1971.

9. T. R. Mager, "Fatigue Crack Growth Characteristics of Nuclear Pressure Vessel Grade Materials," Paper 1, HSST Program 5th Annual Information Meeting, Oak Ridge National Laboratory, Mar. 25–26, 1971.

10. T. Kondo et al., "Fatigue Crack Propagation Behavior of ASTM A 533-B and A 302-B Steels in High Temperature Aqueous Environment," Paper 6, HSST Program 6th Annual Information Meeting, Oak Ridge National Laboratory, Apr. 25–26, 1972.

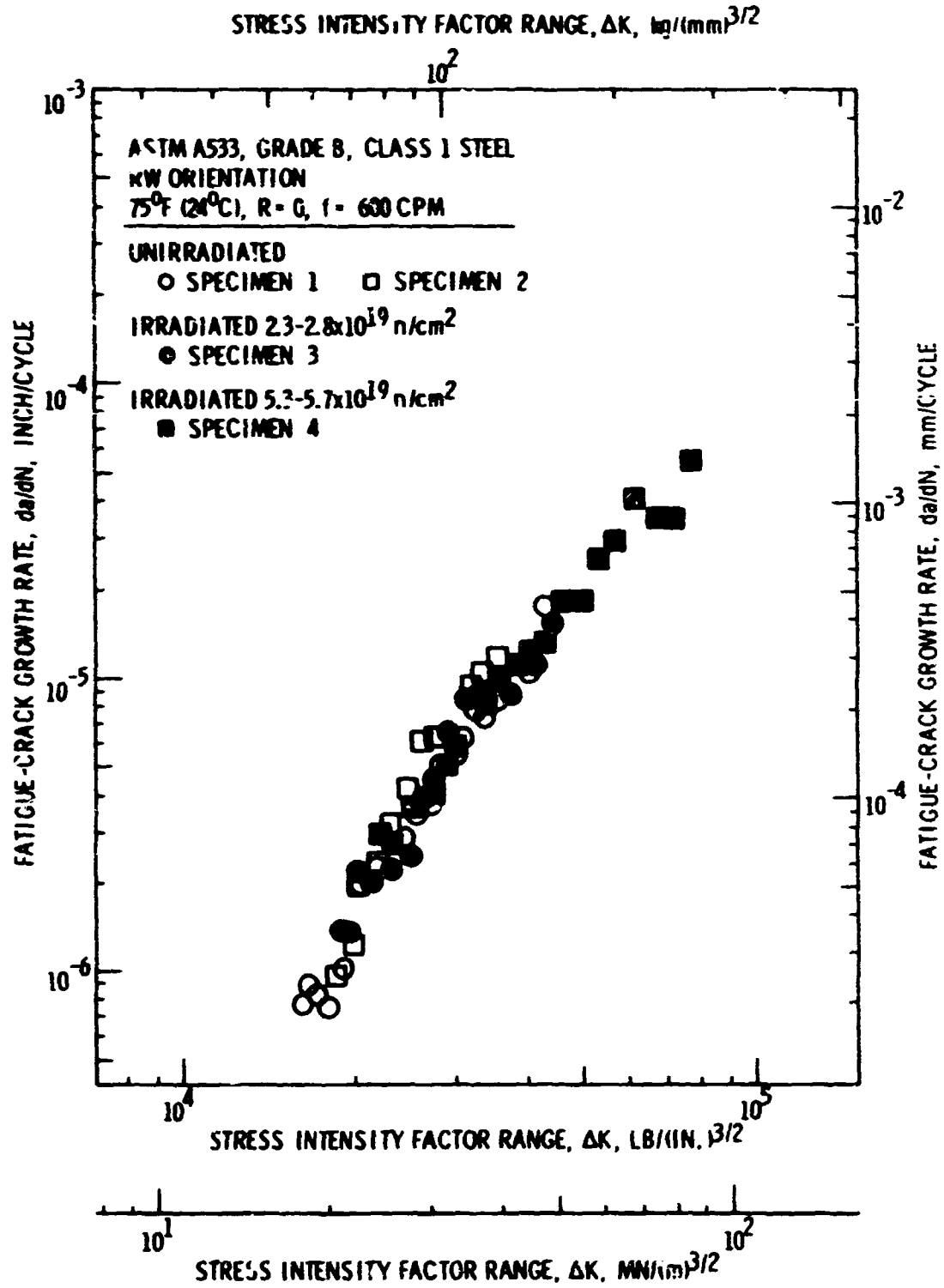

Fig. 3.1. Fatigue-crack propagation behavior of ASTM A533, grade B, class 1 steel at 75°F (24°C). Irradiation temperature: 550°F (288°C).

RW and WR specimens and suggest that the effect of moisture susceptibility between the two orientations is responsible for the difference. Behavioral differences due to crack orientation have been noted in the fatigue of ferritic steels at room temperature (e.g., Heiser and Hertzberg[11]), but such differences are not apparent in the results of Watson et al.[6] for unirradiated specimens at room temperature. Excellent agreement is obtained between the results of Watson et al.[6] and the present study for unirradiated and irradiated specimens in the KW orientation at room temperature.

The fatigue-crack growth rate, at 550°F, of the irradiated material appears to be slightly lower than that of the unirradiated material, as shown in Fig. 3.2. There appears to be no noticeable difference, however, between the results for 2.3 to 2.8 × 10^{19} and those for 5.3 to 5.7 × 10^{19} neutrons/cm^2. Watson et al.[6] found

11. F. A. Heiser and R. W. Hertzberg, "Anisotropy of Fatigue Crack Propagation," *J. Basic Eng.* 93(2), 211–17 (1971).

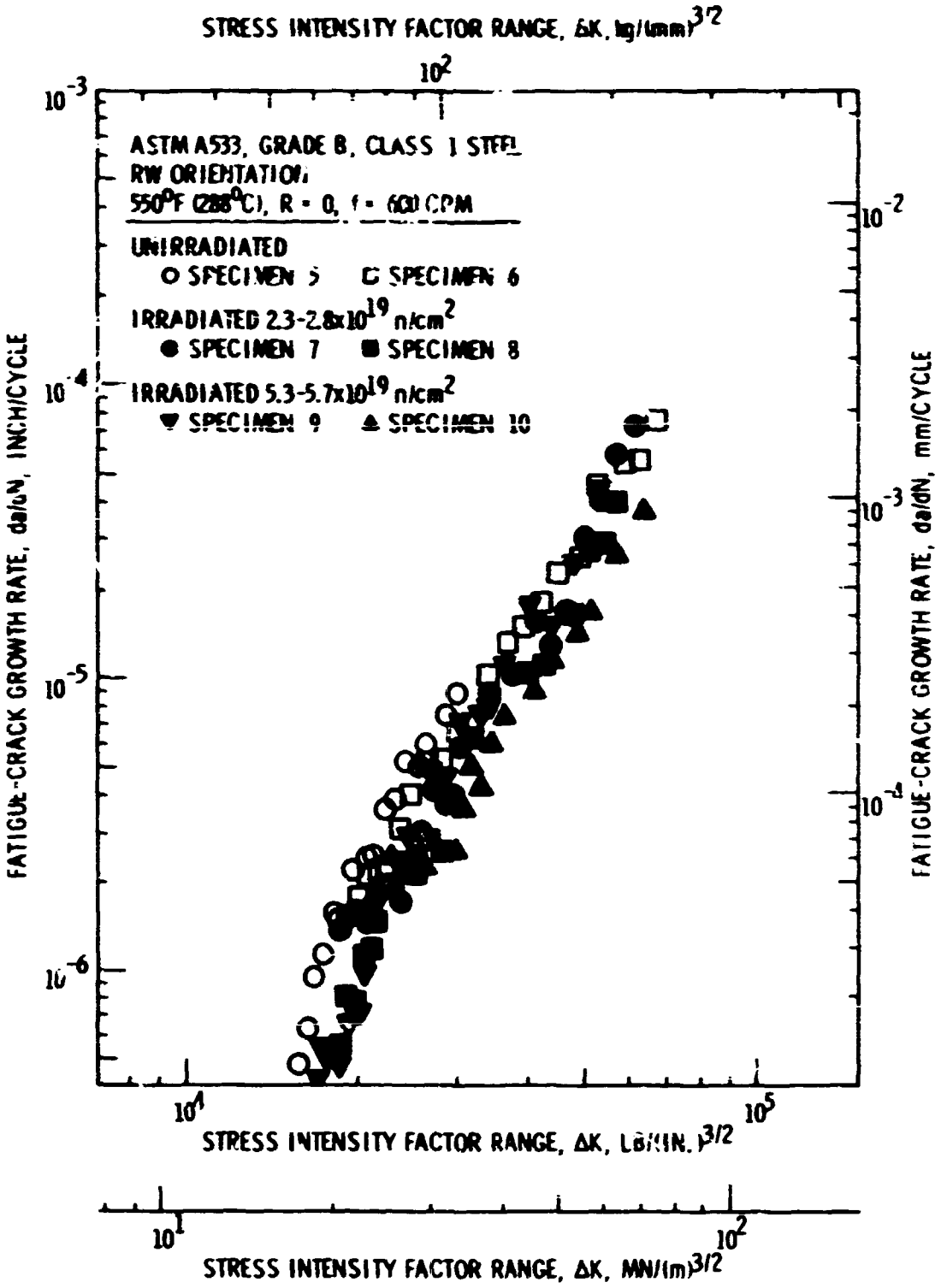

Fig. 3.2. Fatigue-crack propagation behavior of ASTM A533, grade B, class 1 steel at 550°F (288°C). Irradiation temperature: 550°F (288°C).

a slight increase in the cracking rate of the irradiated material relative to the unirradiated material at 550°F, but these tests were conducted at a lower frequency than those of the present study. Results of Watson et al. for unirradiated specimens and those of the present study are equivalent.

It should be pointed out that in the foregoing discussion, behavioral differences are generally slight. For example, all the unirradiated and irradiated material results of the present study could be fitted within a "scatter band" equivalent to those of other investigators[5-9] for unirradiated material tested under similar conditions. Hence for this study, at the conditions of frequency, stress ratio, temperature, and fluence investigated, neither temperature nor neutron irradiation appears to be a significant variable. However, at elevated temperatures, cyclic frequency can be an important variable. For example, Kondo et al.[10] (see also Chap. 2) have shown a significant increase in crack growth rate with decreasing frequency for A533, grade B cycled in water at 500°F (260°C), as shown in Fig. 3.3; that is, as the frequency is lowered from 100 to 0.1

cpm a pronounced increase in crack rate results The agreement demonstrated in Fig. 3.3 between the results of this study and those of Mager[9] for an equivalent cyclic frequency of 600 cpm shows that there is little or no environmental effect between water and air on the fatigue-crack propagation behavior. Frequency will be a variable of future investigation in evaluating fatigue-crack growth in irradiated A533, grade B steel.

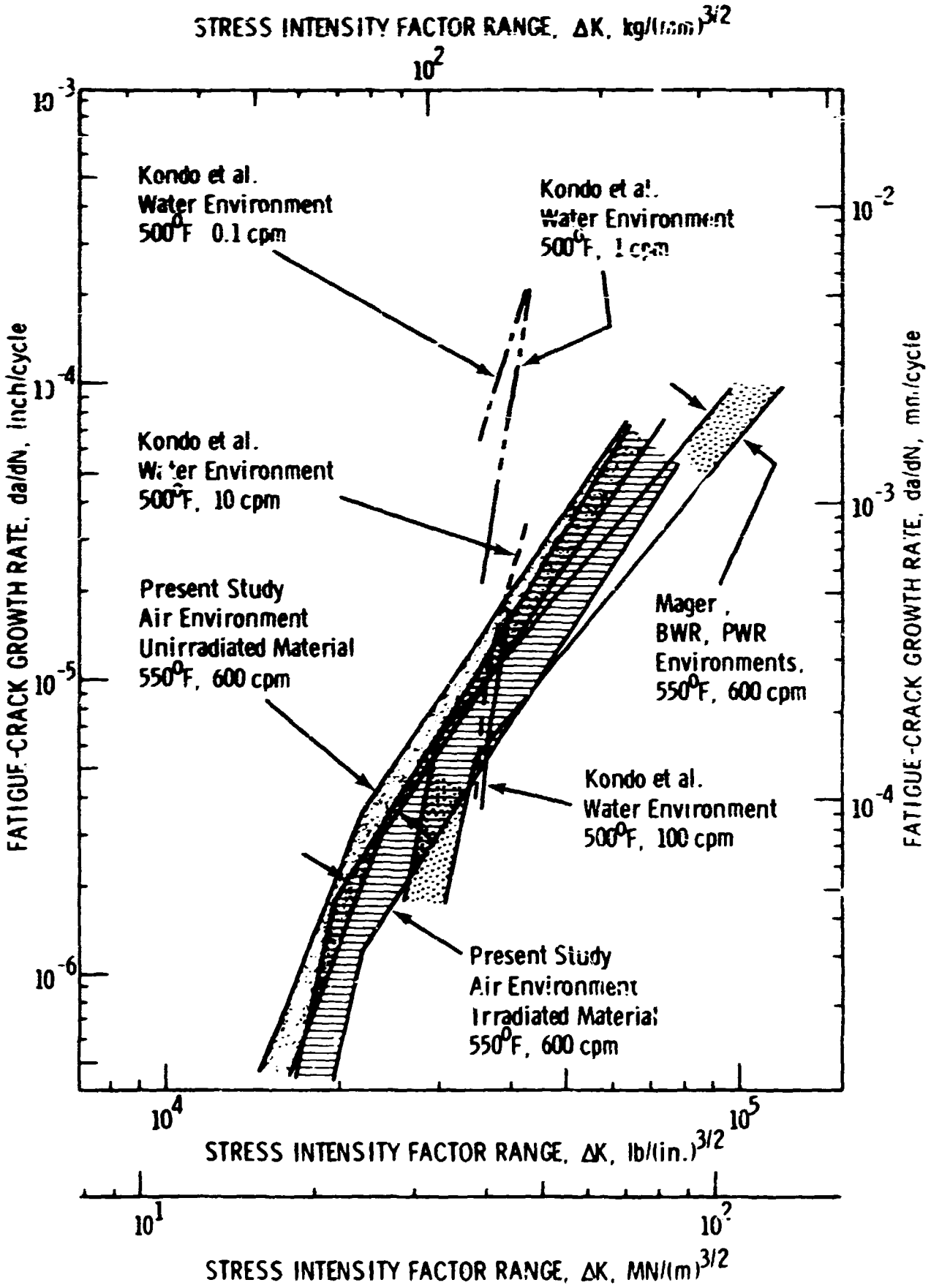

Fig. 3.3. Comparison of elevated-temperature fatigue results for ASTM A533, grade B, class 1 steel between the present study and those of Mager (Ref. 9) and Kondo et al. (Ref. 10).

Irradiation Effect on Toughness of A533, Grade B Submerged-Arc Weldment

The plane strain, K_{Ic}, and equivalent energy, K_{Icd},[12] fracture toughness properties of weldment material from the heat-affected-zone (HAZ) and fusion line (FL) locations were evaluated after irradiation. Witt[12] has described the method for calculation of K_{Icd} (K_{Ic1} for thickness d = 1 in.) used for evaluation of the toughness of fracture specimens which are invalid by K_{Ic} toughness criteria.[13] Witt and Mager[14] have proposed that K_{Icd} is an assessment of the lower bound of fracture toughness at all temperatures (for the valid K_{Ic} range $K_{Icd} = K_{Ic}$).

The testing procedures, crack preparation, and validity criteria of 1-in.-thick compact-tension (1T CT) specimens for K_{Ic} measurements[13] were applied in the 1T CT specimens for K_{Icd} (K_{Ic1}) evaluation. Specimen irradiations were conducted in the ETR and have been described in detail previously.[15] The fracture toughness results of HAZ material irradiated to 0.28 to 0.57 × 10^{19} neutrons/cm^2 ($E > 1$ MeV) and FL material irradiated to 1.8 to 2.7 × 10^{19} neutrons/cm^2 are given in Table 3.1 and Fig. 3.4; irradiation temperature was 540°F. Fracture properties of unirradiated weld center (WC) material[16] and 2.7 to 3.1 × 10^{19} neutrons/cm^2

12. F. J. Witt, "Equivalent Energy Procedures for Predicting Gross Plastic Fracture," paper presented at Fourth National Symposium on Fracture Mechanics, Carnegie-Mellon University, Aug. 24–26, 1970.

13. ASTM Standard E399-70T, Tentative Method of Test for Plane-Strain Fracture of Metallic Materials, ASTM Standards, Part 31, 1970.

14. F. J. Witt and T. R. Mager, *A Procedure for Determining Bounding Values on Fracture Toughness K_{Ic} at Any Temperature*, ORNL-TM-3894 (October 1972).

15. C. W. Hunter and J. A. Williams, "Fracture and Tensile Behavior of Neutron-Irradiated A 533-B Pressure Vessel Steel," *Nucl. Eng. Des.* 17(1), 131–48 (August 1971).

16. C. W. Hunter and J. A. Williams, "Irradiation Effects on the Fracture of Heavy Section Pressure Vessel Steels," *HSST Program Semiannu. Prog. Rep. Feb. 28, 1971*, ORNL-4681.

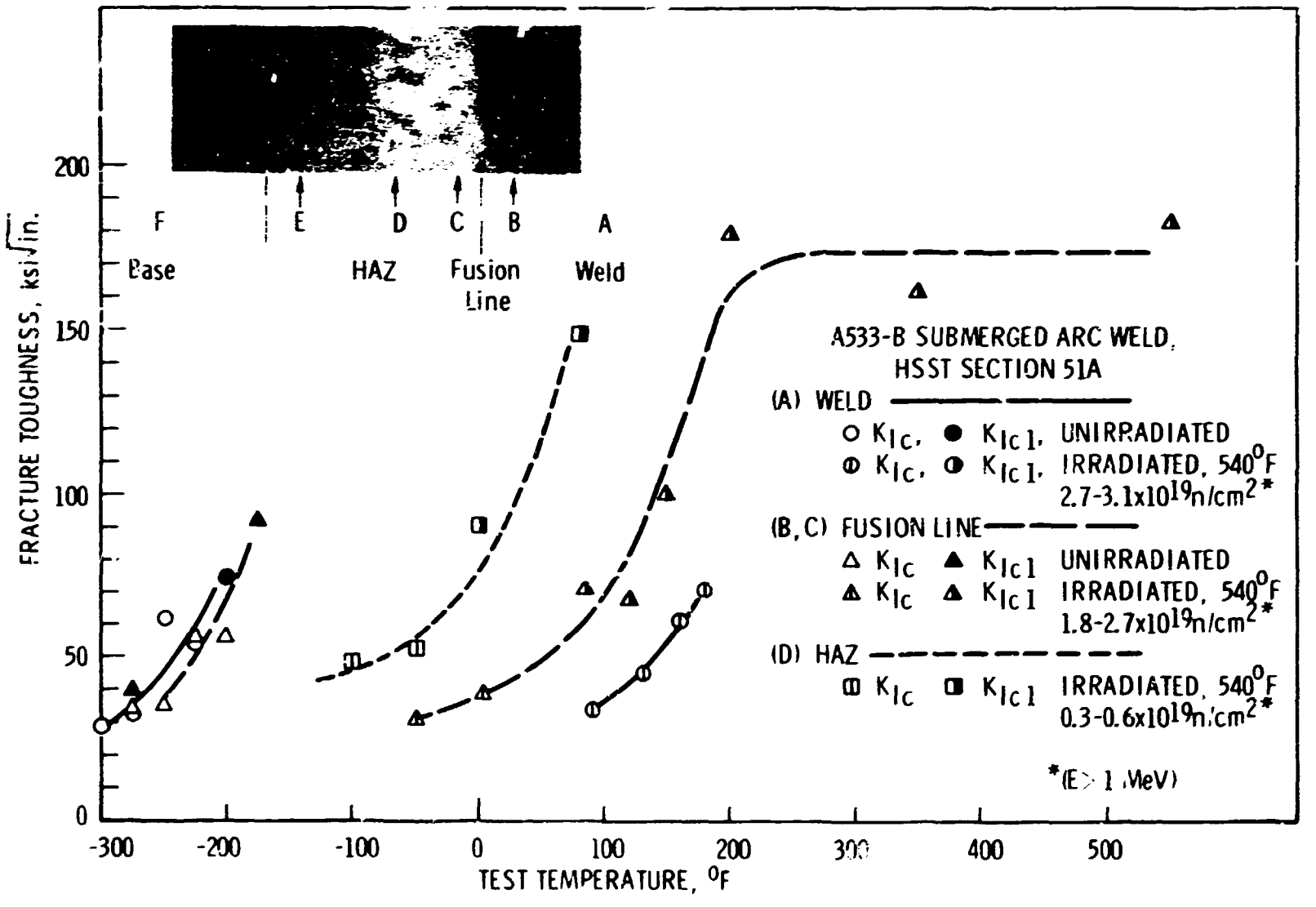

Fig. 3.4. Fracture toughness of unirradiated and irradiated ASTM A533, grade B, submerged-arc weldment materials from HSST weldment section 51A. Inset shows typical section at weld base metal interface and area of material location.

Table 3.1. Fracture toughness of irradiated ASTM A533, grade B, class 1 steel submerged-arc weld section 51A and HSST plate 02

Specimen identification	Test temp. (°F)	Fluence [neutrons/cm^2 ($E > 1$ MeV)]	Plate position (in.)	Location[a]	Yield strength[b] (psi)	Crack length, a (in.)	$K_{fatigue}$ (ksi$\sqrt{in.}$)	K_Q (ksi$\sqrt{in.}$)	K_{Ic} (ksi$\sqrt{in.}$)	K_{Ici} (ksi$\sqrt{in.}$)	$2.5\left(\frac{K_Q}{\sigma_{ys}}\right)^b$
		$\times 10^{19}$			$\times 10^3$						
51A5047	-100	0.28	6.4	D	100	1.046	11.5	48.5	48.5		0.59
51A5049	-50	0.36	6.4	D	95	1.008	10.2	53.0	53.0		0.77
51A5050	0	0.47	6.4	D	91	1.016[c]	10.4	90.8		90.8[d]	2.48
51A5052	80	0.57	6.4	D	86	1.037	10.8	90.0[e]		148.6	
51A5020	-40	1.98	11.4	B*	104	1.000	10.3	31.5	31.5		0.23
51A5042	3	2.7	7.6	C*	101	1.009	10.3	39.2	39.2		0.38
51A5017	85	1.82	11.4	B	97	1.029	10.6	71.9		71.9[d]	1.56
51A5037	121	2.3	7.6	C*	95	1.012	10.4	69.7		69.7[d]	1.35
51A5043	150	2.65	7.6	C*	93	0.980	9.9	100.6		100.6[d]	2.93
51A5019	200	1.96	11.4	B	91	0.99	10.2	108.3[e]		180.7	
51A5039	350	2.55	7.6	C	87	0.957[c]	15.9	101.3[e]		162.7	
51A5018	550	1.95	11.4	B	86	1.075	11.4	98.7[e]		183.8	
02GA11	250	2.0	6.0	RW-02[f]	97	1.034	10.5	90.5[e]		189.8	
02GA12	550	2.0	6.0	RW-02	97	1.072	11.4	93.5[e]		193.5	

[a]Fusion line specimens: B is area of weld dilution; C is area of γ grain growth; * surface of fractured specimen showed intersection of fusion line. HAZ specimen: D is approximate center of this zone. Crack planes oriented parallel to weld direction and weld plane.

[b]Yield strengths interpolated from yield strength of irradiated weld metal (ref. 17).

[c]Crack shape invalid – surface trace <90% average crack length.

[d]K_u listed instead of K_{Ici} because $P_u = P_5$, therefore $K_u \approx K_{Ici}$; invalid by $B \leq 2.5(K_Q/\sigma_{ys})^2$.

[e]$P_u > 1.1P_5$.

[f]HSST plate section 02GA, RW orientation.

($E > 1$ MeV) irradiated WC material[17] and unirradiated FL material[16] previously reported are also shown in Fig. 3.4.

The results to date primarily demonstrate the irradiation effect on a given weldment material at a given irradiation condition over a range of test temperatures. In all cases, WC, HAZ, and FL materials exhibit strong transitional behavior. Relative irradiation sensitivity between material and irradiation conditions cannot be directly assessed, but the results presented in Fig. 3.4 suggest that similar transitional irradiation sensitivity (shift in transition temperature) might be expected from all material conditions.

The results of FL material at temperatures above 200°F are of special interest, since a high toughness, K_{Ic1} of about 175 ksi$\sqrt{\text{in.}}$, is obtained after irradiation to approximately 2×10^{19} neutrons/cm^2 ($E > 1$ MeV). Weld center material might be expected to exhibit equally as tough high-temperature lower-bound behavior after irradiation as does FL material. The tested 1T CT fusion line specimens are to be remachined to Charpy-thickness compact-tension (C_v CT) specimens; direct comparison of weld metal and fusion line material irradiation sensitivity, both transitional and lower-bound high-temperature toughness, can then be made.

High-temperature lower-bound toughness of irradiated A533, grade B steel

Fracture specimens from ASTM A533, grade B, class 1 steel, HSST plate 02, irradiated to approximately 2×10^{19} neutrons/cm^2 ($E > 1$ MeV) at 540°F were tested at 250 and 550°F. The 1T CT specimens exhibited fully plastic behavior during testing. The test results were interpreted for lower-bound equivalent-energy fracture toughness, K_{Ic1}, shown in Fig. 3.5 with data of 2 and 8 $\times 10^{19}$ neutrons/cm^2 previously reported[15,16] and the unirradiated plane strain fracture toughness curve of Shabbits et al.[18] A high K_{Ic1} toughness value, approximately 190 ksi $\sqrt{\text{in.}}$, is obtained at temperatures above

17. J. A. Williams, "Irradiation Effects on Fracture of Heavy Section Pressure Vessel Steels," *HSST Program Semiannu. Prog. Rep. Aug. 31, 1971*, ORNL-4764.

18. W. C. Shabbits, W. H. Pryle, and E. T. Wessel, *Heavy Section Fracture Toughness of A 533 Grade B Class 1 Steel Plate and Submerged Arc Weldment*, WCAP-7414 (December 1969).

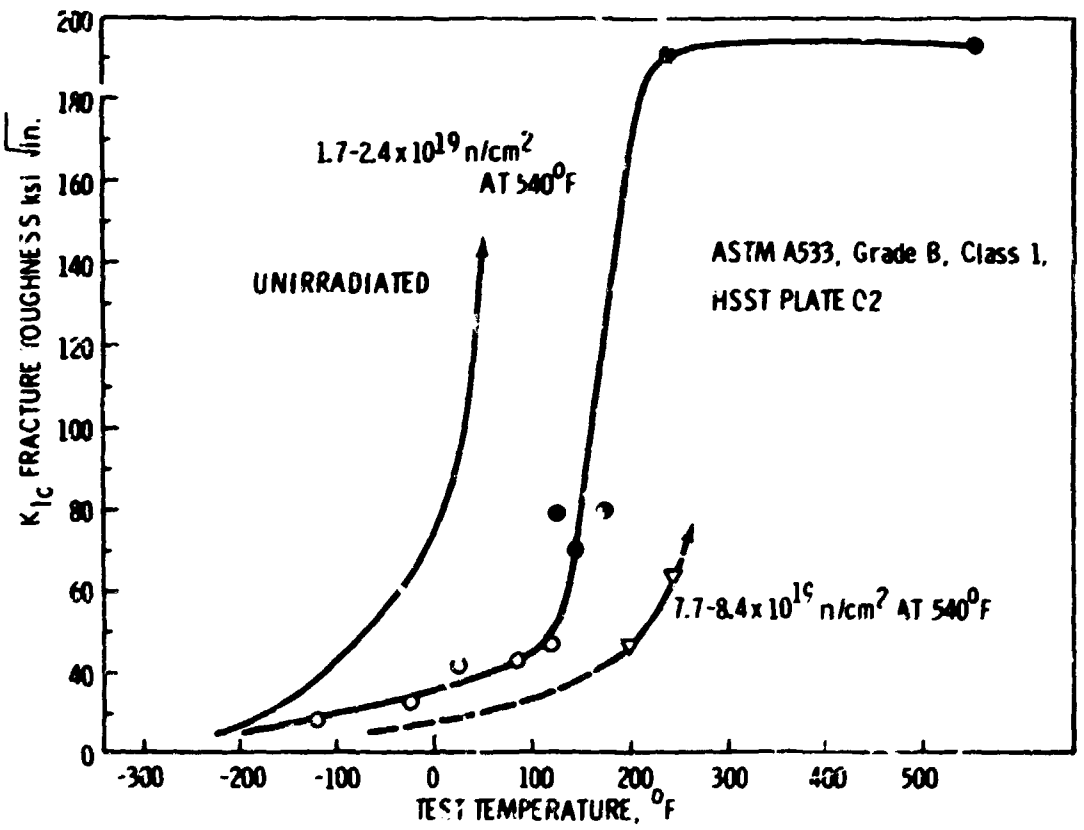

Fig. 3.5. Fracture toughness as a function of temperature for irradiated and unirradiated ASTM A533, grade B, class 1 steel from HSST plate 02. Closed points on the curves are K_{Ic1} values.

250°F. A high-temperature lower-bound fracture toughness for Charpy thickness compact-tension specimens, $K_{Ic}C_v$, was reported previously;[19] there the toughness above 250°F for both the longitudinal and transverse irradiated specimens irradiated to 2×10^{19} neutrons/cm^2 ($E > 1$ MeV) was approximately 150 ksi $\sqrt{\text{in.}}$ The difference in lower-bound toughness with size is consistent with the application of the method.[14]

FRACTURE TOUGHNESS CHARACTERIZATION OF IRRADIATED A533, GRADE B, CLASS 1 STEEL USING 4T COMPACT-TENSION SPECIMENS[20]

S. A. Legge T. R. Mager
P. C. Riccardella

Westinghouse Electric Corporation

Introduction

The objective of this program is to provide irradiated fracture toughness data at test temperatures in the upper transition range. In order to achieve valid test results at these temperatures according to ASTM recommended test procedure E-399, one must use thick-section specimens. ASTM E-399 requires that the specimen thickness B and the crack length a be equal to or greater than $2.5(K_Q/\sigma_{YS})^2$, where K_Q is the fracture toughness measured in the test and σ_{YS} is the yield strength of the material at the test temperature. Thus it is desirable to irradiate specimens as large as possible to obtain data on irradiated, high-temperature fracture toughness.

Unfortunately, there is an inherent difficulty associated with irradiating thick sections, mainly that of obtaining uniform irradiation conditions through the thickness. Neutron flux attenuates in the steel such that the midthickness sees less than 50% of the surface fluence for a 4-in.-thick specimen. This is about the maximum size with which one can obtain a reasonably uniform distribution of fluence. Periodic rotation of the section will result in equal fluences on the faces and therefore a symmetrical distribution through the thickness.

A second problem arises due to internal heat generation caused by gamma absorption and subsequently induced temperature gradients. The temperature peaks about 1 in. in from the front face and drops off slightly at the front face and more considerably at the back face, as shown in Fig. 3.6. Because fluence and irradiation temperature have a synergistic relationship, a given amount of fluence will produce significantly greater material damage at lower irradiation temperatures (<510°F). Hence it is necessary to reduce the temperature gradient as well as maintain the correct peak temperature.

Efforts on the program to date have included the fabrication of six 4T compact-tension specimens and associated smaller specimens and the design and construction of an encapsulation arrangement which will provide the required amount of fluence in a reasonably

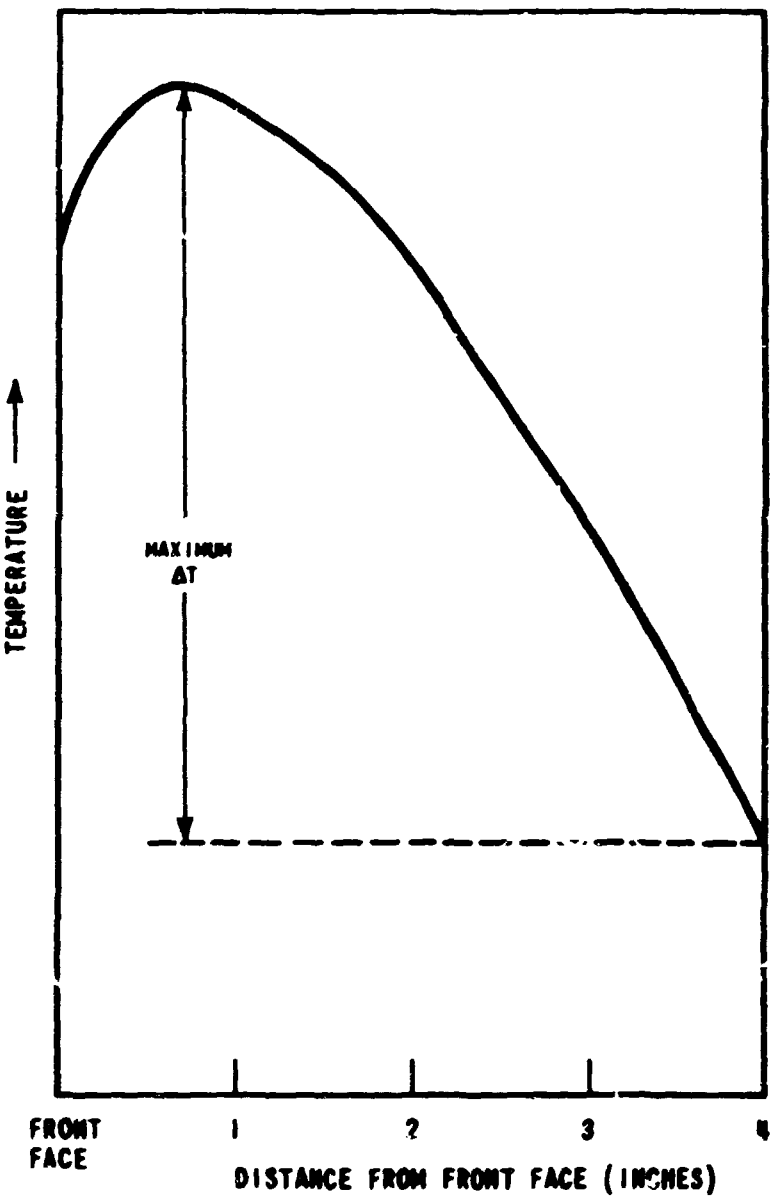

Fig. 3.6. Temperature distribution in 4-in. plate resulting from attenuation and absorption of gamma radiation.

---

19. F. J. Witt and J. A. Williams, "Lower Bound Toughness of Irradiated A 533 Grade B, Class 1 Steel," *HSST Program Semiannu. Progr. Rep. Feb. 28, 1972*, ORNL-4816.

20. Work sponsored by HSST Program under UCCND Subcontract No. 3720 between Union Carbide Corporation and Westinghouse Electric Corporation. Portions of this program being performed at the Battelle Columbus Laboratories are under the technical direction of Neil E. Miller.

short time period (about one year). The encapsulation has been designed to provide irradiation temperature distributions in the test specimens which are uniform enough to provide meaningful test results. The irradiation will be performed in the Battelle Research Reactor (BRR).

Capsule Design Considerations

The specimens must be encapsulated to provide control of their internal temperature distribution. The specimens will be continuously generating heat internally during the irradiation as a result of gamma-ray absorption in the metal lattice. Irradiation of the specimen should take place in the 510 to 590°F temperature range to simulate PWR vessel environment.

Two methods have been employed to establish and regulate the temperature in the specimens to the required levels in the presence of the gamma radiation field. First, gas-filled gaps constituting thermal resistances have been provided at the front and back faces of the specimens (see Fig. 3.7). Heat generated internally is thus retained inside the specimen, raising the total temperature distribution up to the region of interest. Auxiliary electrical heaters located at the faces of the specimens have been employed as the other means of temperature control.

The effect of gamma attenuation through the metal produces a skewed temperature distribution, as was shown in Fig. 3.6. The back face minimum falls substantially below the front face minimum. By selective use of the electrical heaters, it is possible to raise the minimum specimen temperature at the back face at the expense of raising the total temperature distribution somewhat. Thus the maximum temperature gradient through the thickness can be reduced.

Large gas gaps were designed for the top, bottom, and sides of the capsule to impede heat flux in two directions while promoting one-dimensional heat flow through the thickness. The front and back face gap widths were determined by calculating the gap conductance required to place temperatures in the specimen near the acceptable range. Assuming the gap is filled with helium (a high-conductivity gas), the spacing was determined to range from 0.030 in. at the core midplane to 0.041 in. at the top of the capsule or 0.045 in. at the bottom. The gap profile so calculated negates the effect of the cosine-shaped gamma distribution in the axial direction.

A gas mixing system has been incorporated as an integral part of the encapsulation scheme. By mixing nitrogen (one-sixth the conductivity of helium) with the helium, a means exists for altering the total gap conductance and hence controlling the temperature distribution in the specimen.

It should be pointed out that by sizing gaps to a pure helium gas condition, the control flexibility lies entirely in favor of raising capsule temperatures. There are two reasons for doing this: first, if heaters fail in the course of the experiment, total heat input will drop and the difference will have to be counteracted by lower gap conductance; and second, the design calculations were made based on full-power operation. If at any time during the experiment it becomes necessary or desirable to run at reduced power, the gamma heat input will be reduced, and again gap conductance must be reduced to maintain the appropriate temperature levels.

Auxiliary Heat Input

The maximum temperature gradient in the specimen (peak to back face minimum) is primarily a function of the spatial distribution of the heat generation, regardless of the boundary conditions. Alteration of the thermal resistance at the surfaces will raise or lower all temperatures more or less uniformly. By introducing another source of heat at the back face in the form of electrical heaters, it is possible to decrease the gradients resulting from the skewed distribution of gamma heating.

The importance of this function, combined with the requirement of long-term operation, dictates a design emphasis on reliability. The heater is constructed with bayonet-type heating elements embedded in a $\frac{3}{8}$-in.-thick 2024-T4 aluminum plate. The elements are arranged in three zones of three elements each as shown in Fig. 3.8. The partial contribution from each of the zones to the total auxiliary power output can be manipulated to satisfy operating conditions. The heater design calls for an input of 3 kW(t) at the back face. Each of the nine heating elements is rated at 1 kW and is warranted by the supplier to withstand long time exposures in nuclear environments. Two of the three elements in each zone will be operated at approximately one-half of rated power, while the third element is held in reserve. Each heater will be required to operate from 4000 to 5000 hr.

Forced Convective Cooling

Battelle's calculations of the heat flux emerging from the front and back faces of the capsule indicate that boiling of the pool water could occur at full power. One design requirement for the capsule is that boiling must

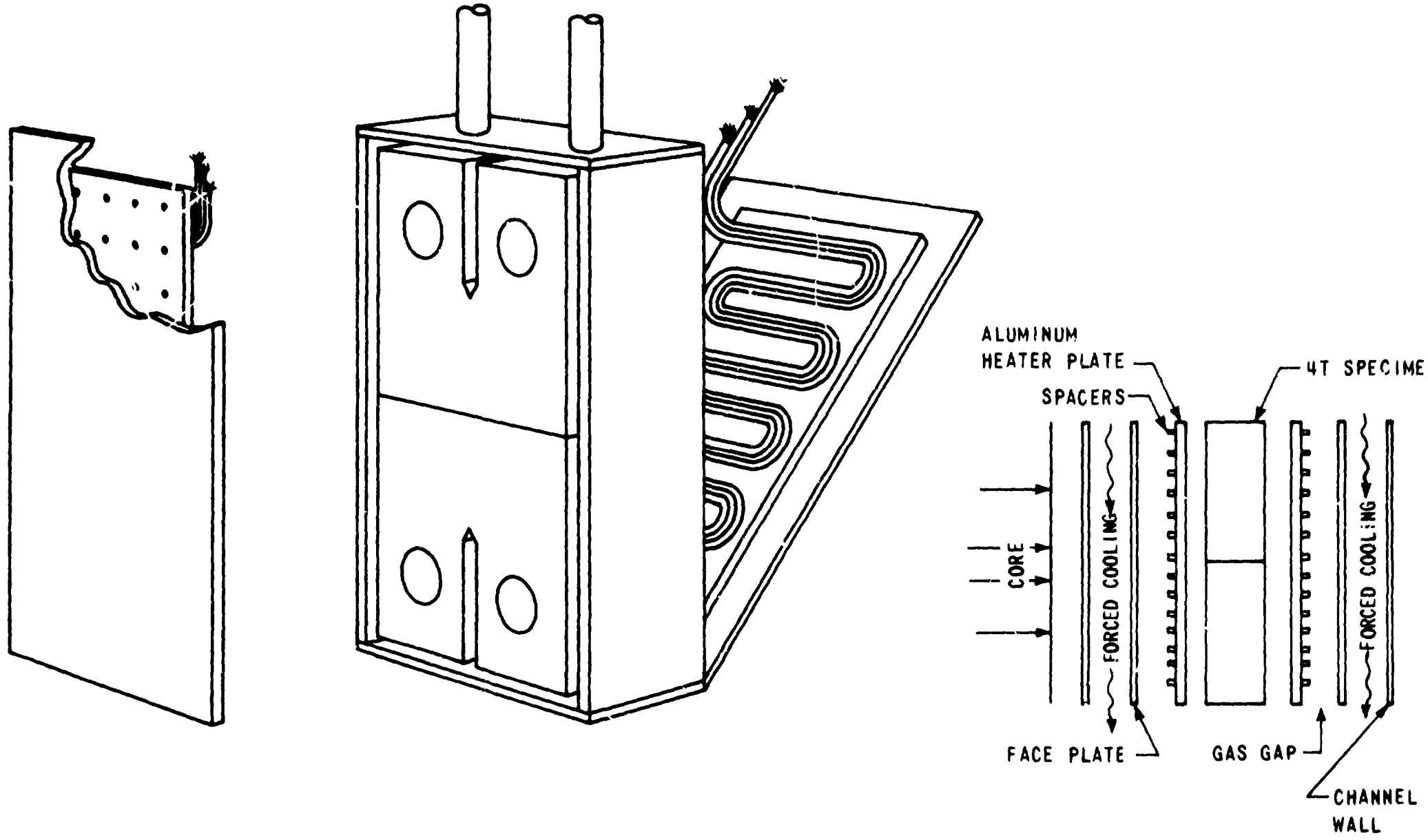

Fig. 3.7. 4T specimen capsule geometry.

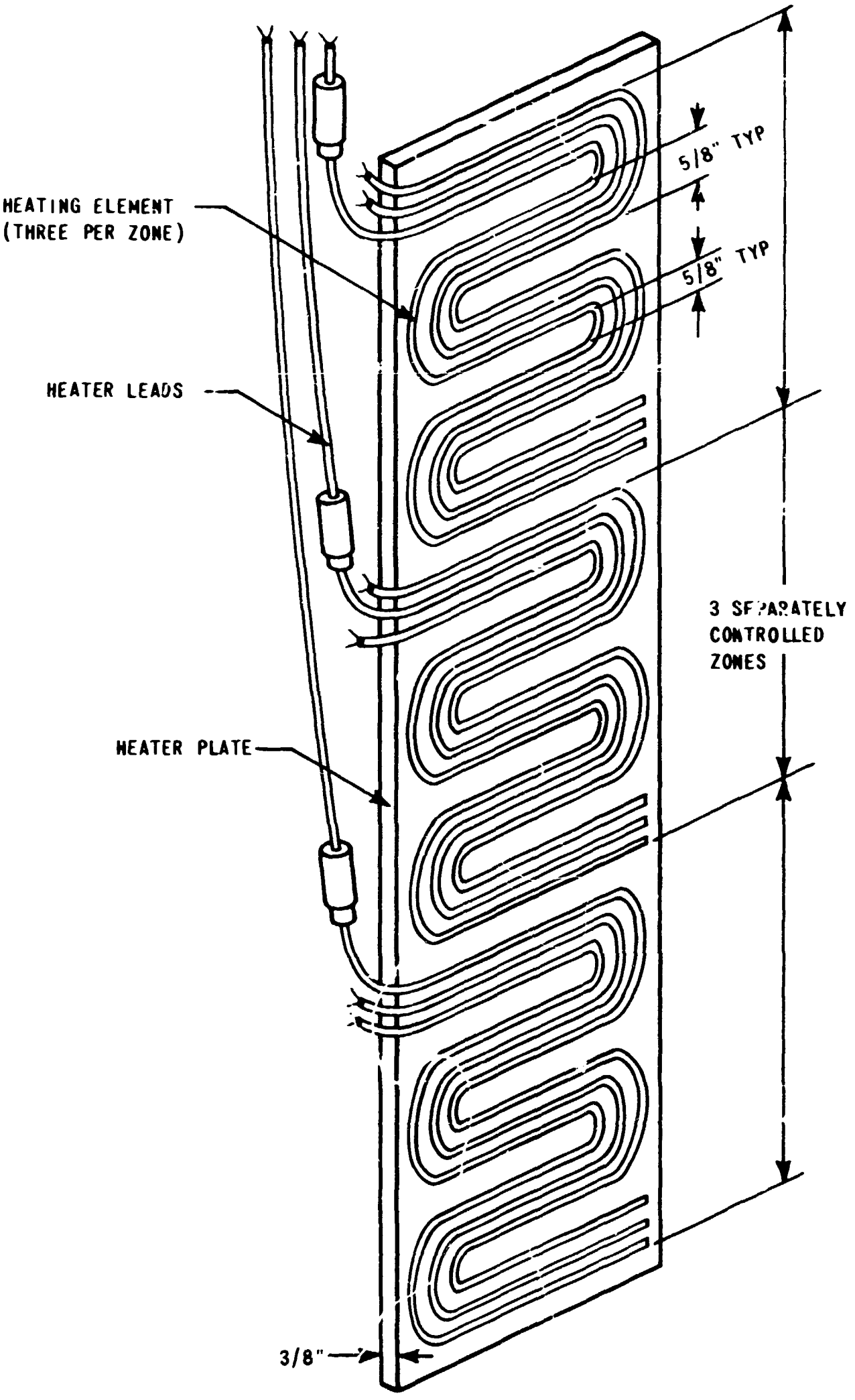

Fig. 3.8. Electrical heater design.

not occur near the reactor core, due to stipulations in the BRR operating license. In order to prevent boiling, a high heat transfer rate from the capsule to the surrounding water must be guaranteed. Calculations by Battelle and Westinghouse have confirmed that neither natural convective cooling nor forced cooling with laminar flow will yield heat transfer coefficients high enough to guarantee that boiling will not occur at the faces normal to the core. At steady-state full power the pool temperature could be as high as 120°F. A temperature drop across the film of 100°F may produce boiling.

The problem has been solved by constructing a channel for forced cooling at the front and back faces having a cross section of $\frac{1}{8}$ by 13 in. (see Fig. 3.7). At flow rates of 6 gpm the flow in the channel becomes turbulent, heat transfer is high, and the film temperature drop falls to the order of 10 to 20°F. The remaining four surfaces are cooled sufficiently by natural convective processes, since heat flux normal to these surfaces is substantially lower.

Capsule Construction

The capsule side, top, and bottom walls are structurally supporting and are fabricated of $\frac{1}{2}$-in.-thick plates of 6061-T6 aluminum alloy. The two face plates are made of the same material but only $\frac{1}{8}$ in. thick. Stainless steel pins are positioned between the face plate and the heater assembly in order to maintain the appropriate gap spacing. The flexibility of the face plates enables the water pressure of the pool to cause the plates to conform to the spacer profile. The four walls constituting the frame are first welded together, and then the face plates are last to be welded to the structure.

Upon completion of the assembly, the capsule integrity will be tested by means of a helium leak test. A net pressure difference of 1 atm (14.7 psia) will be imposed during the test. Experimental conditions will call for an external pressure 3 to 10 psi over internal pressure.

Analytical Verification of Design

Thermal analysis of the proposed capsule design has been carried out by the Battelle Columbus Laboratories and verified by Westinghouse. A parametric study was completed prior to final design acceptance in order to determine the appropriate encapsulation geometry and dimensions. It was further deemed useful to evaluate the sensitivity of the specimen temperature distribution to the various design parameters. Those considered most critical were:

1. Gap conductance
   (a) Width
   (b) He-N composition
2. Auxiliary heat input
3. Radiative heat loss
4. Fluctuation in internal heat generation (directly related to reactor power)
5. Losses through gap spacers
6. Contact resistance through the specimen-heater interface

The results have demonstrated that the contact resistance at the specimen-heater interface and the radiative heat losses at the sides of the specimen affect temperatures by 2 to 3%. The gap widths were established at 0.030 to 0.045 in., as described previously, based on the initial condition of a pure helium gas in the gap.

The percentage of heat conducted through the spacers rather than across the gap has been a matter of some concern. At substantial percentages, one begins to lose the temperature control effectiveness promised by the use of variable gas mixtures. The final spacer configuration chosen was a 1.414-in. square grid of $\frac{1}{8}$-in.-diam stainless steel pins. The pins were interference fitted to holes in the heater plate with the ends contacting the face plate turned down to 0.057 in. The thermal analysis indicates that this configuration will conduct approximately 5% of the total heat crossing the gap. That figure is sufficiently low to maintain the effectiveness of the gas mixture mechanism for controlling heat flow.

Optimal heater power was determined to be 3 kW(t). Effects of this parameter on the temperature distribution are as described in the section on "Auxiliary Heat Input."

Temperature Measurement

Specimen temperatures will be monitored throughout the irradiation by 16 thermocouples placed inside each capsule at the positions shown in Fig. 3.9. The six thermocouples positioned at the bottom of the machined slots will provide the data needed to establish the through-thickness (4-in. dimension) gradient and also the axial temperature distribution. The latter interpolation defines the temperatures in the crack propagation regions for the two specimens. Four of the six measurements would be sufficient to characterize

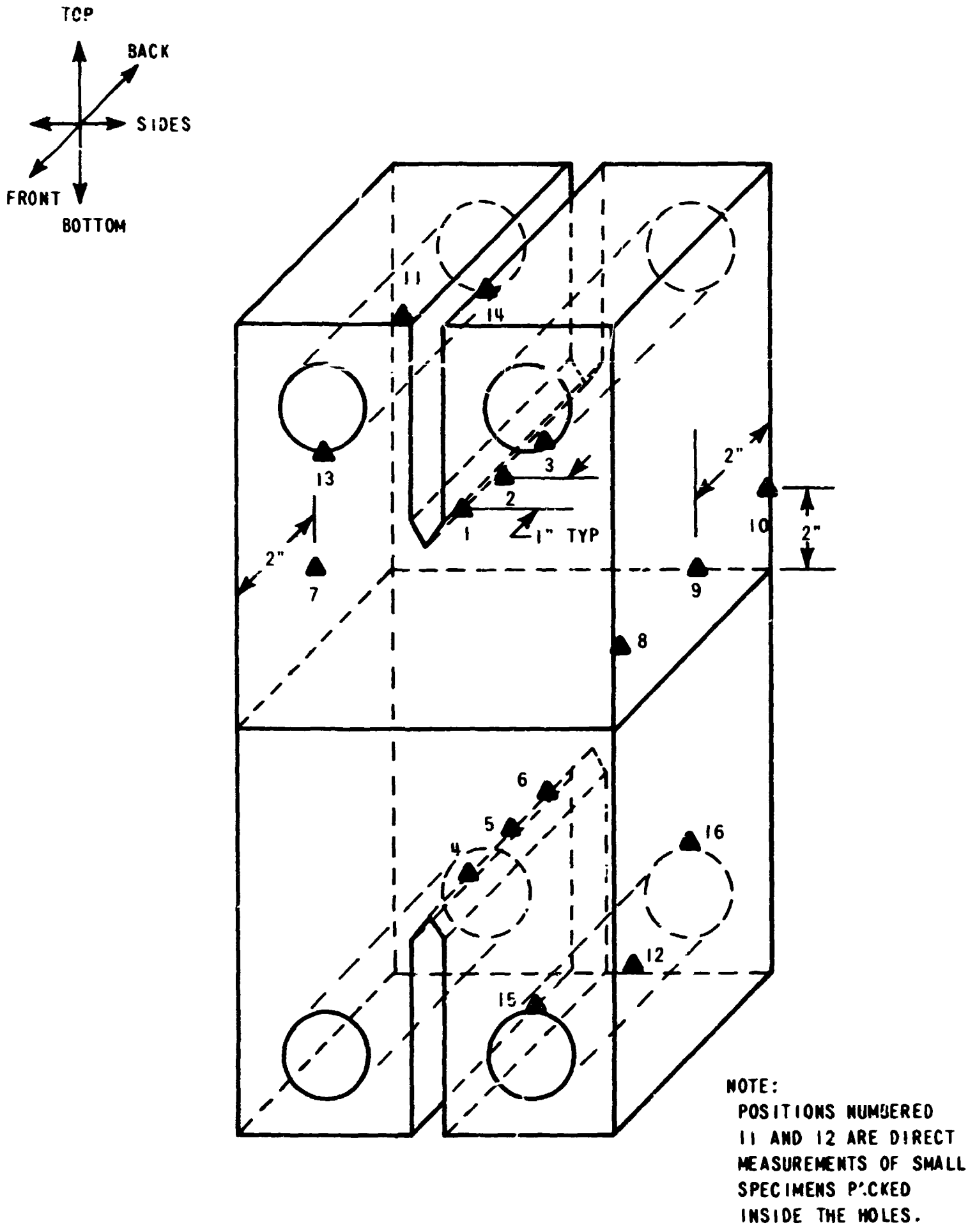

Fig. 3.9. Thermocouple positions inside capsule.

these temperature distributions, but again, as in the case of the heaters, failures are being anticipated in the temperature measurement scheme, and redundancy has been incorporated wherever possible.

Eight more thermocouples are located on the periphery of the specimens and near the holes. With these temperature measurements it will be possible to describe the resultant temperature distributions in the large specimens very accurately by comparing the thermocouple readouts with the computer-generated temperature maps prepared before the experiment. Some of the temperature measurements will be used as feedback in the automatic temperature control circuitry.

In addition to the thermocouples placed on the large specimens, two thermocouples are provided to make temperature measurements in two of the four holes. The prime objective here is to monitor a potential overheating condition among the many small specimens to be packed in the 4T holes. Hot spots may arise locally due to the summed contact resistance occurring for all the interfaces encountered normal to the hole axis (4-in. dimension).

Target Fluence

The program goal is to irradiate the 4T compact-tension specimens as uniformly as possible to a fluence of 5×10^{19} neutrons/cm^2 ($E > 1$ MeV) at a nominal temperature of 550°F. These conditions will most accurately simulate the type of damage incurred in a reactor pressure vessel wall at the end of plant life. The target fluence will be applied to the midthickness of the specimen rather than at the front face.

Four inches of steel attenuate neutron flux very rapidly. Therefore, the capsule will be rotated 180° at the completion of each reactor operational cycle (21 days) to build up a fluence symmetrical about the midthickness.

Measurement of BRR Neutron Environment

Battelle Memorial Institute has conducted detailed studies of the BRR core to characterize the spatial and energy distribution of the neutron flux at the 4T compact-tension specimen irradiation positions. A capsule mockup was constructed consisting of two steel plates, each 2 in. thick, 10 in. wide, and 20 in. high, sandwiched between two aluminum plates. The dimensions of the assembly combined with appropriate positioning relative to the core resulted in thicknesses of water, aluminum, and steel nearly identical to those of the actual irradiation capsule.

Dosimetry experiments were conducted at the north, east, and south faces of the core at the positions where the irradiation capsules will be placed (see Fig. 3.10). At all three faces of the core, the dosimetry included (1) nickel wires wrapped vertically around the outside of the assembly at approximately 2-in. intervals, (2) nickel wire placed vertically on the center line between the two 2-in.-thick steel slabs, (3) iron wires also located at the center line of the capsule, and (4) a self-powered thermal-neutron detector placed on the outside of the aluminum plate facing the core. The self-powered neutron detector was used to monitor the total neutron exposure in the irradiation capsule. The wires provided a description of the spatial distribution of the fast-neutron flux throughout the capsule. At the north face of the core two additional packages of ten dosimeters each were placed at the center of the 10- by 20-in. faces between the aluminum and steel to provide a description of the energy spectrum of the neutron flux at the outside surfaces of the steel slab.

The experiments were conducted with the capsule mockup centered on the core midplane. Short-term irradiation of the assembly was at a core power level of 80 kW(t) for a duration of 5 min. Only preliminary results of the flux measurements are available at this time, but fast flux appears to be attenuated by a factor of 8.7 through the steel specimens. Measured values of the flux at the reactor midplane indicate that the desired target fluence of 5×10^{19} neutrons/cm^2 ($E > 1$ MeV) at the midthickness can be achieved by irradiating for 15 full-power reactor cycles. In the regions of the crack tips the reactor power will be somewhat lower (~10%), and therefore approximately 17 operational cycles, or one calendar year, will be required to meet the target fluence.

Measurement of Fluence in the Capsules

Dosimetry must be placed inside the specimen irradiation capsule so that the total amount of fluence and its spatial distribution may be ascertained in the postirradiation analysis. Two types of dosimeters are to be employed.

The first type of dosimetry monitor, gradient wires, will be inserted in the specimen capsules in the six locations shown in Fig. 3.11. Each wire will be 3¾ in. long and will be oriented through the thickness. Sectioning these wires after the irradiation will produce a number of samples which will yield a range of counts

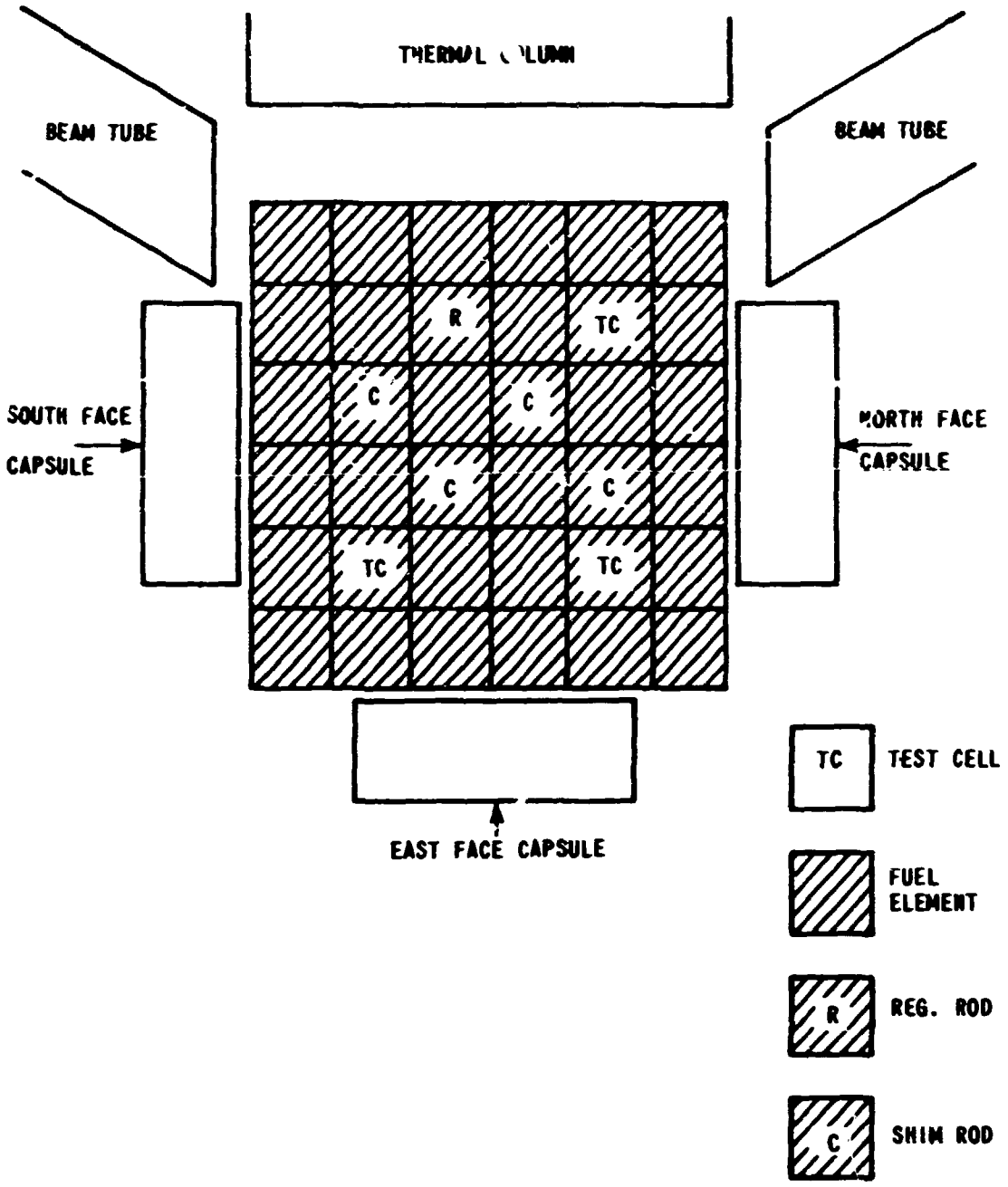

Fig. 3.10. BRR core configuration for 4T irradiations.

through the specimen thickness. It is planned to count five segments for each wire. Iron and nickel wires will be used in each of the six designated measuring points to monitor fast-neutron fluence. Also, unshielded Al–0.15% Co wires will be used at the bottom of the notch in each capsule (positions 2 and 5) to give some measure of the thermal-neutron fluence.

The second type of monitor, ^{238}U, will be placed in each capsule in positions 1 and 4. It will consist of depleted ^{238}U powder encapsulated in a small brass vial, shielded by $\frac{1}{8}$ in. of cadmium oxide powder. These monitors will provide point measurements of fluence only and are incorporated as supporting data to the gradient wire activity measurements.

The internal dosimetry, described in Table 3.2, has been procured, prepared, and incorporated in the irradiation specimens at this time.

Additional dosimetry will be placed external to the capsule to continuously monitor the accumulation of dose. This will take two forms: removable dosimeters and self-powered neutron detectors (SPND). The latter will remain in position at all times and produce an electrical output which can be monitored continuously above the pool. All external dosimetry will be located adjacent to the face closest to the neutron source. Although the SPND registers only those neutrons in the thermal energy range, this is simply convertible to a measure of fast flux by applying a fixed fast/thermal

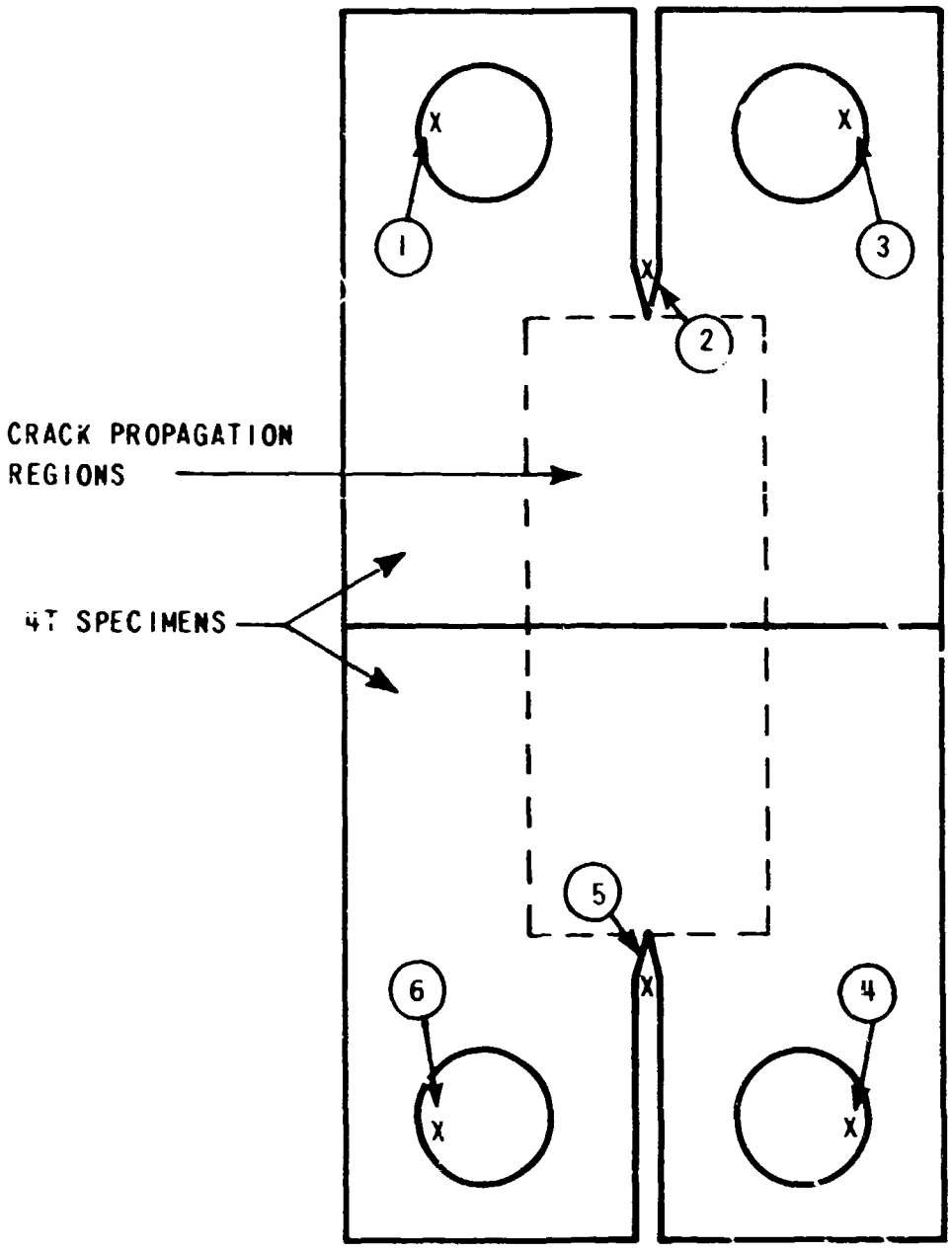

POSITIONS 1. 4:

Ni^{58} WIRE
Fe^{54} WIRE
U^{238} (SHIELDED)

POSITIONS 2. 5:

Ni^{58} WIRE
Fe^{54} WIRE
Co^{59} (UNSHIELDED) WIRE

POSITIONS 3. 6:

Ni^{58} WIRE
Fe^{54} WIRE

Fig. 3.11. Capsule internal dosimetry.

Table 3.2. Capsule internal dosimetry

Material + reaction	Half-life	Threshold energy (MeV)	Form	Number per capsule
$^{59}Co(n,\gamma)^{60}Co$	5.2 y	Thermal	4-in.-long wire, 0.020 in. diam, Al--0.15% Co	2
$^{54}Fe(n,p)^{54}Mn$	313 d	2.4	4-in.-long wire, 0.009 in. diam	6
$^{58}Ni(n,p)^{58}Co$	71.4 d	2.5	4-in.-long wire, 0.030 in. diam	6
$^{238}U(fission)^{137}Cs$	30 y	1.7	Depleted ^{238}U, CdO shielded	2

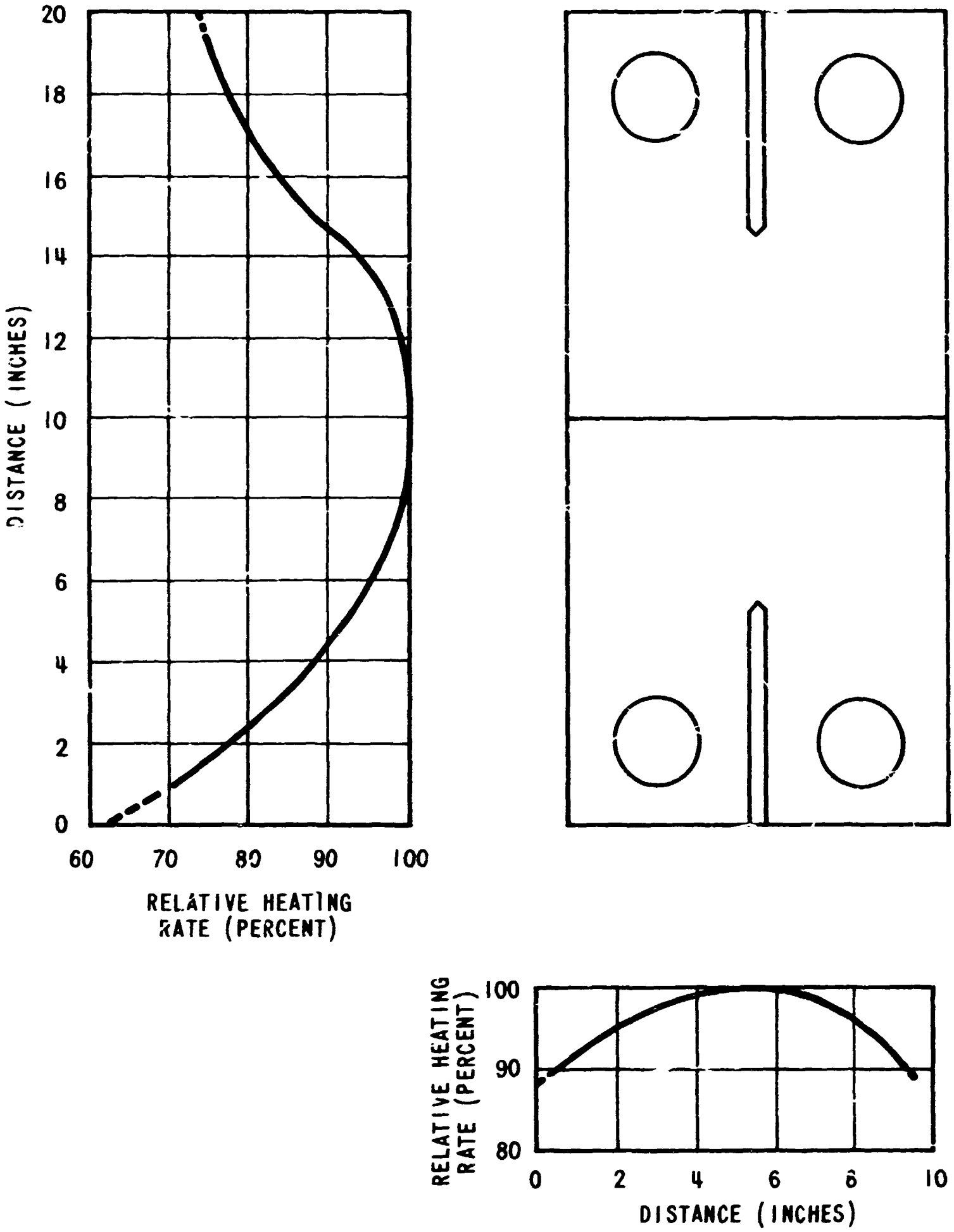

Fig. 3.12. Relative gamma heating rates predicted for 4T specimen assemblies.

ratio obtained in the dosimetry experiments discussed previously.

Prediction of Internal Gamma Heat Generation

Another experiment was conducted in the BRR to evaluate the amount of internal heat generation occurring at full core power. A 6 X 6 X 4 in. steel block was positioned adjacent to the core face in the location to be occupied by an irradiation capsule. The top, bottom, and sides were insulated with foamed polystyrene to promote one-dimensional heat flow, and the block was instrumented with a thermocouple on each face and at seven interior positions along the block center line. Temperature measurements were recorded at a reactor power of 1.5 MW(t) following the attainment of thermal equilibrium.

The experiment was modeled by a Battelle heat transfer computer code (SADSON). Temperature distributions were calculated on an iterative basis with estimated volumetric heating rates until the experimentally determined distribution was closely matched. The local volumetric heat generation rates finally determined appear in Table 3.3 as SADSON program input. Integration of the values in the right-hand column of the table will yield total volumetric heat generation rates.

Measurements were also made to map the relative gamma heating rates in the axial direction (20-in. capsule dimension) and the azimuthal direction (10-in. capsule dimension). The results are shown in Fig. 3.12. As expected, the heat input profiles are nearly described by the superposition of two cosine curves, one in each direction. Note that heating rates drop to approximately 90% of the peaks in the region of the notch roots.

Table 3.3. BRR gamma heating rates

Thermocouple No.	Location from front face (in.)	Measured temperature extrapolated to 2 MW (°F)	SADSON calculated temperature (°F)	SADSON program input, capsule heat generation rates (Btu $in.^{-3}$ hr^{-1})
1	0	173	174	187
2	1/4	186	188	137
3	1/2	191	196	101
4	3/4	194	201	68.4
5	1	195	203	45
6	1 1/2	194	202	27
7	2	190	196	12.6
8	3	178	177	4.5
9	4	158	155	

4. Pressure Vessel and Piping Investigations

These investigations encompass the complex stress state task, the simulated service test task, and that part of the specific safety research task dealing with the extent of ductile pipe rupture. No work was performed this reporting period under the complex stress state task. The flawed tensile specimen tests and pressure vessel tests discussed herein as well as the supporting properties testing and acoustic emission monitoring for the pressure vessel investigations are part of the simulated service test task.

1. Research sponsored under UCCND Subcontract No. 3202 between Union Carbide Corporation and Southwest Research Institute.

TESTING OF 1- AND 6-in.-THICK TENSILE SPECIMENS[1]

S. C. Grigory
Southwest Research Institute

A final series of four 6-in.-thick tensile specimens were tested. Three of these contained fatigue-sharpened flaws, while the fourth was tested without a flaw. Results from these tests are summarized in Table 4.1. Two tests of the series were unique, in that specimen 15, which contained a flaw, was tested at −40°F and failed at a stress of about half yield as predicted by fracture mechanics, and specimen 17 did not contain a flaw and was pulled in tension past necking strain. A

Table 4.1. Tensile test data for longitudinal specimens 14 to 17

Gage length, 24 in.; width, 18 in.; thickness, 6 in.; gross area, 108 in.^{2}

Specimen No.	Test temp. (°F)	Net area (in.^{2})	Elastic limit load (kips)	Elastic limit stress (ksi)		Maximum load (kips)	Maximum stress (ksi)		Average strain[a] (%)	
				Gross section	Net section		Gross section	Net section	At maximum	At separation
14	200	94.0	5800	53.7	62.4	6800	63.0	72.4	1.81	4.22
16	75	95.05	6200	57.4	65.2	6200	57.4	65.2	0.15	0.15
15	−40	95.05	3400[b]	31.5[b]	36.7[b]	3400	31.5	36.7	0.09	0.09
17	200	95.09	7560	70.0		9100 (8100)[c]	84.3 (75.0)[c]		10.30	21.00[d]

[a]Results obtained from test-section displacement gage readings across flaw divided by gage length (24 in.).
[b]Failed below yield.
[c]These were apparent maximum values prior to 48-hr hold period.
[d]Necked down but did not separate.

BLANK PAGE

rather anomalous result not yet fully understood was obtained. Maximum load was reached at about 8 million pounds and a strain of 3%. With this load or less, the specimen was strained to about 5%. Some 48 hr elapsed before attempting to separate the specimen. During this time the specimen was maintained at temperature but without being loaded. At the end of this time it took over 9 million pounds to reinitiate plastic deformation. The specimen was never actually separated due to displacement limitations on the machine. These results as well as those of the other two specimens have been reported.[2]

CHARACTERIZATION OF INTERMEDIATE VESSEL V-1

W. J. Stelzman

Mechanical properties of material obtained from the 6-in.-thick prolongation of intermediate vessel V-1 were determined. These data were necessary to assist in the prediction of failure for the preflawed vessel study in which vessel V-1 is the first to be studied. However, before reporting the data, it was necessary to redefine the specimen orientation notation because of the cylindrical shape of the material tested. Figure 4.1 illustrates both the orientation and the notation used to describe the attitude of the specimens tested.

Results from drop-weight tests[3] using CA-oriented specimens indicate nil ductility transition (NDT) temperatures of 0°F at the $^1/_{24}$T depth and 10°F at the $^7/_{16}$T and $^{11}/_{16}$T depths from the outer surface of the vessel. Results from standard 0.505- and 0.178-in.-gage-diam tensile specimens at room temperature for various depths through the wall thickness are listed in Table 4.2. Yield strength differences are evident and are due to apparent difference in cooling rates at the inner and outer surfaces during the quenching. The outer surface, which would be the most easily cooled, shows a yield stress in excess of 76,000 psi. The yield stress then drops rapidly to 70,000 psi by the $^1/_4$T depth and remains relatively constant through the vessel thickness. At the $^{23}/_{24}$T depth ($^1/_4$ in. from the inner wall), the yield strength indicates a maximum of 72,000 psi.

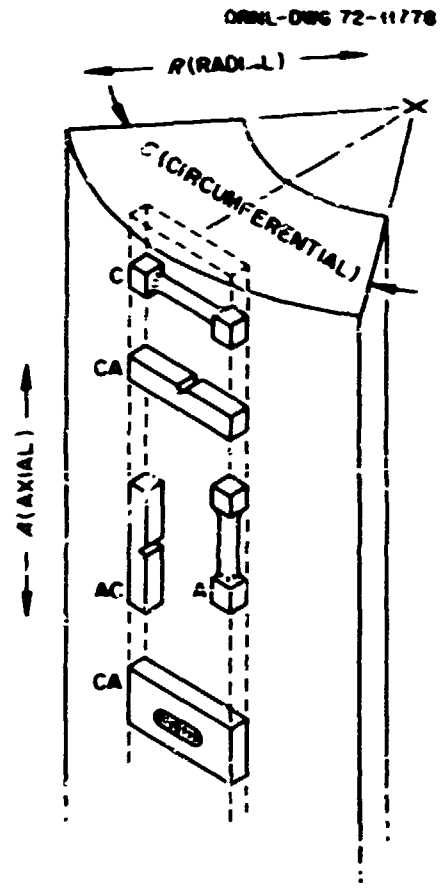

Fig. 4.1. Specimen orientation notation for HSST intermediate vessel materials showing tensile, Charpy V-notch, and drop-weight specimens.

Table 4.2. Tensile properties[a] of 6-in. wall thickness HSST intermediate vessel V-1 from circumferential-oriented specimens of ASTM A508, class 2 forging steel

Depth[b] (d/6)	Strength property (kpsi)		Total elongation[c] (%)	Reduction in area (%)
	Lower yield	Ultimate tensile		
1/16	75.8	96.1	20.0	65
1/12	74.5[d]	96.4[d]	23.0[d]	54[d]
1/4	71.1	92.6	19.5	65
3/?	68.8	89.5	21.5	66
1/2	70.6[d]	91.2[d]	25.5[d]	59[d]
3/4	68.6	89.5	21.0	65
3/4	70.3[d]	91.6[d]	24.5[d]	62[d]
23/24	69.5[e]	91.4[e]	23.0[e]	62[e]
23/24	71.6[e]	92.6[e]	20.0[e]	55[e]

[a]Average of two specimens tested at 75°F and strain rates of 0.015 min^{-1} for 0.178-in.-gage-diam specimens and 0.0089 min^{-1} for 0.505-in.-gage-diam specimens.

[b]Fraction of wall thickness (6 in.) from outer surface of vessel.

[c]Length-to-diameter ratio of 7.

[d]Results from standard 0.505-in.-gage-diam specimens; remainder of results from 0.178-in.-gage-diam miniature specimens.

[e]Results of individual specimens.

2. S. C. Grigory, *Tests of 6-Incl.-Thick Flawed Tensile Specimens Third Technical Summary Report, Longitudinal Specimens Numbers 14 through 16, Unflawed Specimen Number 17*, HSSTP-TR-22, Southwest Research Institute (October 1972).

3. *1971 Annual Book of ASTM Standards*, Part 31, pp. 590–609, American Society for Testing and Materials, E 208–69, July 1971.

These data indicate that the cooling rate for inner surface material during the quench cycle was not much higher than for the central material but quite a bit lower than for the outer surface material.

Standard Charpy V-notch impact results from $\frac{3}{8}$T and $\frac{5}{8}$T CA-oriented specimens are shown in Fig. 4.2. A correlation energy of 33 ft-lb based upon the drop-weight NDT temperature (10°F) for these depths and orientation and a ductile shelf energy of 90 ft-lb are indicated. A Charpy impact energy scan was made of the surface and central ($\frac{1}{4}$, $\frac{1}{2}$, and $\frac{3}{4}$T) materials at four test temperatures (−50, 0, 50, and 100°F). The results show that, within experimental scatter, the fracture energies for the outer surface material were approximately 20 ft-lb higher than those for the inner surface or the central materials. No significant difference was noted between the central or inner surface materials, and both correlated with the $\frac{3}{8}$T and $\frac{5}{8}$T results over the same temperature range. The energy scan also indicated a correlation energy of approximately 49 ft-lb at the NDT temperature of 0°F for the outer surface material.

Charpy V-notch impact results from $\frac{1}{3}$T and $\frac{1}{4}$T, AC-oriented specimens indicated a ductile-brittle transition temperature of −40°F at the 32 ft-lb fracture energy level and a ductile shelf energy of approximately 135 ft-lb. Therefore the dynamic fracture properties for a radial crack propagating in the circumferential direction are superior to those of a radial crack propagating in the axial direction.

Static lower-bound fracture toughness data, K_{Icd}, were also obtained from standard Charpy V-notch specimens fatigue cracked to a total depth of 0.210 to 0.240 in. (a/w = 0.532 to 0.609). The precracked specimens were then tested in slow bend at seven test temperatures (−50, 0, 50, 76, 100, 130, and 200°F) and the fracture parameters determined by the equivalent-energy method proposed by Witt[4] and the ASTM standard E 399-70T.[5] The results from central material are shown in Fig. 4.3, where they are compared with results, to be discussed later, which were obtained by Westinghouse from 0.85T and 4T compact-tension

4. F. J. Witt, "The Equivalent Energy Method for Calculating Elastic-Plastic Fracture." Paper 12, HSST Program Fifth Annual Information Meeting, Oak Ridge National Laboratory, Mar. 25–26, 1971.

5. *1971 Annual Book of ASTM Standards*, Part 31, pp. 919–35, American Society for Testing and Materials, E 399-70T, July 1971.

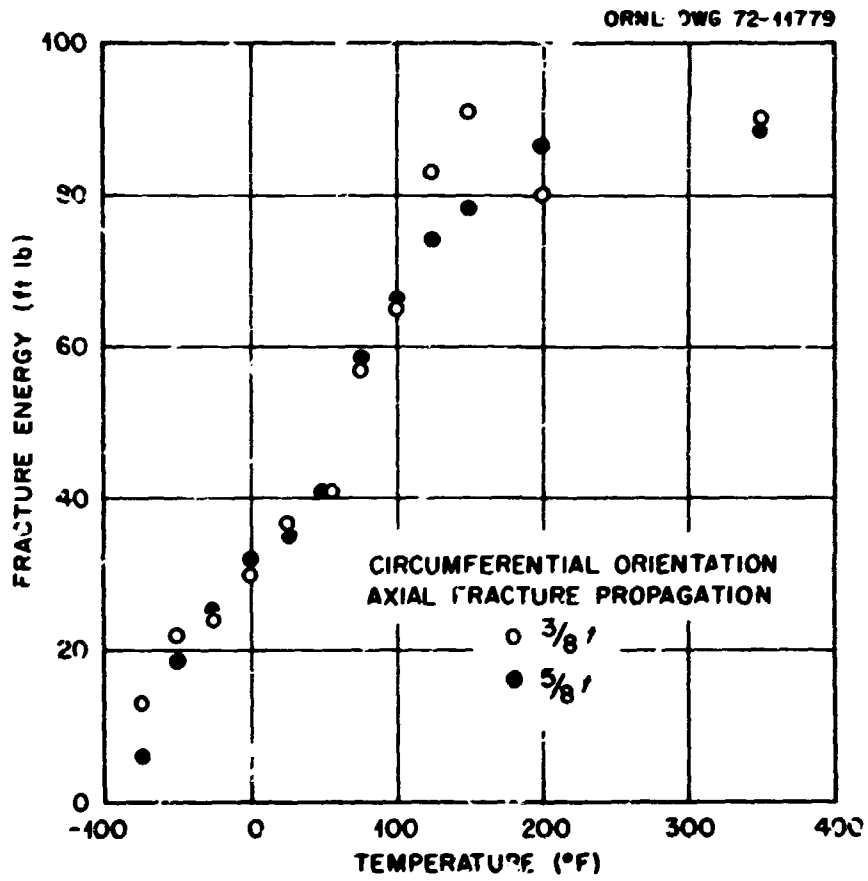

Fig. 4.2. Charpy V-notch impact test results obtained from intermediate vessel V-1, 6-in.-thick, ASTM A508, class 2 forging steel.

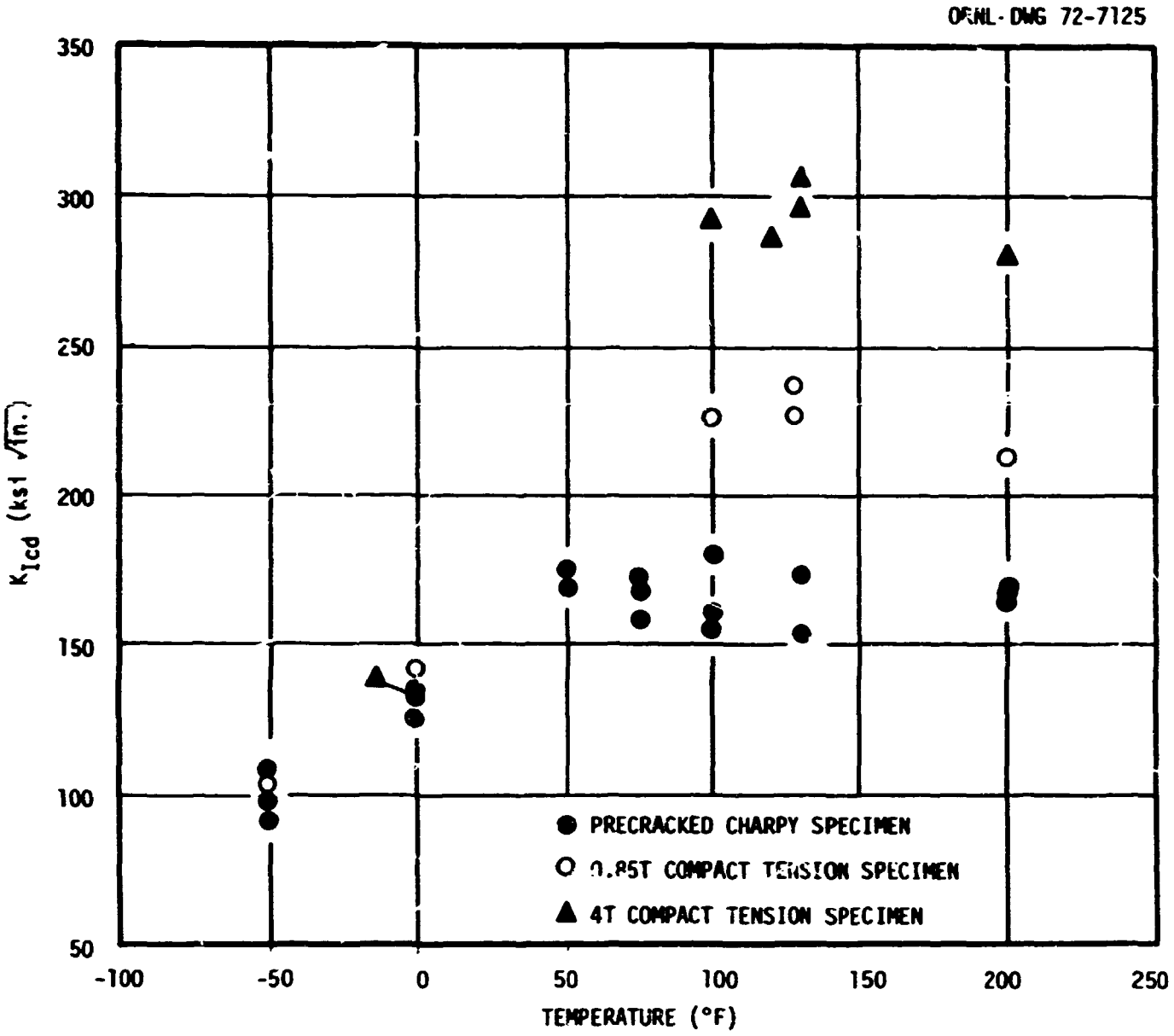

Fig. 4.3. Lower-bound fracture toughness values obtained from intermediate vessel V-1 center material, circumferential orientation, 6-in.-thick ASTM A508, class 2 forging steel.

specimens of the same material and at similar depths. The precracked Charpy specimen results adequately describe the lower-bound fracture toughness characteristics as defined by the lower-bound procedure.[6] Data from the inner surface material correlated with the central material when experimental scatter was considered. The outer surface material data indicated a static fracture toughness transition range below --50°F. Otherwise the K_{Icd} plateau values from all materials including both surfaces appear to be similar.

A similar study of the dynamic fracture toughness parameter, K_{Idd}, obtained from precracked Charpy V-notch specimens fatigue cracked to a depth of 0.210 to 0.240 in. and tested in impact over the temperature range 0 to 350°F is in progress. Load-time traces of the impact loading to fracture are being used to determine the energy values required for the K_{Idd} calculation.

Materials from intermediate vessels V-2, V-3, and V-4 are also being studied to obtain similar data.

FRACTURE TOUGHNESS CHARACTERIZATION OF HSST INTERMEDIATE PRESSURE VESSEL MATERIALS[7]

P. C. Riccardella T. R. Mager L. R. Singer
Westinghouse Electric Corporation

Introduction

In order to demonstrate the capability to predict failure of large, heavy-walled pressure vessels under service-type loading conditions, the HSST program includes a series of pressure vessel tests which are

6. F. J. Witt and T. R. Mager, *A Procedure for Determining Bounding Values on Fracture Toughness K_{Ic} at Any Temperature*, ORNL-TM-3894 (October 1972).

7. Work sponsored by HSST Program under UCCND Subcontract No. 3196 between Union Carbide Corporation and Westinghouse Electric Corporation.

intermediate between conventional laboratory tests and a full-scale vessel. The intermediate pressure vessels contain a cylindrical test course approximately 54 in. long and 6 in. thick. The first two vessels are fabricated from ASTM A508, class 2 forging steel. In order to characterize the material properties of the test vessels, 24-in. prolongations of the test courses were removed prior to welding on the heads. This section describes the fracture toughness testing of the forging prolongations from the first two vessels. The specimens were tested over the range 0 to 200°F in order to establish a lower-bound curve of the fracture toughness of the pressure vessel material using Witt's[8] equivalent-energy concept.

8. F. J. Witt, "A Procedure for Determining Bounding Values on Fracture Toughness K_{Ic} at Any Temperature," Paper 13, HSST Program Fifth Annual Information Meeting, Oak Ridge National Laboratory, March 1971.

Specimen Fabrication

A total of 44 compact-tension specimens were machined from the forging prolongations from the first two pressure vessels (22 each). The specimens included seven 0.85T CT specimens from the outside surface of each vessel, six 0.85T CT specimens from the center thickness region of each vessel, two 0.85T CT specimens from the inside surface of each vessel, six 4T CT specimens from the center region of each vessel, and one 4T CT specimen from the inside surface of each vessel. Figure 4.4 contains sketches which show the exact location from which each type of specimen was machined. The specimens were fatigue precracked according to the methods specified in ref. 9.

9. Tentative Method of Test for Plane-Strain Fracture Toughness of Metallic Materials, ASTM E399-70T.

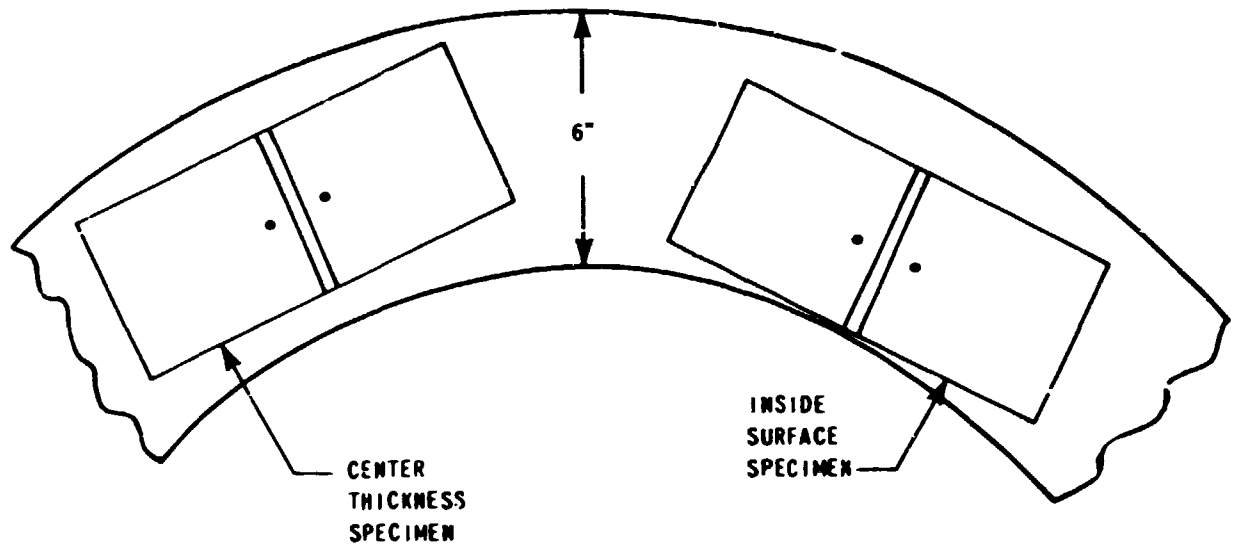

Fig. 4.4. Machining of fracture toughness specimens from HSST intermediate pressure vessel prolongations.

Test Program

Specimen test temperatures were specified during the test program in order to establish pressure vessel test temperatures which would yield failures in the desired fracture regimes (frangible, transitional, or ductile). Test temperatures of 130°F for the first vessel (V-1) and 32°F for the second vessel (V-2) were selected on the basis of this and the study discussed in the previous section. These test temperatures are in the range where very large specimens (greater than 6T CT) would be necessary to perform valid fracture toughness testing according to the ASTM recommended procedure.[9] For this reason, the equivalent-energy concept[8] was used to interpret the data in terms of lower-bound values of the actual fracture toughness.

Test Results

The results of the tests for vessels V-1 and V-2 are summarized in Tables 4.3 and 4.4 respectively. Lower-bound values of fracture toughness computed from the test data using the methods of ref. 9 are listed in these tables and are plotted as a function of temperature in Figs. 4.5 and 4.6 (see also Fig. 4.3).

The results of these tests indicate that the toughness of the forging material used for the first two intermediate pressure vessels is comparable to toughness

Table 4.3. Fracture toughness results from 4T and 0.850T compact-tension specimens from ORNL vessel forging prolongation V1B

Specimen No.	Test temp. (°F)	Crack length (in.)	Maximum load (lb)	Energy to maximum load (in.-lb)	P_Q (lb)	Energy to P_Q (in.-lb)	K_{Icd} (ksi$\sqrt{\text{in.}}$)
0.850T compact-tension specimens (outside surface)							
V1B-13	−100	0.958	8,390	230.2	3,000	17.6	113.0
V1B-12	−50	0.883	10,750	266.2	3,100	17.0	112.0
V1B-7	0	0.888	12,300	1,037.7	4,100	32.4	214.0
V1B-8	+100	0.868	12,090	813.3	4,100	29.6	192.0
V1B-10	+130	0.871	11,800	842.9	4,000	26.7	202.0
V1B-11	+130	0.896	11,100	945.8	3,500	21.4	219.0
V1B-9	+200	0.858	11,850	1,036.9	4,100	30.7	209.0
0.850T compact-tension specimens (center thickness region)							
V1B-19	−50	0.880	10,250	209.7	5,000	41.0	103.0
V1B-14	0	0.888	11,370	410.8	4,000	28.0	142.0
V1B-15	+100	0.881	11,400	1,059.2	4,200	30.9	225.0
V1B-17	+130	0.888	10,950	1,391.6	3,600	29.7	228.0
V1B-18	+130	0.868	11,350	1,312.4	3,100	18.7	237.0
V1B-16	+200	0.880	11,000	1,005.0	4,000	29.5	213.0
0.850T compact-tension specimens (inside surface)							
V1B-20	+130	0.880	11,600	975.5	3,000	15.7	215.0
V1B-21	+130	0.883	11,390	1,100.7	3,600	22.6	230.0
4T compact-tension specimens (center thickness region)							
V1B-6	0	4.098	149,000	5,264.0	62,000	900.0	136.0
V1B-2	+100	4.123	232,000	27,550.0	80,000	1632.0	292.0
V1B-1	+120	4.328	204,500	22,372.0	60,000	924.0	285.0
V1B-5	+130	4.120	227,500	28,130.0	42,000	450.0	295.0
V1B-4	+130	4.273	213,500	27,172.0	78,000	1584.0	305.0
V1B-3	+200	4.100	228,500	25,134.0	80,000	1584.0	280.0
4T compact-tension specimen (inside surface)							
V1B-22	+130	4.133	232,000	35,520.0	80,000	2464.0	270.6

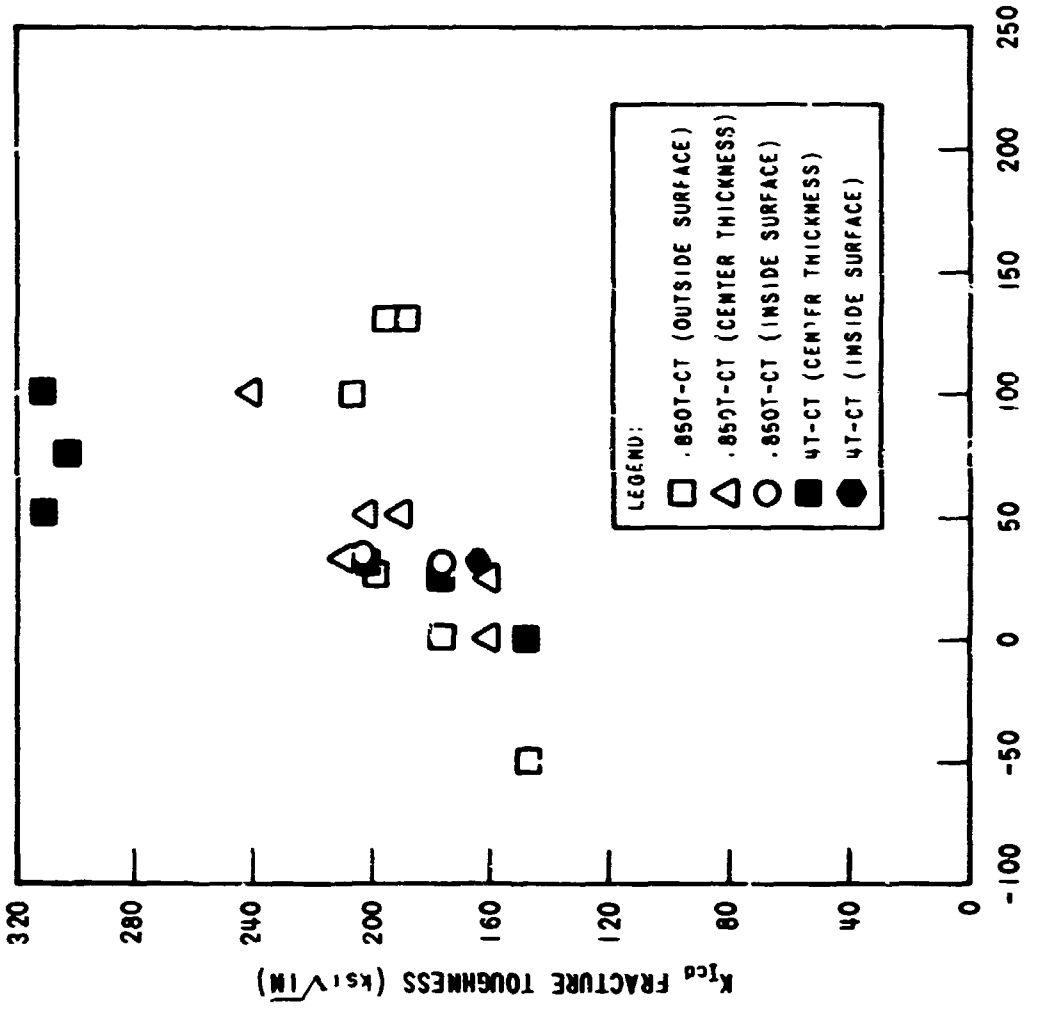

Fig. 4.6. Fracture toughness data for HSST intermediate pressure vessel V-2.

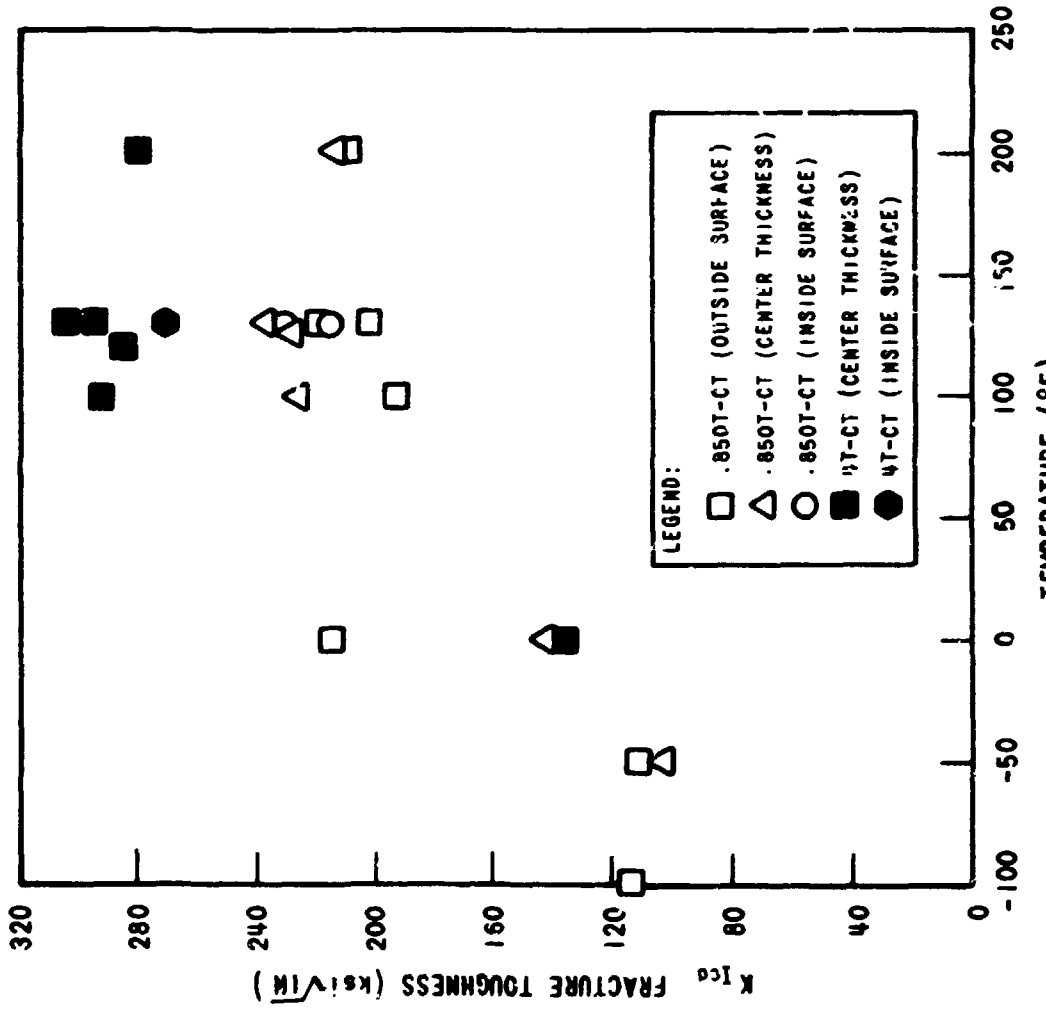

Fig. 4.5. Fracture toughness data for HSST intermediate pressure vessel V-1.

Table 4.4. Fracture toughness results from 4T and 0.850T compact-tension specimens from ORNL vessel forging prolongation V2B

Specimen No.	Test temp. (°F)	Crack length (in.)	Maximum load (lb)	Energy to maximum load (in.-lb)	P_Q (lb)	Energy to P_Q (in.-lb)	K_{Icd} (ksi$\sqrt{\text{in.}}$)
0.850T compact-tension specimens (outside surface)							
V2B-11	−50	0.886	12,200	437.8	4,000	27.6	146.3
V2B-9	0	0.851	12,200	760.2	4,000	28.9	176.7
V2B-10	+25	0.873	12,250	911.4	4,000	29.9	198.0
V2B-12	+32	0.873	12,440	852.6	4,000	25.8	206.2
V2B-8	+100	0.860	12,450	910.1	4,000	26.2	206.5
V2B-13	+130	0.855	12,300	736.2	4,000	25.0	188.2
V2B-7	+130	0.873	11,550	860.2	4,000	28.8	196.0
0.850T compact-tension specimens (center thickness region)							
V2B-16	0	0.913	10,500	493.2	4,000	28.6	160.5
V2B-17	+25	0.860	11,800	575.9	4,000	27.5	160.2
V2B-18	+32	0.890	11,260	958.4	4,000	30.0	209.0
V2B-15	+50	0.885	11,500	729.9	4,000	26.3	190.1
V2B-19	+50	0.885	11,200	941.4	4,000	31.2	201.3
V2B-14	+100	0.893	11,400	1,173.0	4,000	28.0	241.2
0.850T compact-tension specimens (inside surface)							
V2B-20	+32	0.876	12,120	911.8	4,000	28.5	204.1
V2B-21	+32	0.886	11,600	697.3	4,000	29.5	178.7
4T compact-tension specimens (center thickness region)							
V2B-4	0	4.125	164,000	6,768.0	80,000	1564.0	148.0
V2B-6	+25	4.133	184,500	9,344.0	80,000	1512.0	177.1
V2B-2	+32	4.295	186,000	10,772.0	80,000	1516.0	202.4
V2B-5	+50	4.115	236,000	29,584.0	80,000	1532.0	311.3
V2B-1	+75	4.326	210,500	26,992.0	80,000	1724.0	304.7
V2B-3	+100	4.120	237,500	30,420.0	80,000	1620.0	311.4
4T compact-tension specimen (inside surface)							
V2B-22	+32	4.100	180,500	14,260.0	80,000	2576.0	165.7

data which have previously been determined for A533, grade B, class 1 steel.[10]

FIRST INTERMEDIATE VESSEL TEST

R. W. Derby

Introduction

The first 6-in.-thick, 39-in.-OD intermediate-size pressure vessel was flawed and burst during the reporting period. Six 0.85-in.-thick models were also fabricated, flawed, and burst. The models were geometrically similar to the prototype except for flaw geometry and were made from the prolongation of the cylindrical forging which had been given the same heat treatments as the vessel. The test procedures and significant results are summarized below.

Fatigue Sharpening of the Machined Flaw

One problem encountered during preparation of the first intermediate vessel was the growing of a suitable fatigue crack from a starter notch. The basic approach was identical to that used previously to sharpen the

10. T. R. Mager, "Experimental Verification of Lower Bound K_{Ic} Values Utilizing the Equivalent Energy Concept," Paper 23, HSST Sixth Annual Information Meeting, Oak Ridge National Laboratory, April 1972.

cracks in the 6-in.-thick tensile specimens.[11] However, it was necessary to develop special tools to manufacture the starter notch, because the vessel was too heavy to fit under any of the locally available machine tools. A vessel with the fixture for machining the crack attached is shown in Fig. 4.7.

The ultrasonic monitoring techniques which had worked so well for the tensile specimens were not strictly applicable to a cylindrical geometry, because a shear wave is always generated when a longitudinal wave arrives at an interface. Hence it seemed essential to make several trial runs on a prolongation before actually trying the technique on a vessel. After several practice runs, it became apparent that there was a definite trend for a fatigue crack in the cylindrical body to grow more slowly than in the tensile specimens. In fact, it was necessary to use more than three times as many cycles (90,000 instead of 25,000) to obtain the target growth of ½ in.

Instrumentation and Test Facility

The vessel was instrumented with strain gages, thermocouples, and acoustic emission transducers as shown in Fig. 4.8. Special techniques were developed for bonding the strain gages and protecting them against the environment. Both inside and outside gages were sealed, since leakage at the closure was considered a distinct possibility.

A perspective view of the test facility is shown in Fig. 4.9, and a general view of the test pit is given in Fig. 4.10. Two views of the fully instrumented vessel in the test pit are shown in Figs. 4.11 and 4.12.

11. A. A. Abbatiello and R. W. Derby, *Notch Sharpening in a Large Tensile Specimen by Local Fatigue*, ORNL-TM-3925 (November 1972).

PHOTO 79426

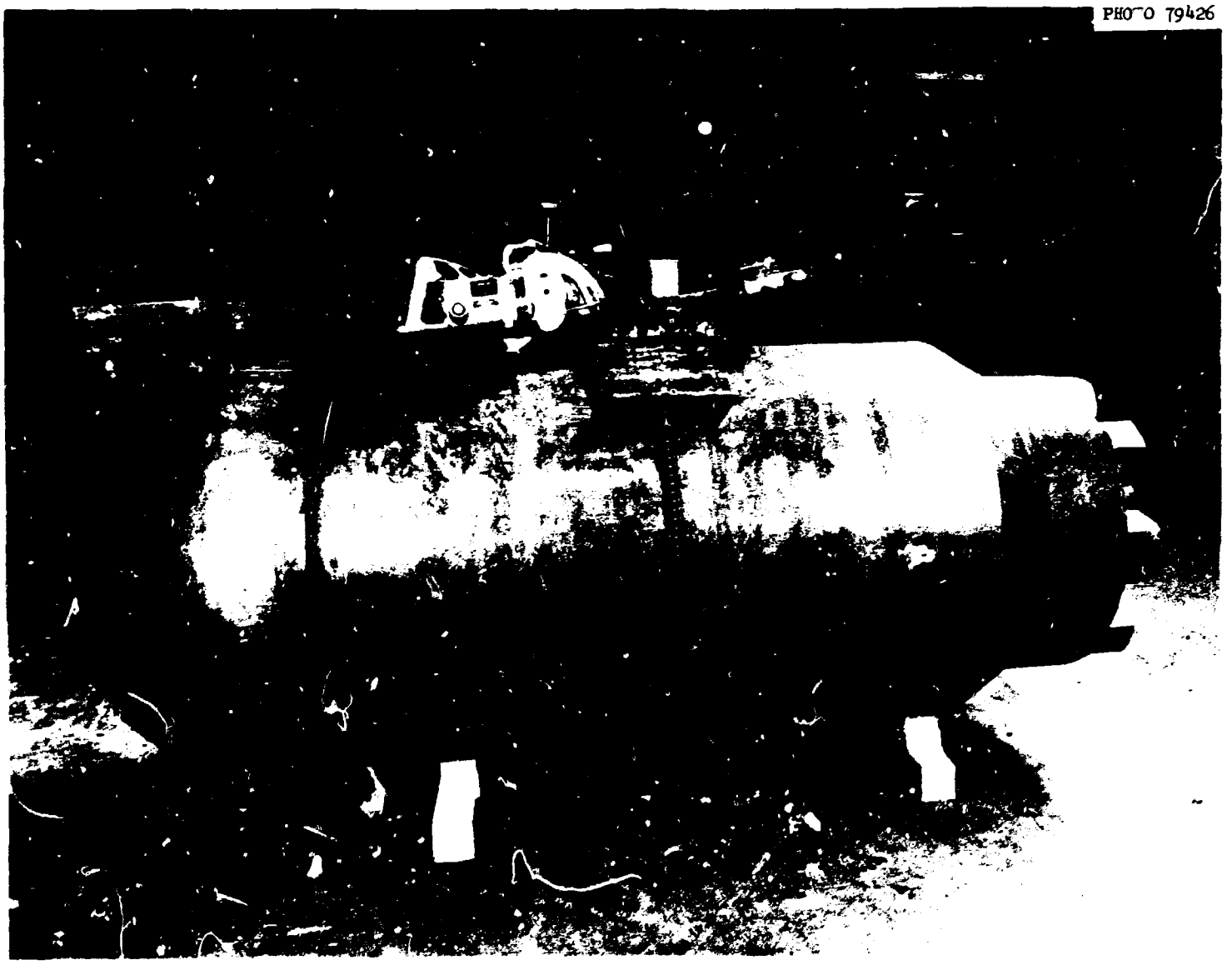

Fig. 4.7. Masonry saw crack preparation fixture.

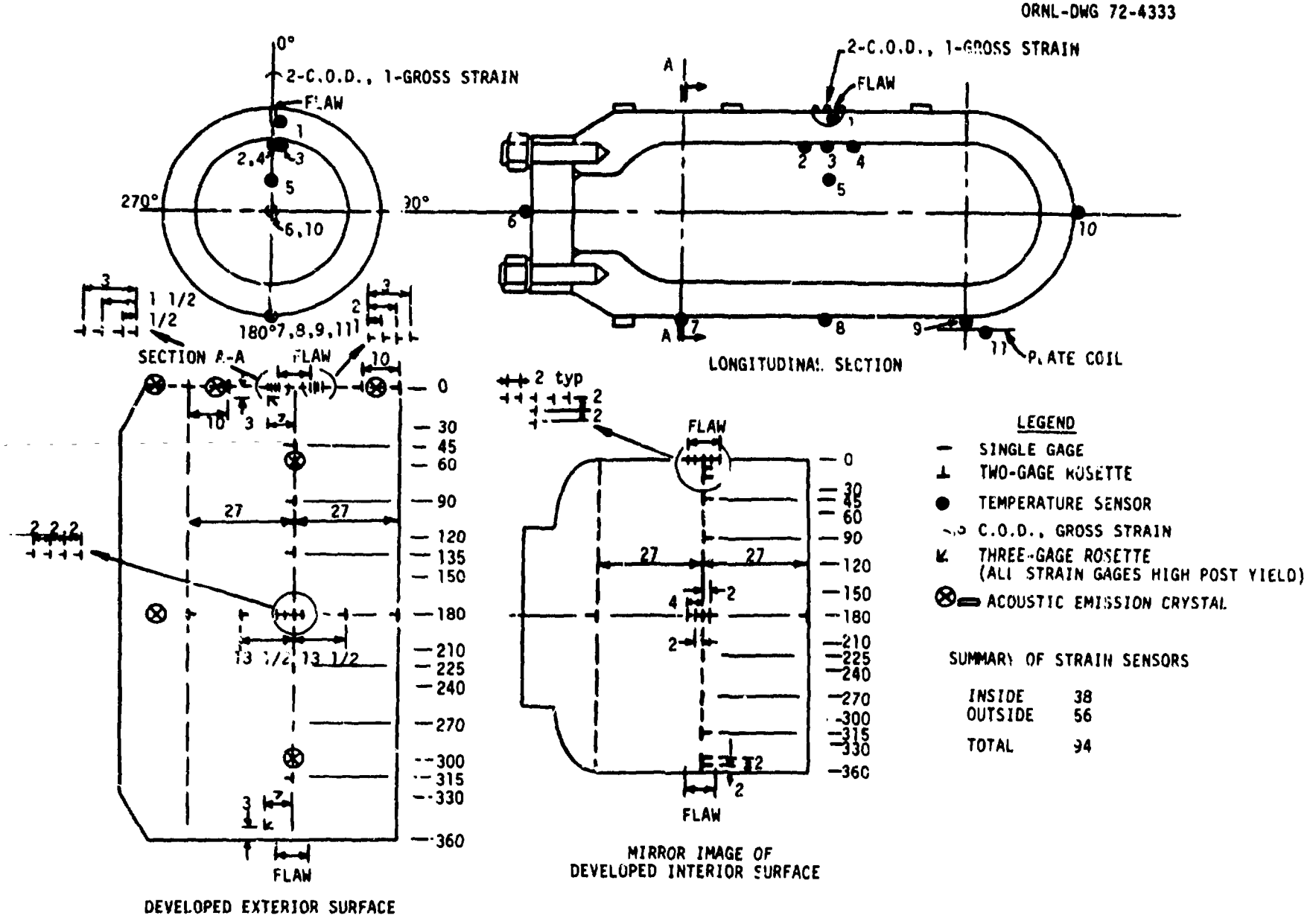

Fig. 4.8. *Instrumentation of the intermediate test vessel V-1.*

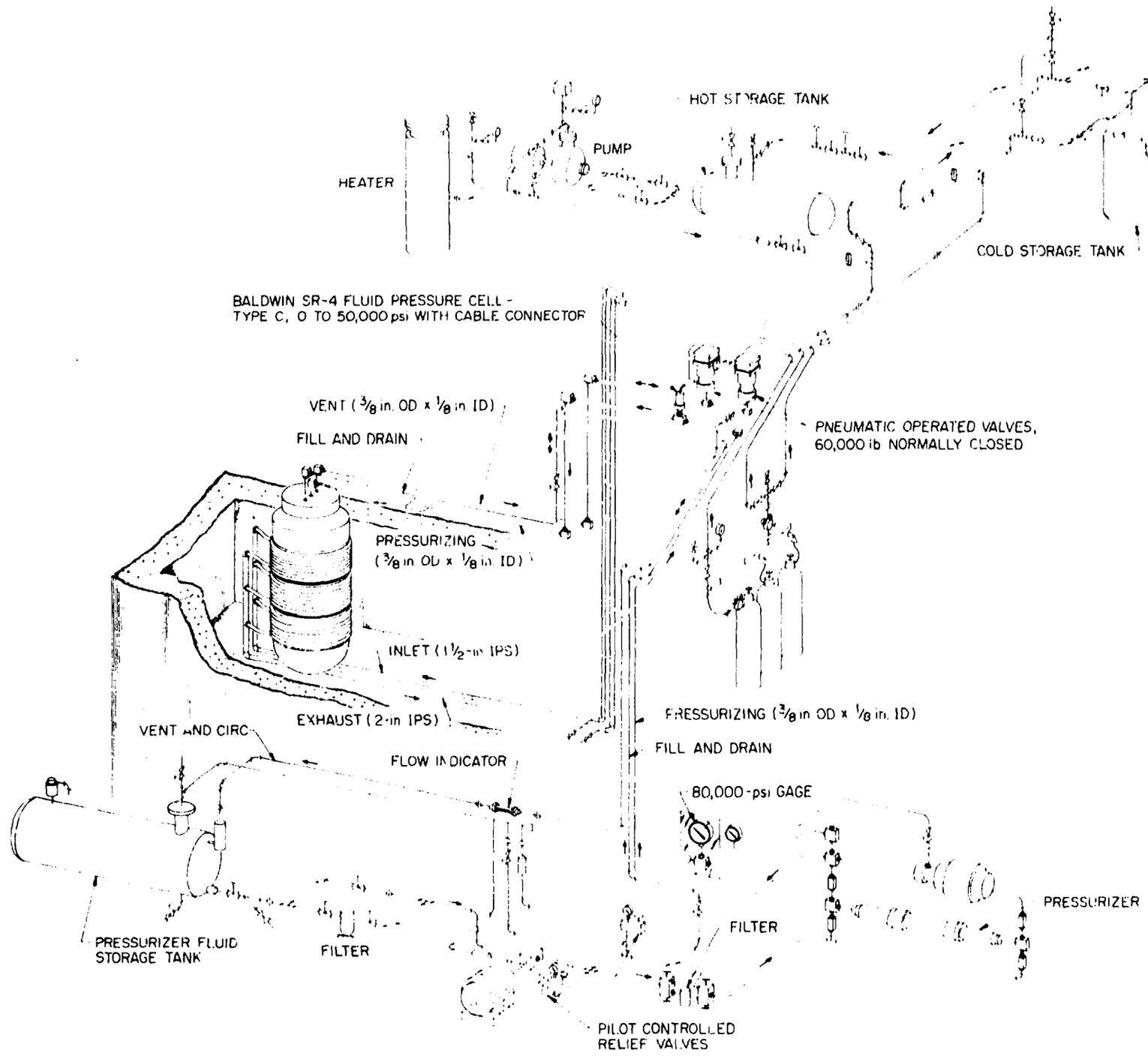

Fig. 4.9. Perspective view of intermediate vessel test facility.

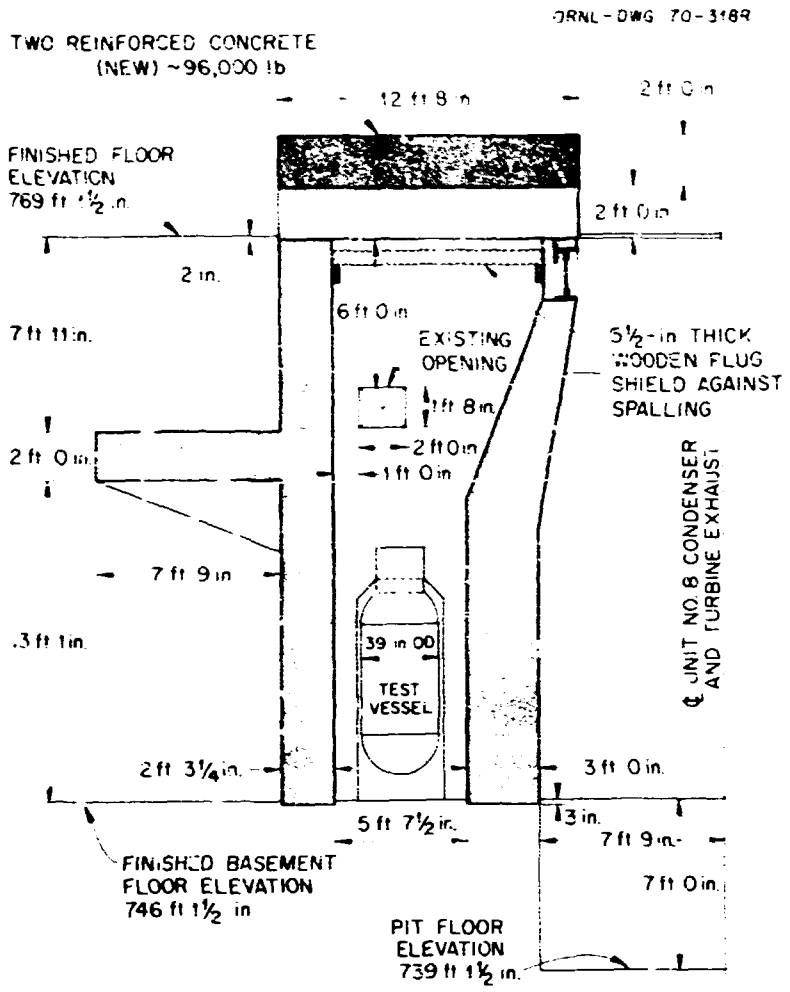

Fig. 4.10. Test part of the intermediate vessel test facility.

Pressure Seals in the Closure

The only significant problem encountered with the high-pressure system used during the burst test occurred at the interface between the lead-through devices manufactured by Autoclave Engineering and the vessel. Each of these devices allows the passage of eight stainless steel sheaths through the vessel head. These sheaths contained thermocouples or strain-gage leads. A number of these devices had been tested to 40,000 psi on a small-scale autoclave with no leakage. On the intermediate vessel, four of the lead-throughs leaked, three at pressures as low as 19,000 psi. After several attempts to reach pressure, it became obvious that there were three conditions that were slightly different than those encountered in a laboratory test. First, the finish on the seats was not as good as that on the small-scale autoclave. Second, the tolerances on the perpendicularity of the seats to their holes could not be the same on a big head as on a small laboratory vessel. Finally, the head probably bends during loading and thus accentuates the other two problems. The solution was quite direct; the seats were polished by a special device designed in the field, and the lead-throughs themselves were screwed down much more tightly than had been the practice under laboratory conditions.

The most significant strain-gage data acquired during the burst test of the first IVT are shown in Fig. 4.13. This pressure-strain curve, obtained from an XY recorder, reflects the gross strain in the vessel. (Gross strain is defined as the hoop strain 180° removed from the flaw.) Four model vessels were also tested at 130°F. Shown for comparison in Fig. 4.14 are the results of these model tests with the prototype results. The most significant data from both models and the prototype are summarized in Table 4.5. As mentioned earlier, the models were made from a prolongation of the cylindrical forging used to make the prototype. The flaws, however, were not to scale; thus the fracture pressure and strain of the models cannot be directly associated with that of the prototype. Also, since the forging is quenched and tempered, such properties as tensile strength and toughness show a considerable systematic variation through the thickness.

Table 4.5. Model data for V-1

Test temperature (°F)	Burst pressure (kpsi)	Strain (%)	Remarks
130	32.2	1.65	
130	32.5	1.90	
130	31.5	2.60	Center material flaw
130	32.0	2.60	Center material flaw
0	35.0	1.8	
−35	31.0	0.9	
130	28.8	0.72	Prototype

In addition, at any given location, there must be a certain amount of anisotropy due to the working of the metal during the forging operation. Thus it is not possible to make a model from a prolongation and have it be truly similar to the prototype. If one considers anisotropy to be dominant, then the flaw in the model ends up on surface material. If, on the other hand, one places the flaw in the model so that its tip resides in base metal, as does the tip of the flaw in the prototype, then the flaw in the model is no longer properly oriented. The problem is illustrated in Fig. 4.15. As a compromise, two models with each of the possible orientations mentioned above were tested. Returning to

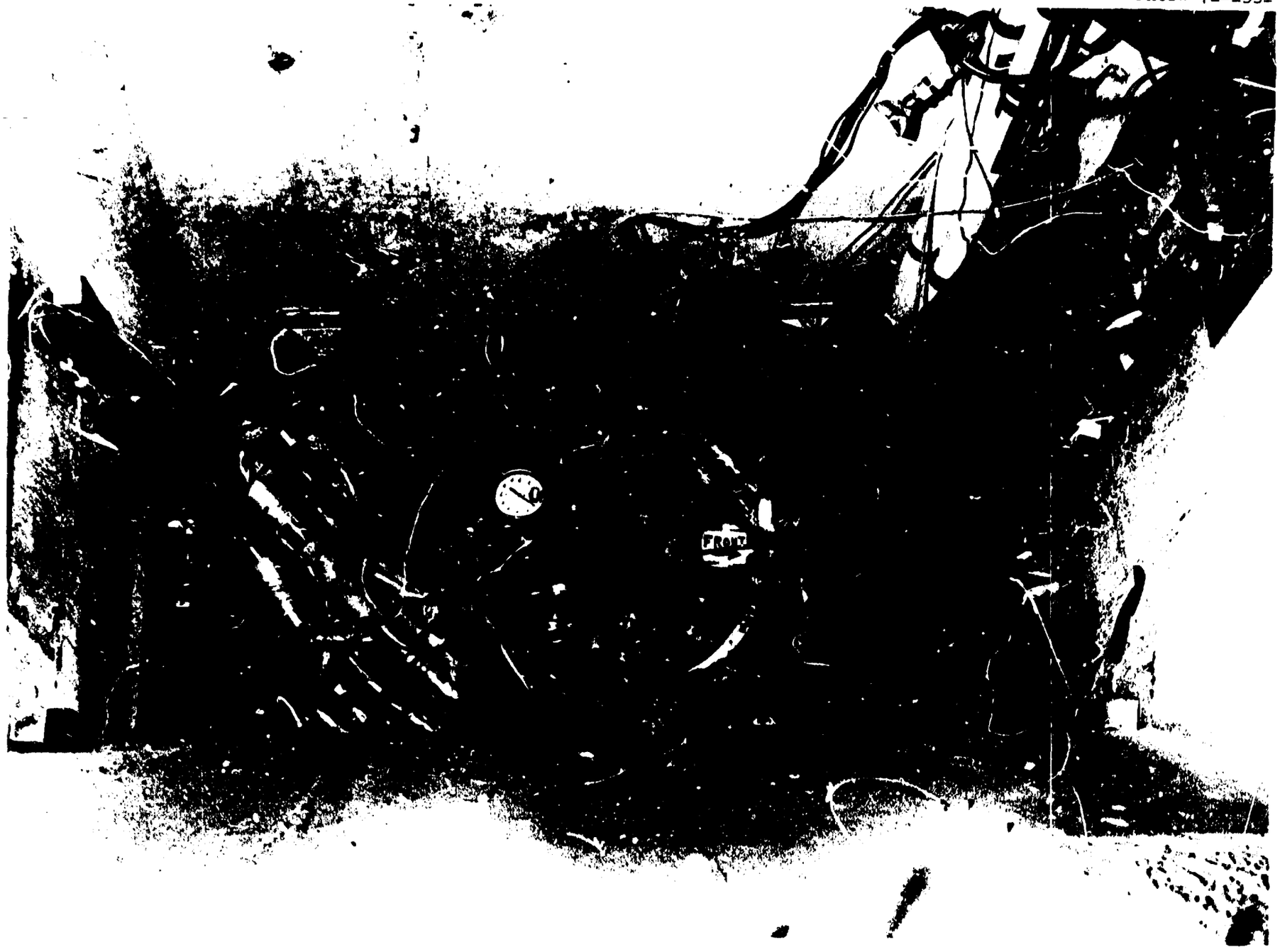

Fig. 4.11. View of top of instrumented intermediate test vessel.

ORGDP
PHOTO 72-1344

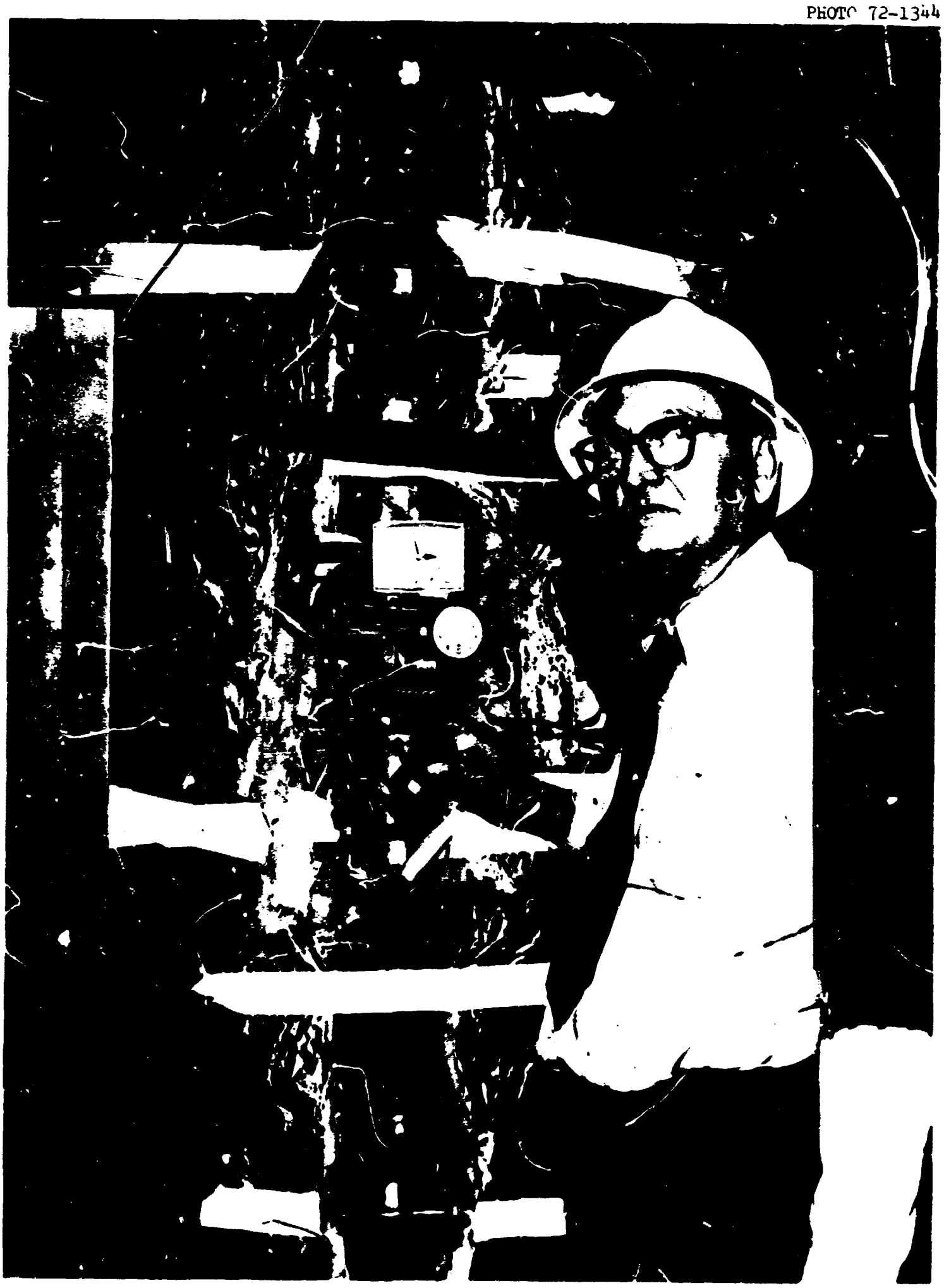

Fig. 4.12. View of flaw of instrumented intermediate test vessel.

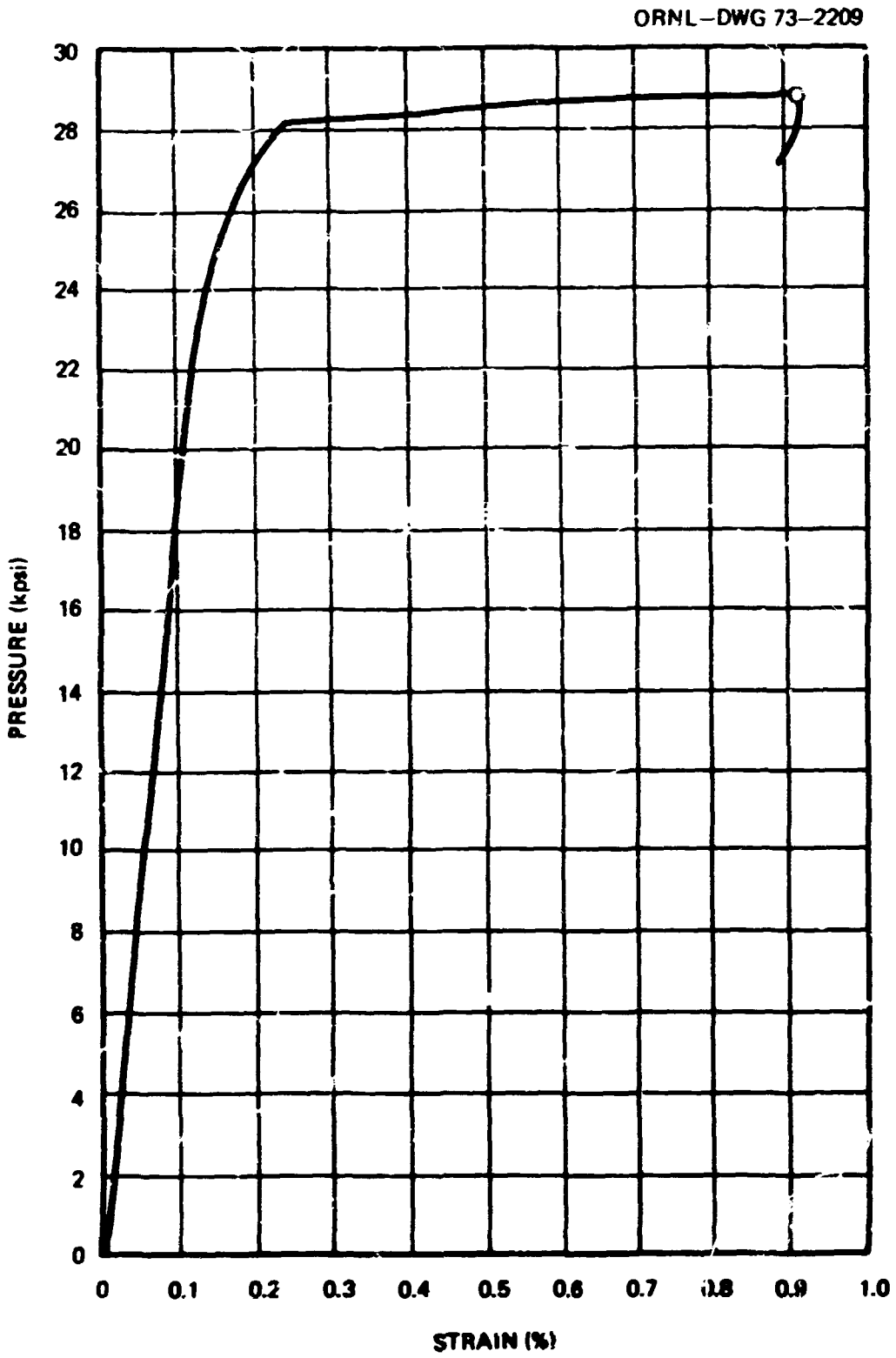

Fig. 4.13. Pressure-strain curve for intermediate test vessel V-1, outside surface 180° from the flaw.

Fig. 4.14, one can see that the actual curve for the vessel fell somewhere between those of the two models. Because of the expanded scale in the figure, the strains at failure in the models are not plotted. (The complete curves are shown later.) The figure clearly illustrates the point frequently made during discussions of size effects – the normalized load-deflection curve for a large flawed structure is identical to that of a model except that the strain at failure is smaller in the large structure.

A more detailed summary of model test results is shown in Fig. 4.16, in which the scale has been compressed to allow the burst conditions for the models to be plotted. Failure points are indicated by stars radiating from the final data point. Ignoring some difference in flaw geometry, several points of considerable interest are demonstrated by this figure. First, the pairs of 130°F models showed excellent reproducibility. Furthermore, the burst pressures for all four

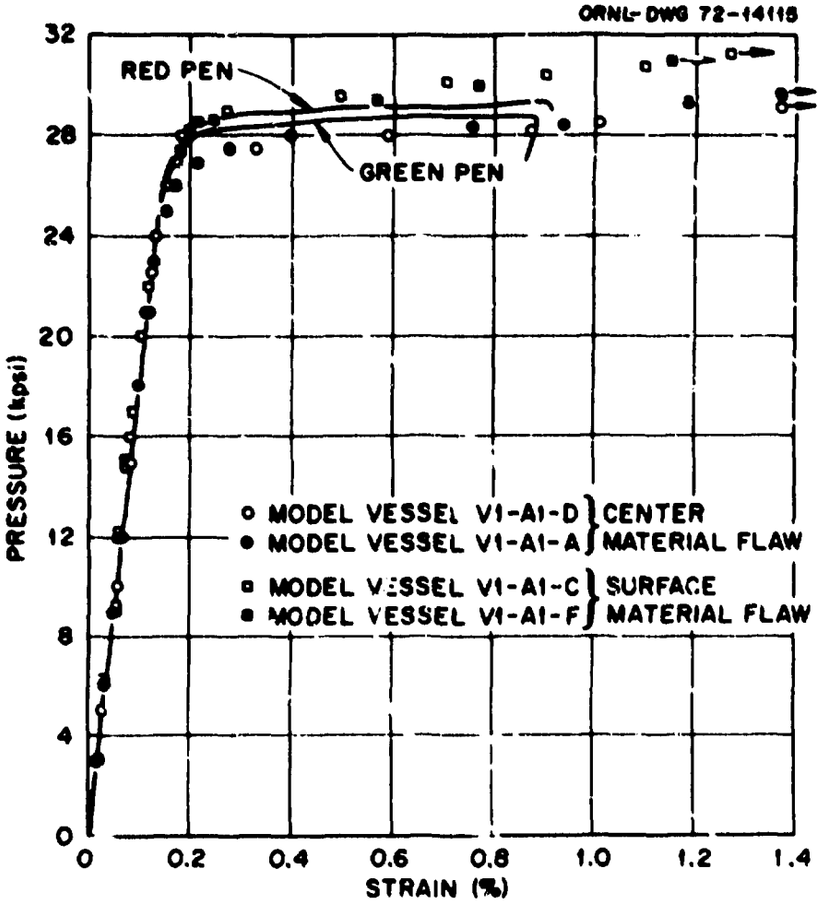

Fig. 4.14. Comparison between XY recorder intermediate vessel test and four model vessels (all at 130°F).

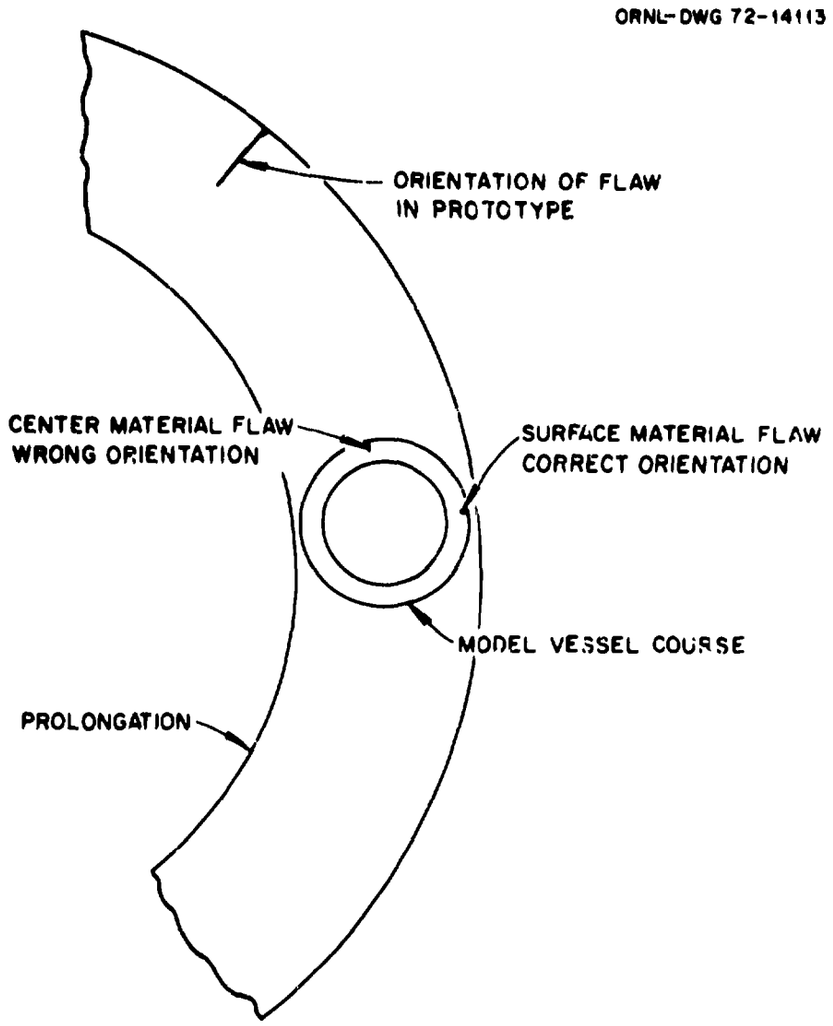

Fig. 4.15. Orientation of model vessels in intermediate test vessel prolongation.

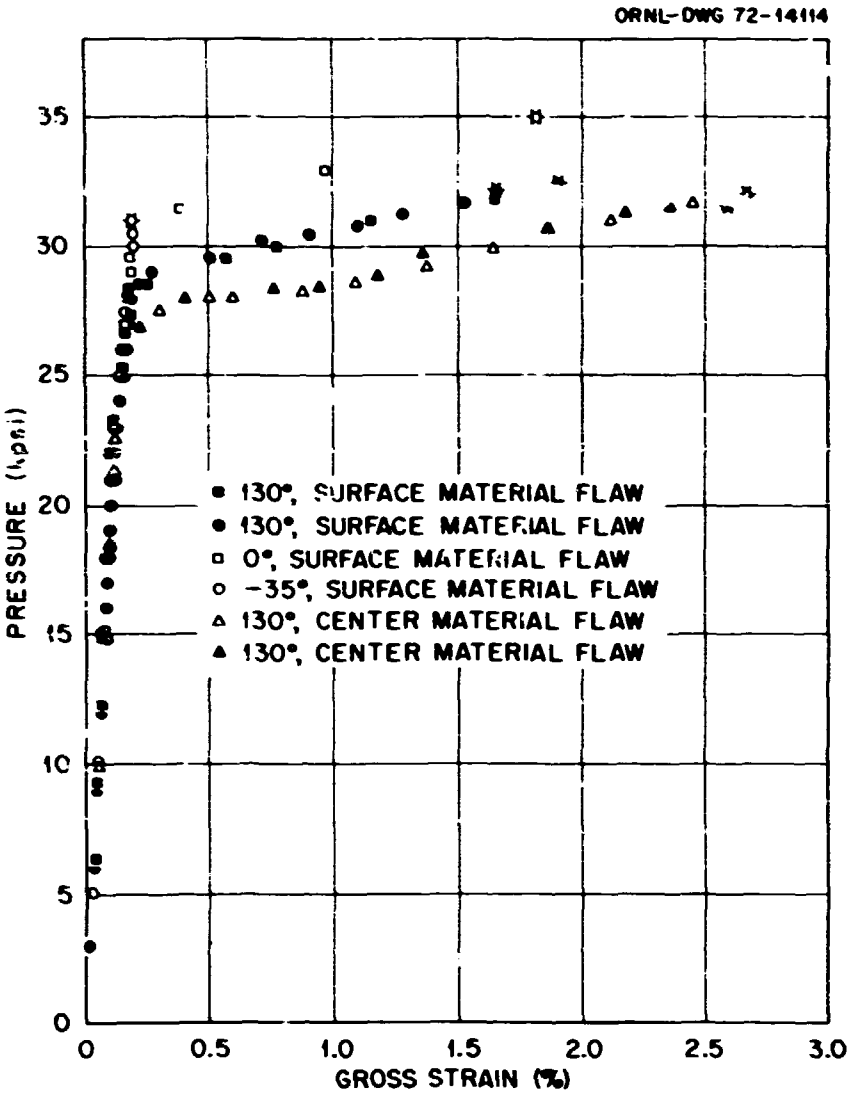

Fig. 4.16. Burst tests of 0.85-in.-thick models, vessel V-1.

130°F tests were very similar and close to 32,000 psi. Thus the decrease in burst pressure due to size effect is relatively small, from 32,000 to 28,800, whereas the decrease in strain is from around 2% to around 0.9%. A surprising result of the model tests was the burst of the −35°F vessel at something less than 0.2% strain (see Table 4.5). So far, this is the only model vessel tested in the HSST Program which did not develop gross yielding before failure.

The exact significance of this test remains to be explained. The 0°F test was also noteworthy; the strain at failure in this test was almost exactly the same as for the 130°F tests of the same orientation. The burst pressure, however, was higher. Unfortunately, considerable difficulty was encountered with freezing of the pressurization medium, and it is believed that the indicated pressures may be too high. The strain data, however, appeared to be correct. For future low-temperature tests, alcohol will be used as the pressurizing medium in the hopes that the problem of freezing can thus be eliminated.

Crack-opening-displacement (COD) results were also obtained on vessel V-1. This COD device consisted essentially of a dial indicator mounted to show the increase of distance between two pins mounted at the edge of the notch. The dial was read by means of a closed-circuit TV camera. A plot of COD as a function of pressure is shown in Fig. 4.17. The numbers adjacent to the curves indicate the attempts to reach burst pressure. For example, on runs 1, 2, and 3, the lead-throughs leaked at approximately 19,000 psi. On the fourth run, a pressure above 25,000 was reached, and on the fifth and final run the burst pressure of 28,800 psi was reached. The curve shown in Fig. 4.17 is a typical one for crack opening displacement – a large change in COD with small changes in pressure as burst pressure is approached.

Mounted next to the TV camera mentioned above was a remotely operable 35-mm still camera. The principal purpose of the still camera was to serve as a backup for the TV system. Two frames taken by the still camera are shown in Fig. 4.18. The counter at the

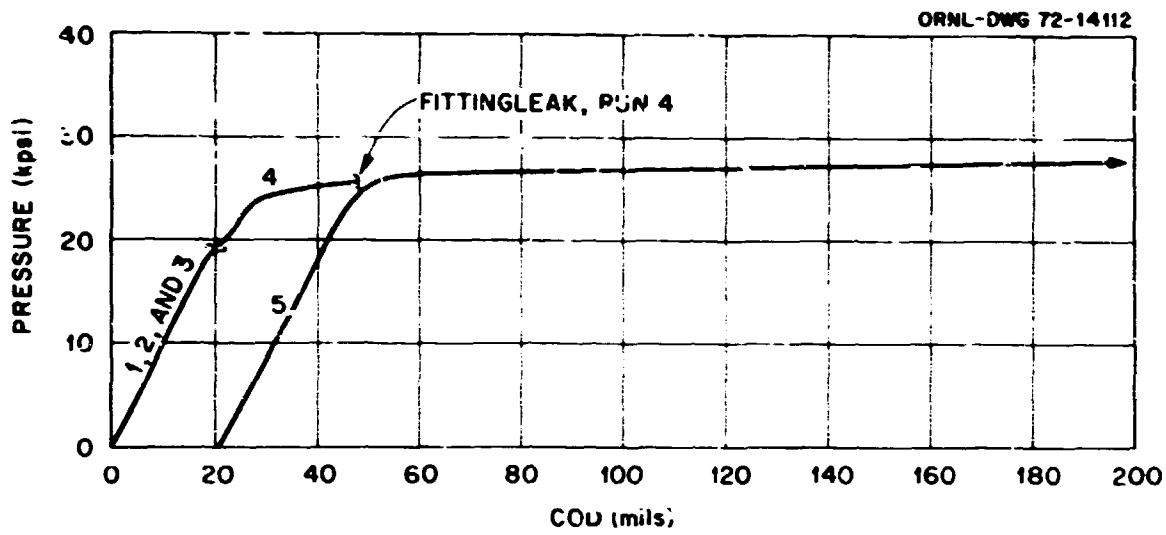

Fig. 4.17. Plot of crack opening displacement vs pressure, vessel V-1.

bottom of the pictures is used to keep track of the sequence of pictures, whereas the clock at the upper right is extremely convenient when reviewing the TV tapes. Unfortunately, all of the most interesting frames, which would have shown a large increase in the size of the notch, were ruined when a jet of high-pressure water from the failing vessel completely destroyed the camera.

The effect of size was illustrated by the mode of failure as well as by the pressure and gross strain at failure. Figures 4.19 and 4.20 show the fracture patterns of a typical model and of the prototype. The important point is that the flaw in the model arrests, whereas the flaw in the prototype runs the full length of the specimen. A reason for this phenomenon is suggested below.

The energy stored in a vessel due to pressurization is a function of volume, whereas the energy needed to generate a new surface depends more on area. Thus the energy available increases as the cube of a dimension, whereas the energy needed increases to a lesser degree. Hence the propensity to fragment increases with size. Although the prototype did not actually fragment, that is it did not break into two pieces, in no way can the failure be called a leak. It also seems likely that without the restraining influence of the large bolted manway at one end of the vessel, a fragment would have been formed. Furthermore, had the temperature been lower or the working medium more compressible, the formation of a fragment would have been almost a certainty.

A companion vessel will be tested under the same conditions except at a lower temperature. A more extensive discussion on vessel V-1 results and related fracture calculations will be presented in conjunction with results from the second vessel test.

Summary and Conclusions

The first intermediate vessel was successfully tested. The importance of size was illustrated both by the lower strain or less normalized energy to failure in the prototype than in the models and by the mode of failure.

The test also illustrated that a large flawed vessel, despite a size effect, will still retain a large margin of safety. The design pressure for the intermediate vessel was 9700 psi. Even with the large flaw, the vessel held almost three times the code-allowable pressure.

The test facility, including pump and computer, as well as numerous experimental techniques performed exceptionally well.

ACOUSTIC EMISSION MONITORING OF FIRST INTERMEDIATE VESSEL TEST[12]

E. R. Reinhart S. P. Ying
Southwest Research Institute

Introduction

The nondestructive test technique of acoustic emission holds considerable promise for use in the safety monitoring of nuclear pressure vessels because of its

12. Research sponsored under Purchase Order No. 11Y-2222V between Union Carbide Corporation and Southwest Research Institute.

PHOTO 2348-72

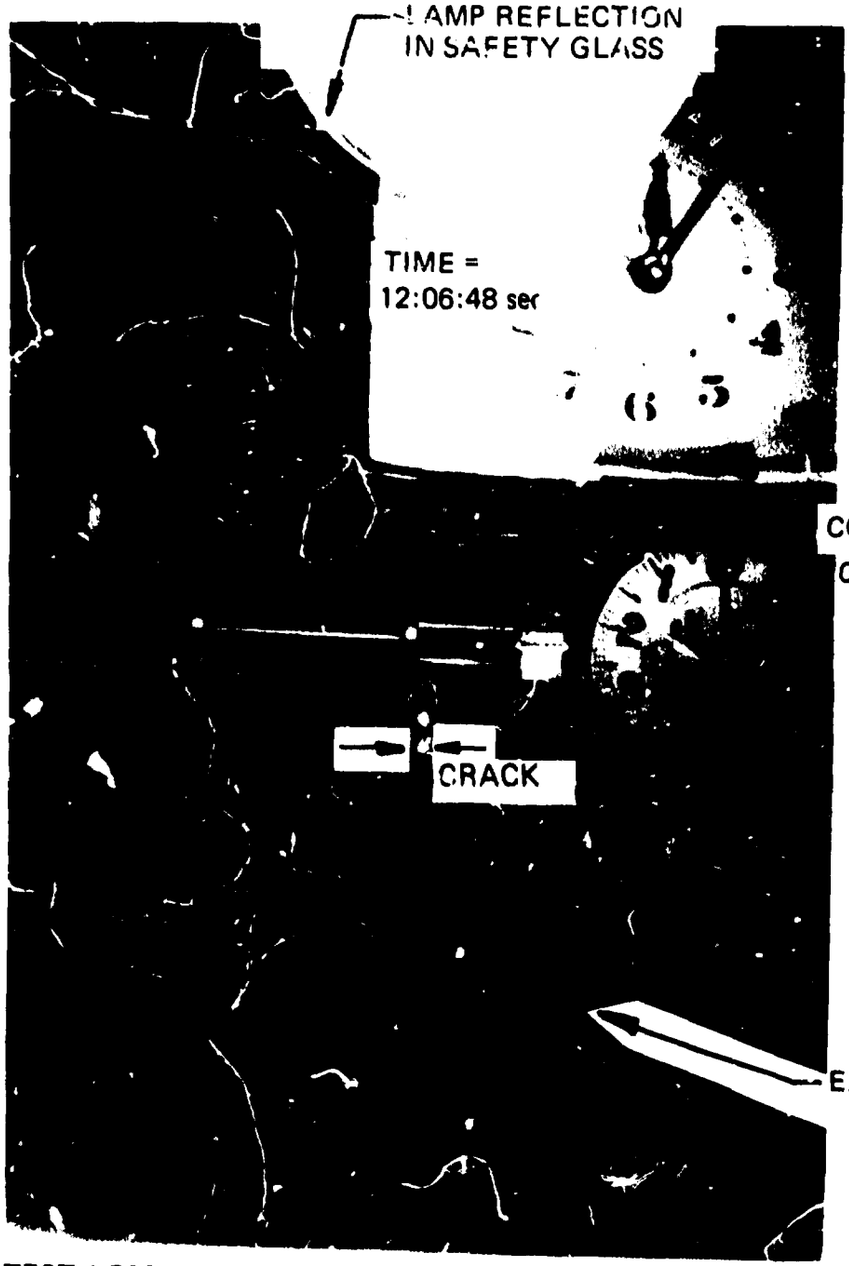

TEST 1 500 psi RESTARTING 6-29-72 12:06:48 PM

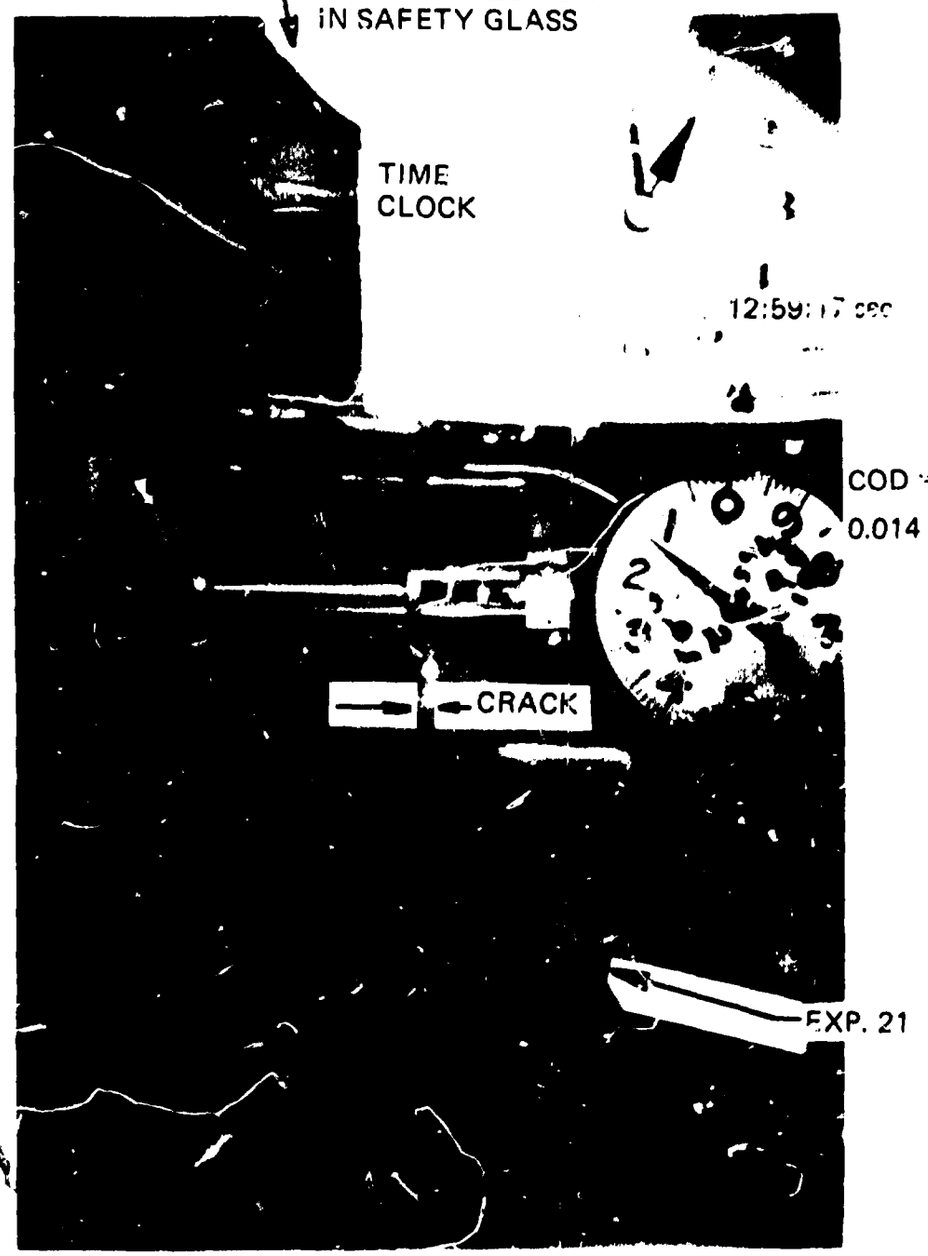

TEST 1 15,000 psi AND RISING 6-29-72

Fig. 4.18. Typical photograph and TV tape data – intermediate vessel test (approximately ½ of full size).

PHOTO 4646-72

Fig. 4.19. Opening of model vessel after burst. Note scale.

PHOTO 79977

Fig. 4.20. Opening of full-scale vessel after burst. Although not visible in the photograph, the crack ran up to the closure at the left end of picture.

ability to interrogate the total volume of the vessel while under hydrostatic or operating stress conditions. To gain necessary background information regarding the acoustic emission signal characteristics of heavy-walled reactor-grade steels, Southwest Research Institute (SwRI), in conjunction with Oak Ridge National Laboratory, has monitored over the last two years the 1-in.-thick specimen and 6-in.-thick specimen tensile tests. The results of these tests have been reported.[13,14]

The next logical step in the development of this technique was to add to the tensile test information the complexity of real three-dimensional pressure vessel loading and geometry as offered by the intermediate vessel tests. The following sections describe the preliminary results of the first Intermediate Vessel Test conducted at ORNL June 29–30, 1972.

Test Preparation

After a review of the proposed ORNL test setup, a number of areas on the pressure vessel were identified as possible sources of extraneous noise which could possibly mask actual acoustic emission signals during the test. The areas of concern were: (1) the vessel coolant circulation coils, (2) the metal seal in the vessel head, and (3) bolt and flange noises in the vessel head.

As shown in Fig. 4.21, the vessel coolant coils are attached directly to the vessel wall and limit access to the vessel outside surface. It was thought that as the vessel expanded under pressure and temperature, relative movement between the coolant coils and the vessel could cause extraneous noise signals. The nature and extent of this noise were unknown.

The metal pressure seal was also considered as a potential source of extraneous noise, since the seal will undergo considerable deformation as the pressure in the vessel increases. It was thought that once the seal was properly seated, this noise should be minimal, but background data were again unavailable.

The third area of potential extraneous noise was anticipated to occur near the bolted head flange. Rotation of the flange, elastic elongation of the studs,

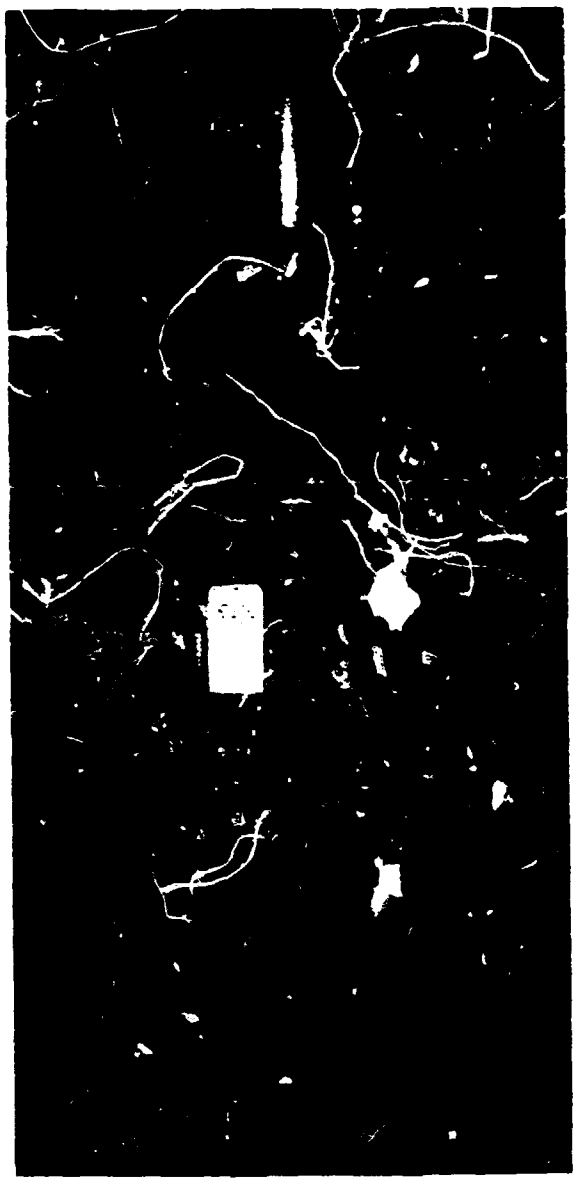

Fig. 4.21. Coolant coils mounted on vessel mockup.

and elastic movement of all the associated hardware in the head were all anticipated as possible noise sources. It should be mentioned that the majority of these mechanical noises are in the low-frequency spectrum (<80 kHz) of the acoustic emission monitoring system and are eliminated by frequency filtering. However, for the anticipated test a more refined method of data recording was felt warranted.

Since the primary interest of this test was the recording of the acoustic emission as generated in the region of the flaw, a data processing technique known as coincident detection was employed to exclude the recording of extraneous noise. This technique employs a multiple sensor array and a coincident circuit to permit the recording of only those signals which arrive at the sensor array within a preselected time gate. All other signals are excluded. The sensor array pattern used for this technique is shown in Fig. 4.22. Sensors L, G, and J comprise the coincident detection sensor

13. S. P. Ying, "Acoustic Emission Monitoring of the Six-Inch-Thick Flawed Tensile Specimens," Paper 23, HSST Program Fifth Annual Information Meeting, Oak Ridge National Laboratory, Mar. 25–26, 1971.

14. S. P. Ying, "Acoustic Emission Monitoring of One-Inch-Thick and Six-Inch-Thick Flawed Tensile Specimens," Paper 15, HSST Program Sixth Annual Information Meeting, Oak Ridge National Laboratory, Apr. 25–26, 1972.

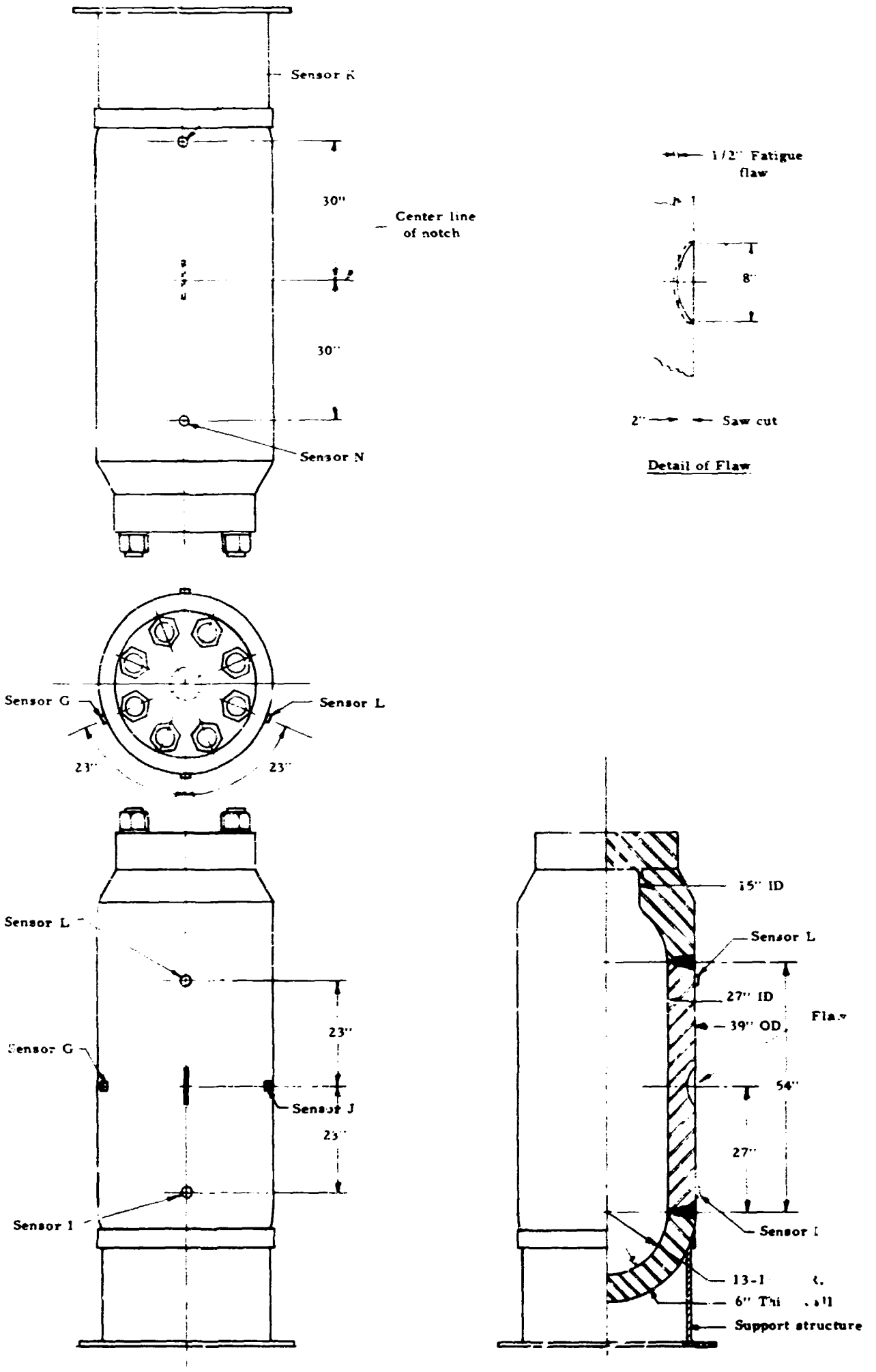

Fig. 4.22. Location of transducers on vessel.

array. The coincidence technique functions in the following manner.

1. When sound (acoustic emission) is transmitted from the region of the flaw as a surface wave on the outside surface of the vessel, transducers L, G, and J will be excited at nearly the same time. For this case, the coincident circuit compares the arrival time of signals from information channels G and J, and if they are within acceptable time gate limits, the coincident circuit is then open to accept data from sensor L, the actual data channel. This is termed two-channel coincidence. If a signal has arrived within the same time gate as the information channels, the data from this channel are accepted and recorded. This final step comprises three-channel coincidence.

2. It should be noted that two-channel coincidence could occur if sensors G and J were excited by a noise source equidistant from the sensors or by simultaneous sound transmission from either end of the vessel. For this case the data channel would not be excited in the necessary time gate, and no data would be recorded.

3. Noise sources outside the area of the flaw will usually not provide the necessary three-channel coincidence, and therefore the majority of extraneous signals are eliminated.

Noise sources outside the flaw area could also cause three-point coincidence and the recording of erroneous data if (1) the noise source was located at an area that would cause a wave front to strike sensors G and J at the same time that a noise wave front from another area strikes sensor L; and (2) a high-amplitude constant noise source could also be recorded, since a signal will always be in the time gate of the data channel.

These two conditions were not anticipated to occur, since any noise from the coolant coils or other areas of the vessel would probably be intermittent and have a point-source location. The preliminary results of the test verified these assumptions. It also appears that the severity of the noise problem may have been overemphasized; however, the number of pressure cycles that were conducted prior to the final fracture test may have eliminated much of the anticipated mechanical noise.

Instrumentation

Typical instrumentation for monitoring acoustic emission for the test is illustrated in Fig. 4.23 and 4.24. Figures 4.25 and 4.26 show the transducers mounted on the vessel wall. Figure 4.27 is a detailed photograph of the transducer, and Fig. 4.28 is the schematic diagram of the experiment. In general, the output from each transducer was fed into a high-input-impedance, low-noise-level preamplifier through a short coaxial cable. A second-stage amplifier was used for each channel operating in 100 to 500 kHz to achieve a gain of about 90 dB for the overall system. Since the amplifiers were designed for general purpose with a wide frequency band, band-pass filters, acting in the frequency range from 100 to 300 kHz, filtered out most mechanical and electrical noises. The signals obtained from the data channel fed into a digital counter. Only those signals significantly above electric noise level are counted as acoustic emission. The digital-to-analog converter changed the digital counts into analog signals which were applied to the Y axis of the X-Y recorder. The X axis was reserved for the information obtained from the pressure transducer mounted in the test system. The X-Y recorder thereby provides an on-line graphic presentation of accumulative counts as a function of vessel pressure.

The outputs of the band-pass filters of the data channel and two information channels were also fed into a coincident circuit, recorded on magnetic tape, and displayed on the oscilloscope. Since the sensors of the data channel and the information channels were mounted at an equal distance from the precracked notch area, only the emissions from the notch area could pass through the coincident circuit; these were counted in the counter at the output of the coincident gate, as previously discussed. However, the counter before the coincident circuit could count all detectable acoustic emissions from the vessel. The amplitudes as well as the durations of acoustic emission pulses were also recorded in a chart recorder through a detector and an operation amplifier. As shown in Fig. 4.28, three additional channels and the oscilloscope were used to periodically monitor other areas of the vessel during the test.

Results

Acoustic data were taken during all the pressure tests; however, data presented and discussed in this report will be confined to the final fracture test. Figures 4.29 and 4.30 show the accumulation of the emission counts obtained from the digital counters before and after the coincident circuit respectively. Since the counters counted every frequency cycle of each emission pulse, and usually a pulse with a higher amplitude has a longer duration, the accumulation counts directly relate to amplitudes and durations of emission pulses as well as the number of pulses. The counts in Fig. 4.30 represent

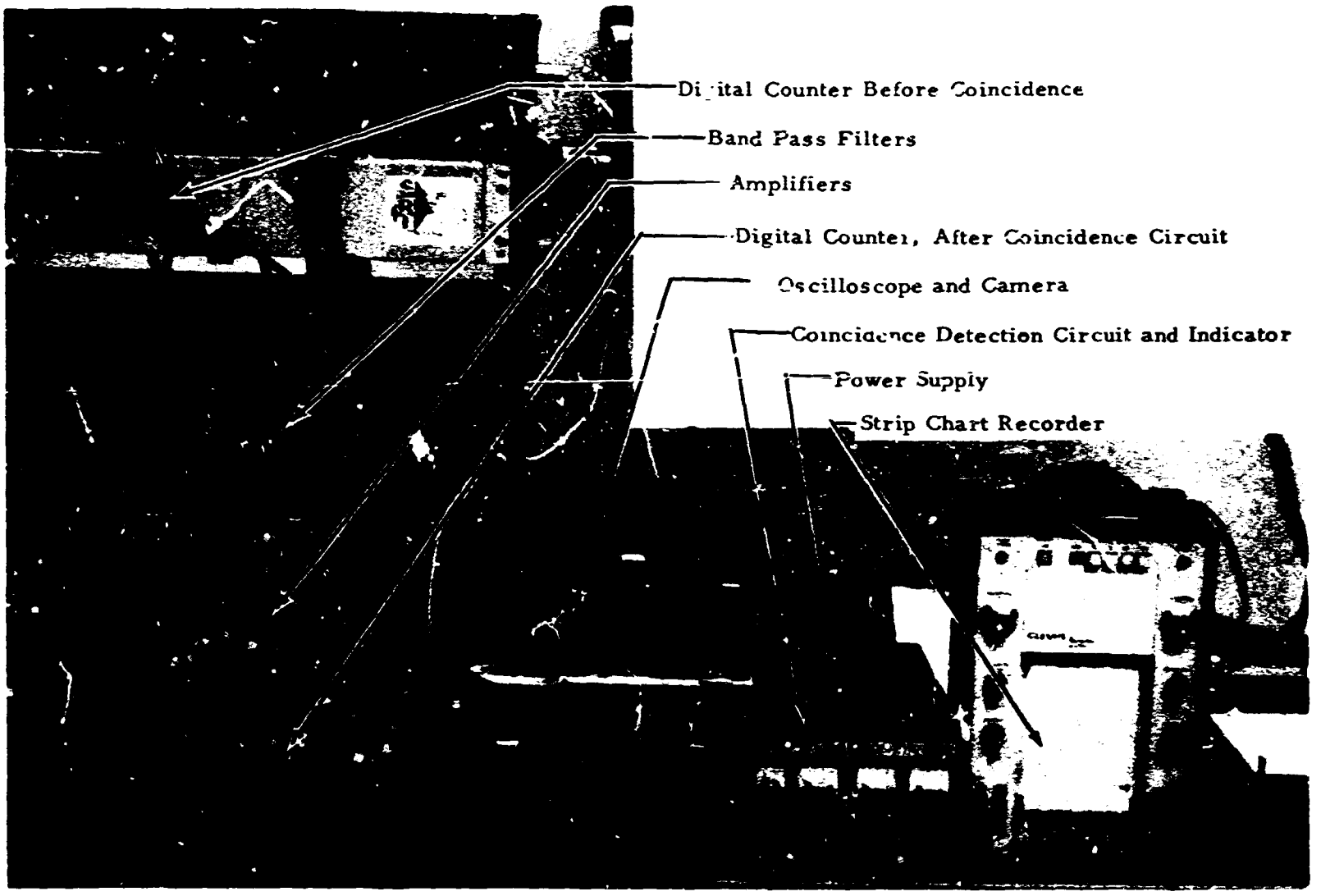

Fig. 4.23. Acoustic emission monitoring system.

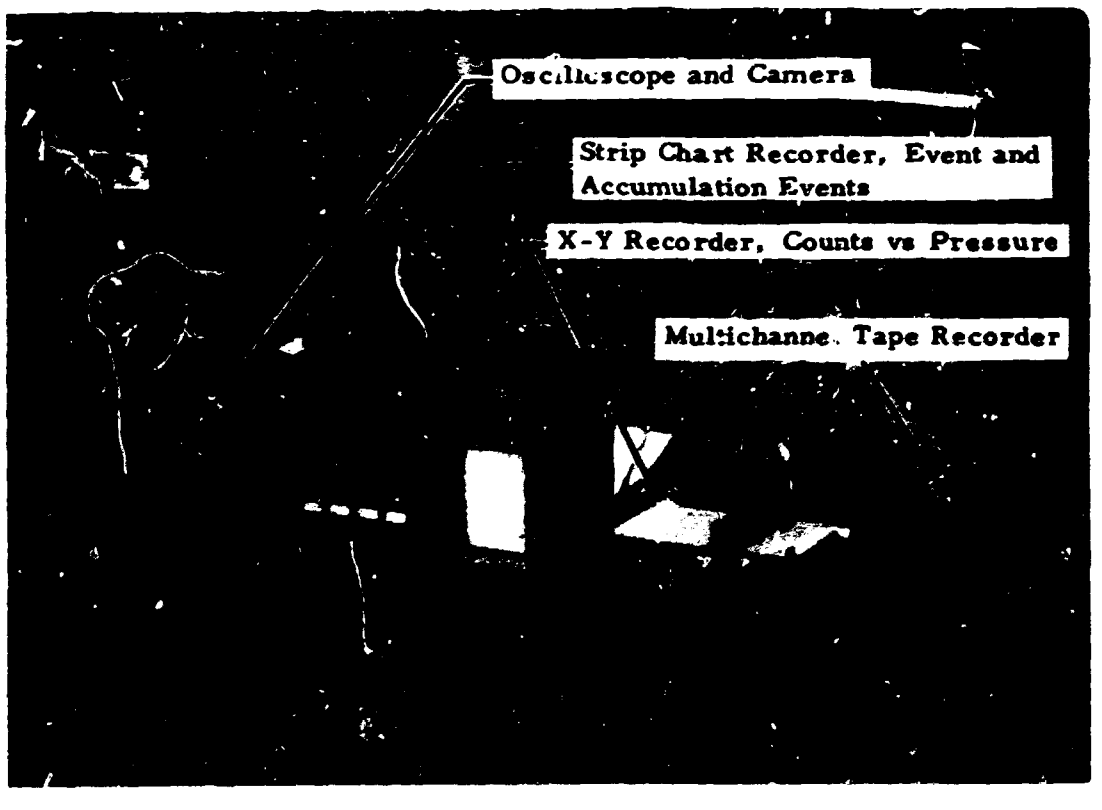

Fig. 4.24. Acoustic emission data acquisition.

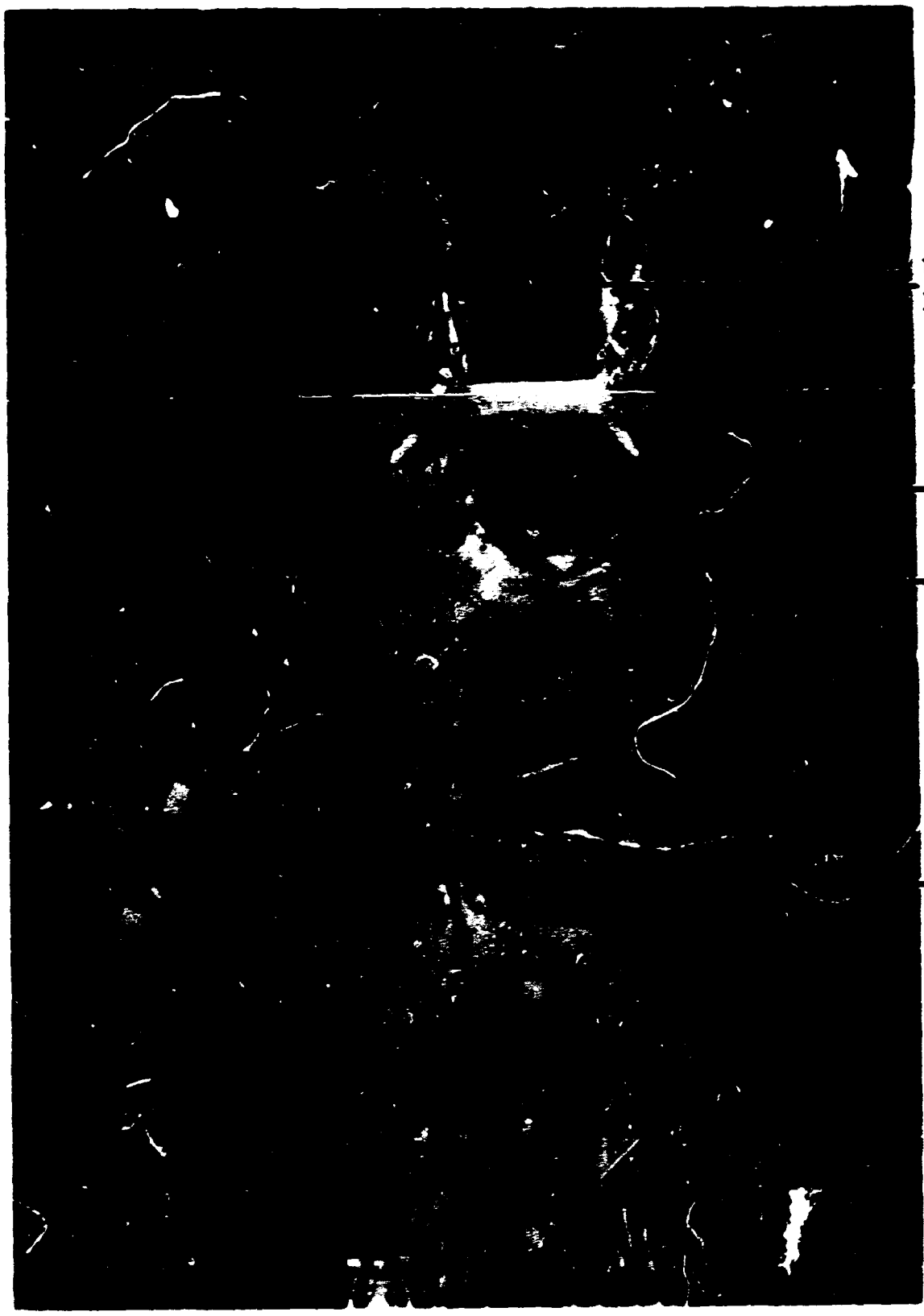

Fig. 4.25. Location of acoustic emission transducers above and below flaws.

the detectable emission from the vessel, and those in Fig. 4.29 correspond to the emission from the notch area. These two curves are similar in shape to that obtained from flawed specimens during the HSST tensile tests. The counts increase rapidly before the yield point, there are smaller counting rates during yielding, and the counting rates increase again prior to the failure of the vessel. Figure 4.31 shows the size of the flaw after failure. The counts prior to failure in Fig. 4.30 are greater than those for Fig. 4.29 for the following reason. The counter for Fig. 4.29 was placed after the coincident circuit and detected bursts in a limited notch area which was smaller than the final crack area. The counter for Fig. 4.30 was placed prior to the coincident gate and at vessel failure detected all the emission from the entire fracture area of the vessel.

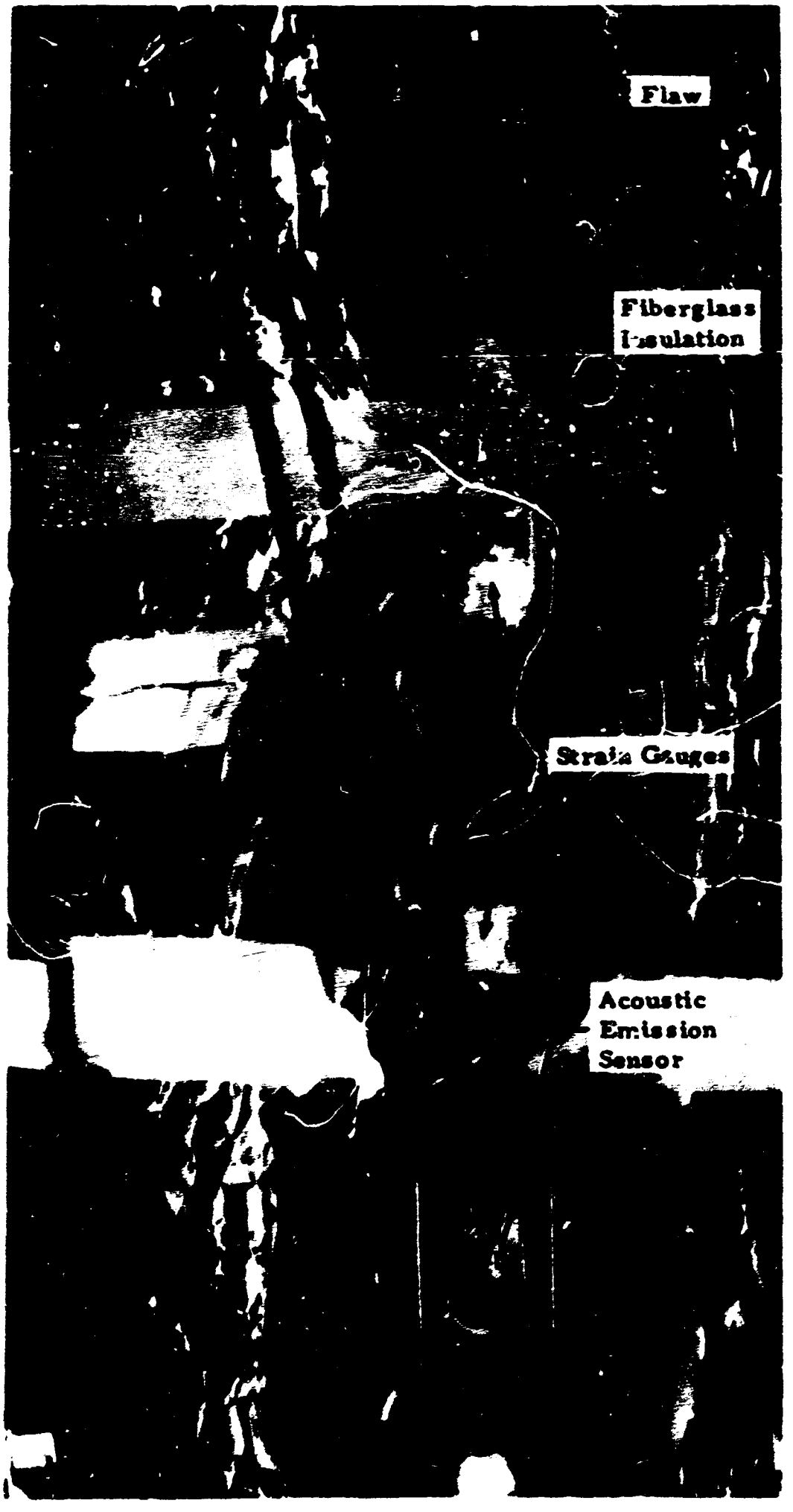

Fig. 4.26. Acoustic emission transducer mounted below flaw.

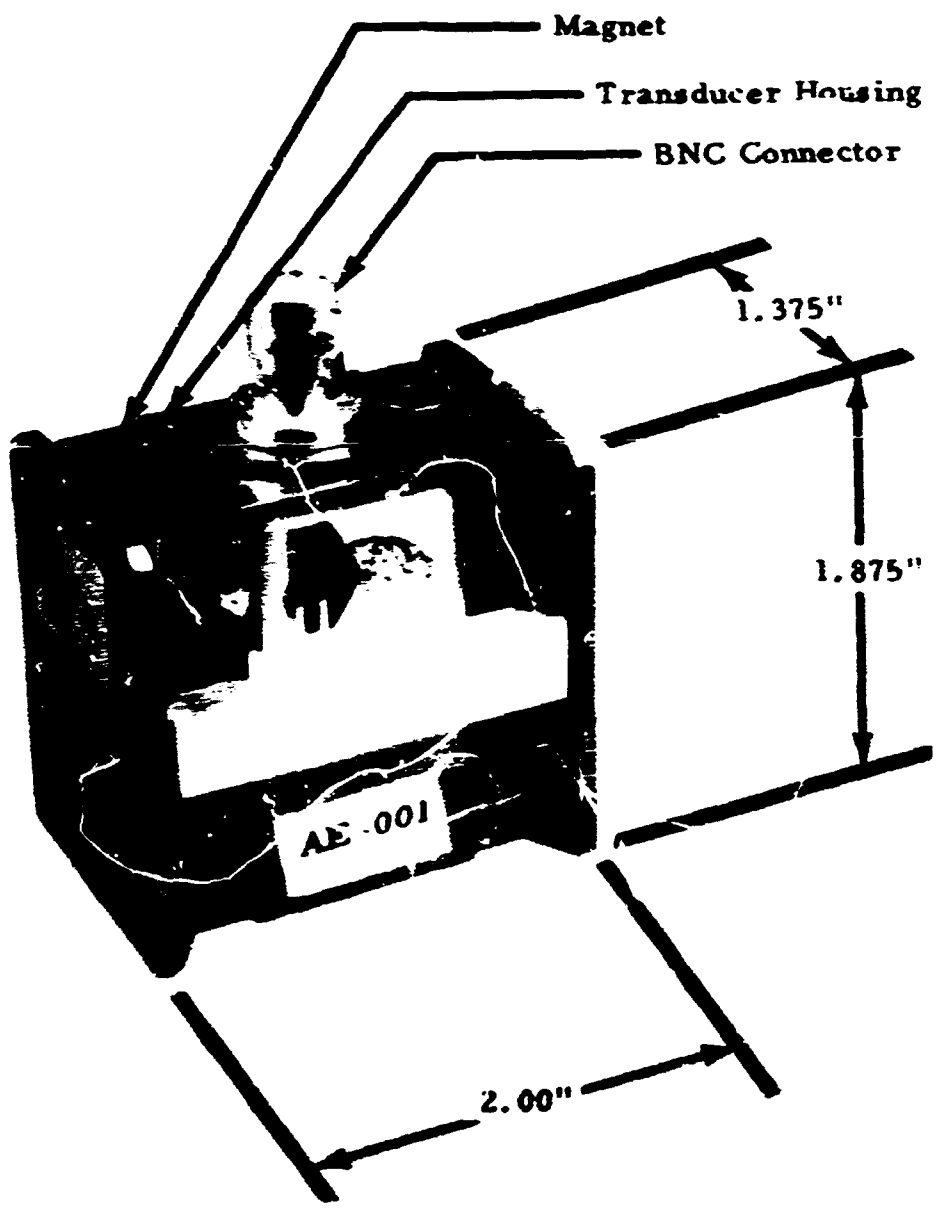

Fig. 4.27. Acoustic emission transducer.

Figure 4.32*a* is a typical record of acoustic emission from the strip chart. The length of each line represents the amplitude and the duration of individual emission pulses. The emission pulses shown in Fig. 4.32*a* were recorded at the vessel pressures from 25 to 28 ksi. Figure 4.32*b* is the record of acoustic emission prior to the failure. Both the amplitudes and the rate increased tremendously during this period up to failure.

INVESTIGATION OF MODE III CRACK EXTENSION IN REACTOR PIPING[15]

R. J. Podlaseк
Battelle Columbus Laboratories

This report summarizes the results of a program investigating the nature and extent of mode III, tearing shear fractures, in nuclear reactor piping.

The program was initiated as a result of a previous research program in which 34 full-scale pipe tests[16,17] were conducted to define the critical flaw sizes necessary to initiate fracture in nuclear reactor piping and also the extent of fracture propagation. The results of this research program indicated that the axial propagation of flaws could be controlled by the saturation

---

15. Work sponsored by HSST program under UCCND Subcontract 3678 between Union Carbide Corporation and Battelle Columbus Laboratories.

16. R. J. Eiber et al., *Investigation of the Initiation and Extent of Ductile Pipe Rupture, Phase I Final Report, Task 17, USAEC*, BMI-1866 (July 1969).

17. R. J. Eiber et al., *Investigation of the Initiation and Extent of Ductile Pipe Rupture, Task 17, Final Report USAEC*, BMI-0908 (June 1971).

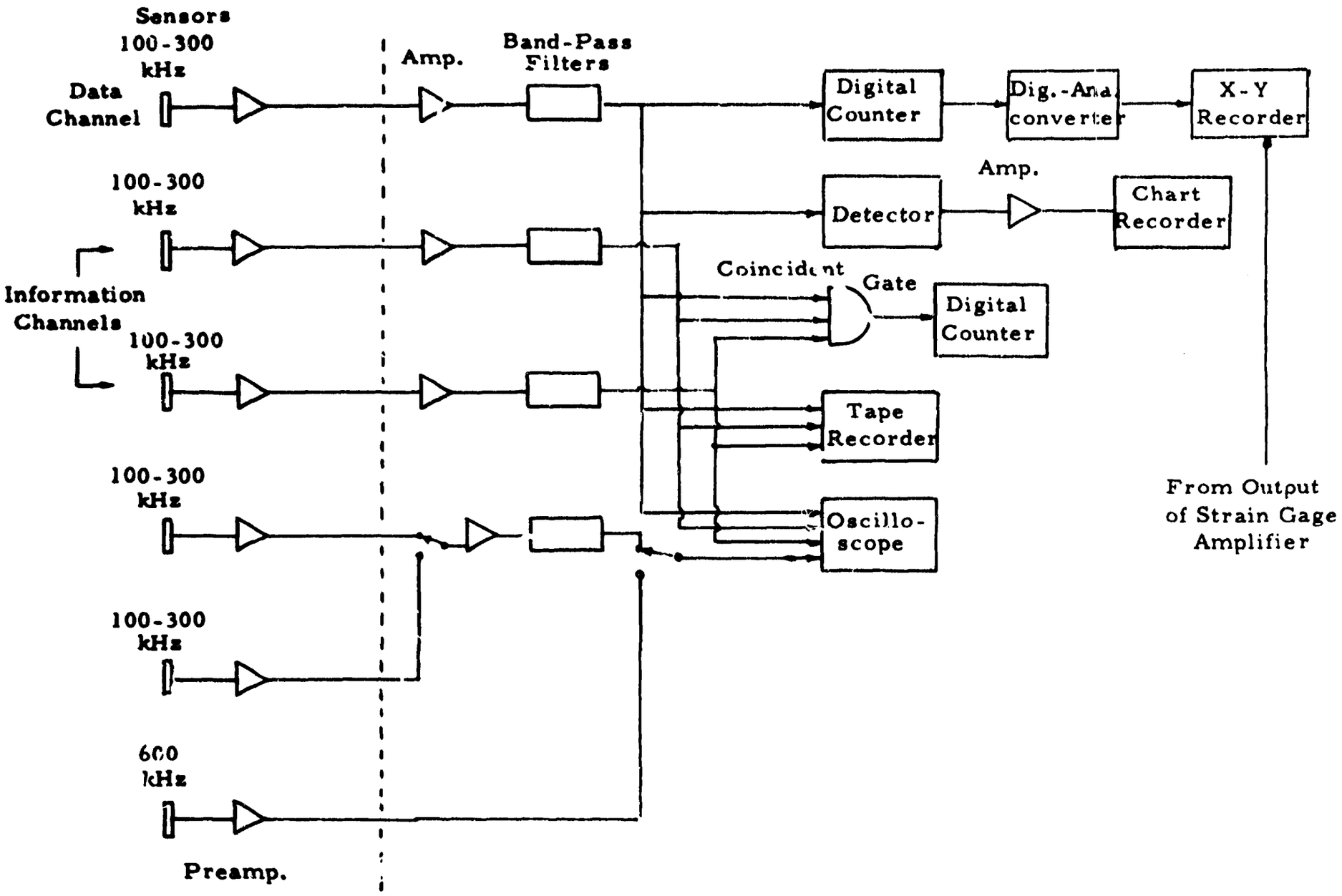

Fig. 4.28. Block diagram of acoustic emission monitoring system.

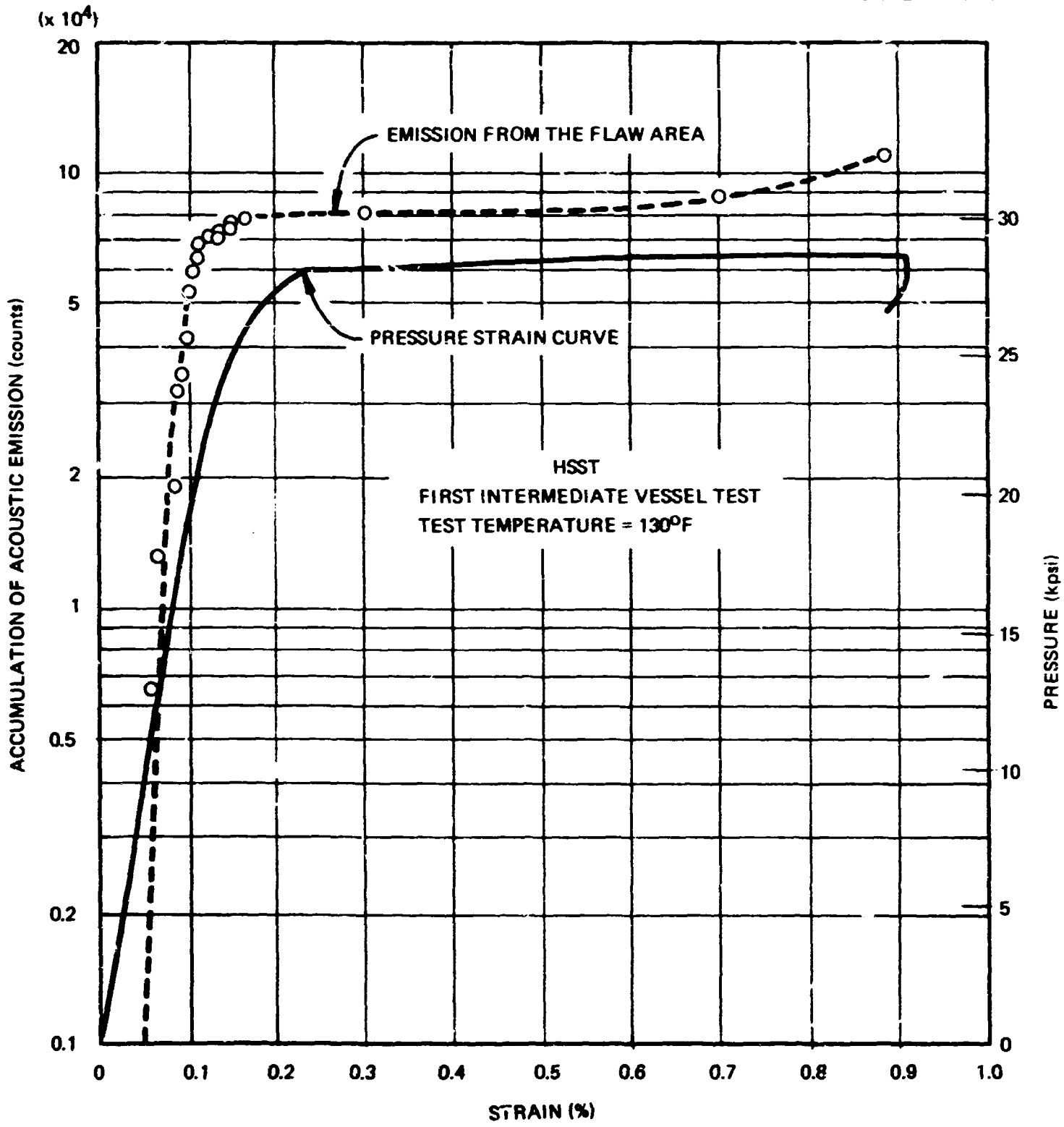

Fig. 4.29. Acoustic emission from the precracked notch area.

pressure hoop stress level. However, the results of one test in the second phase demonstrated that even though the stress level is below the threshold stress for axial extension of a mode I propagating shear fracture, a mode III, or tearing shear fracture, could still spiral along the pipe. The current research program was initiated to investigate this fracture behavior in depth.

In the initial investigation, 34 full-scale tests on A106-B carbon steel and type 316 stainless steel pipe were conducted. The specimens were 8- to 22-ft-long capped vessels with an artificial surface or through-wall defect machined in the center. The OD of the pipe was 7.5 to 24.0 in., and the wall thickness ranged from 0.375 to 1.70 in. Each pipe was pressurized with superheated water or saturated water at 469 to 686°F, and the failure pressures varied from 940 to 5410 psig. In plotting the saturation pressure hoop stress level at failure vs the artificial flaw length for all tests, it was

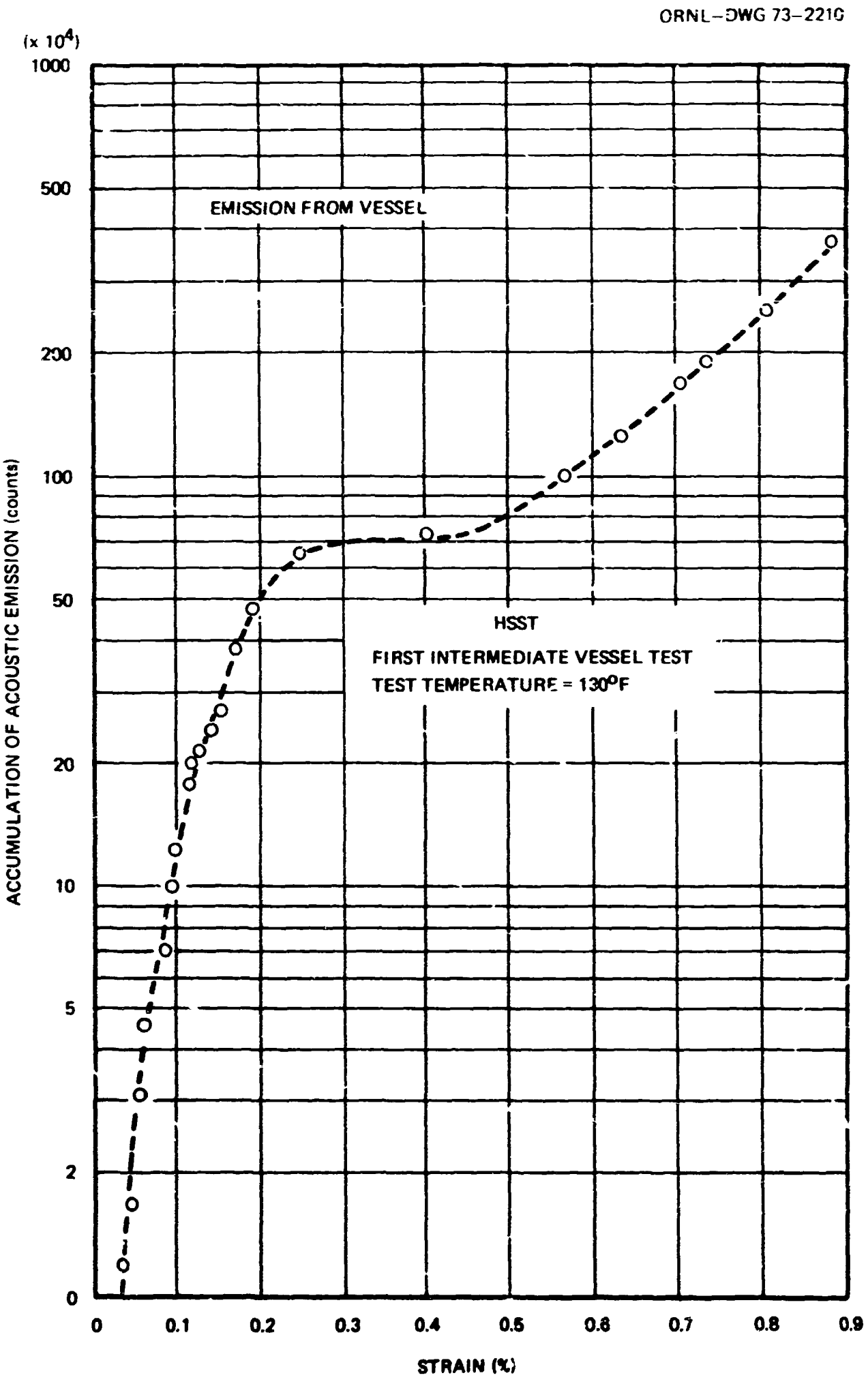

Fig. 4.30. Acoustic emission from the vessel as a function of strain.

ORGDP
PHOTO 72-1337

Fig. 4.31. Posttest condition of flaw.

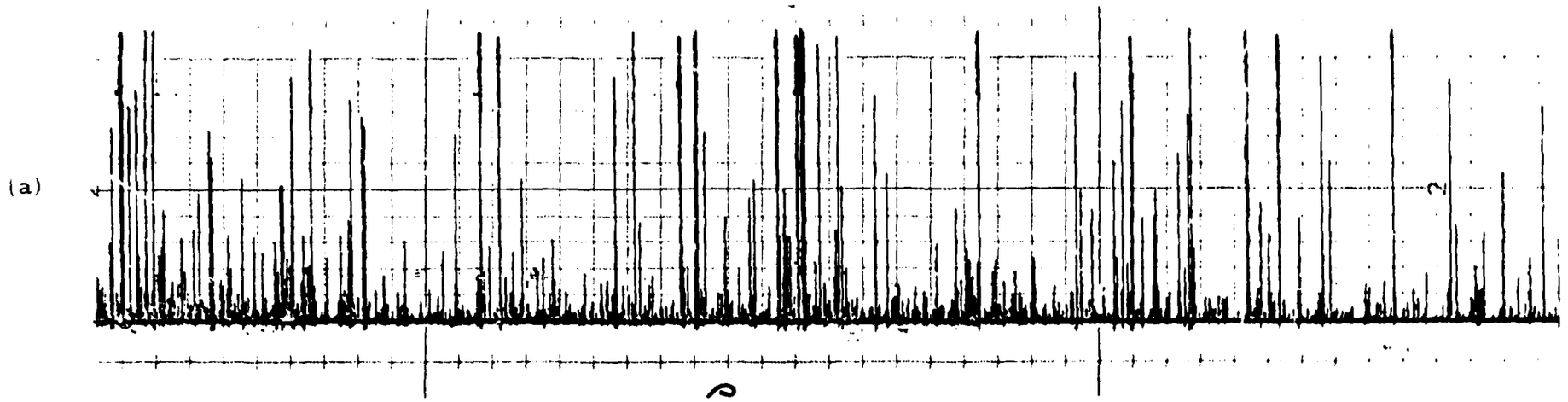

Fig. 4.32. Records of acoustic emission bursts.

noted that for saturation hoop stresses above 12 ksi an unstable rupture resulted, and for saturation pressure hoop stresses below 12 ksi, short crack extension resulted. Thus 12 ksi was deemed the threshold stress for mode I propagating shear fracture, for the A106-B pipe in the sizes investigated. The fracture appearance of all specimens depicted the 45° slant surface typical of ductile fractures. To simulate reactor conditions more precisely, one experiment (test 32) consisted of a 10-ft-long, 7.5-in.-OD by 0.500-in.-wall cylindrical section to which 5-ft-long, 34-in.-OD reservoirs were welded at each end. The result of this experiment with a 20-in.-long, 85% through-the-wall surface flaw was of particular interest, since at a saturation hoop stress of 7.1 ksi the pipe ruptured and a mode III tearing shear fracture propagated for 5 ft. This experiment demonstrated that the possibility of unstable crack extension by mode III fracture existed. For comparison, Fig. 4.33 illustrates the difference in fracture appearance between mode I, propagating shear fracture, and mode III, tearing shear fracture.

To date, two experiments have been performed as part of the current investigation of mode III crack extension. The objective of these tests has been to try to produce a mode III fracture without using the reservoirs on each end of the cylindrical test specimen. In test 1, a 10-ft cylindrical test section was fabricated with the same flaw geometry as in test 32. The fracture initiated at the same temperature and pressure as in test 32. However, the mode III fracture only extended axially 14 in. in one direction and 13 in. in the other direction. A photograph of the fracture is shown in Fig. 4.34. Test conditions for test 1 were identical to those for test 32 with the exception of the reservoirs at each end of the test section.

For test 2, the geometry of the test specimen was identical to that for test 1, except that the initial surface flaw was 40 in. long instead of 20 in. The failure temperature in test 2 was 20°F higher, and the pressure was 18% higher than in test 1; however, the mode III fracture did not extend by spiraling around the pipe. The crack propagated axially 16.5 in. in one direction

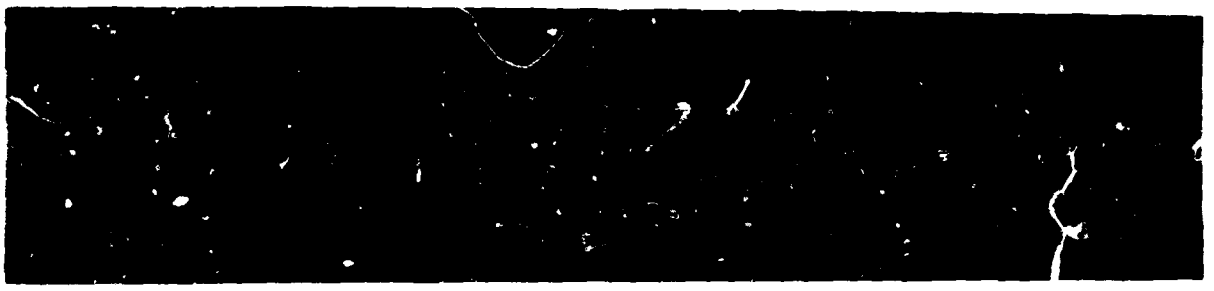

23226

a. MODE I, PROPAGATING SHEAR

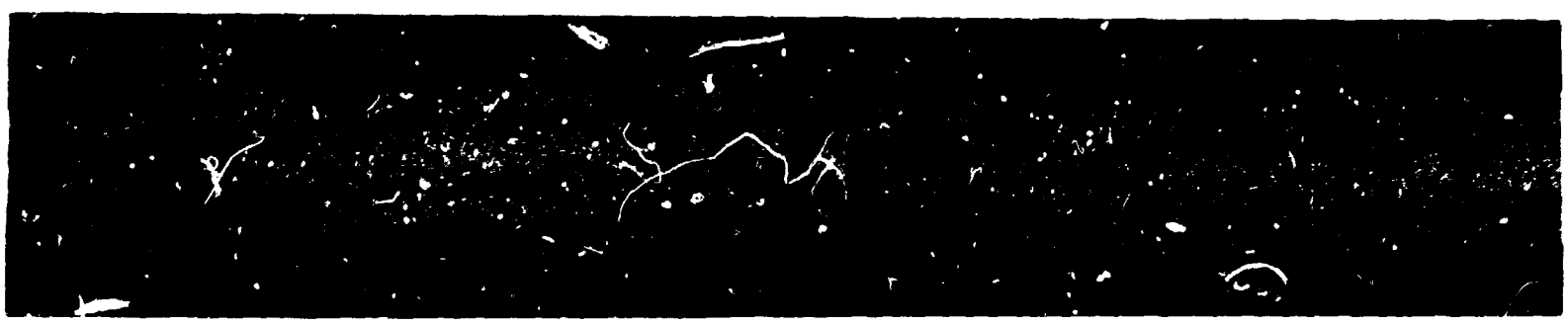

23506

b. MODE III, TEARING SHEAR

Fig. 4.33. Two types of shear fracture.

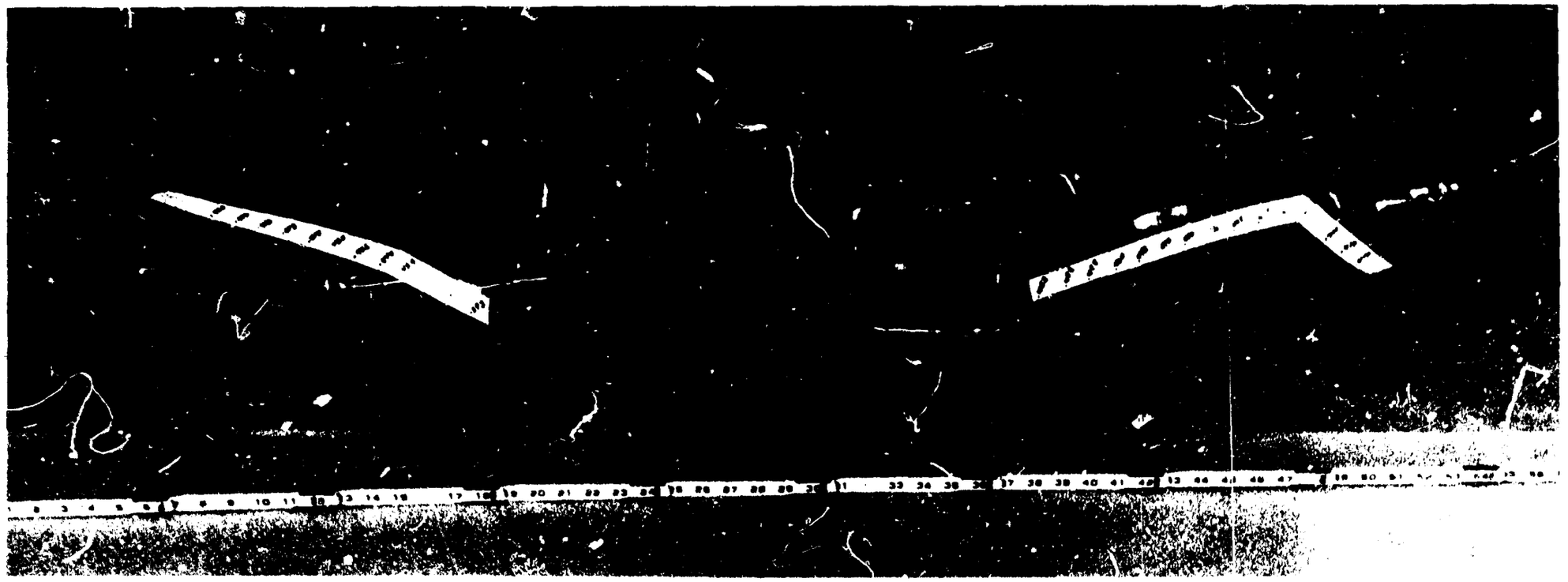

Fig. 4.34. Resulting fracture of test 1, test temperature 550°F, failure pressure 1640 psig, saturation pressure 1080 psig.

and axially 20.0 in. in the other. Figure 4.35 illu. .rates the fracture as it arrested on the 16.5-in. extension end.

In the future another test will be conducted using a test specimen without reservoirs and with the saturation pressure hoop stress level just below 12.0 ksi. If a tearing shear or mode III fracture which extends unstably does not result, the remaining tests will use reservoirs.

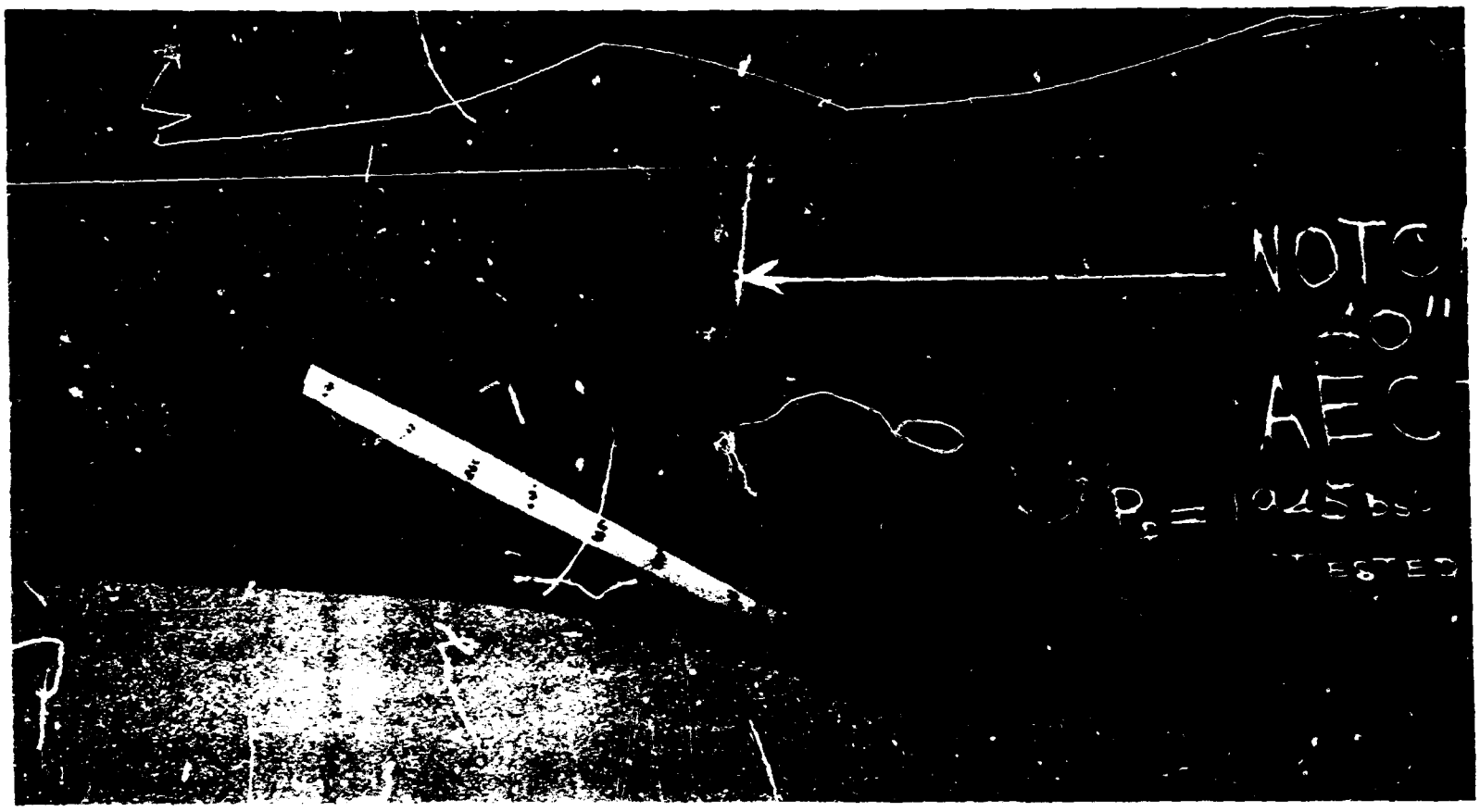

Fig. 4.35. Resulting fracture at one end of test 2, test temperature 575°F, failure pressure 1940 psig, saturation pressure 1280 psig.